THE FLORIDA STATE UNIVERSITY

COLLEGE OF ARTS AND SCIENCES

PROVENANCE OF MIOCENE SEDIMENTARY SEQUENCES IN HENGCHUN PENINSULA, SOUTHERN TAIWAN, AND IMPLICATIONS FOR THE MODERN TAIWAN OROGEN

BY

JIUN-YEE YEN

A Dissertation submitted to the
Department of Geological Sciences
in partial fulfillment of the
requriements for the degree of
Doctor of Philosophy

Degree Awarded:
Fall Semester, 2003

The members of the Committee approve the dissertation of Jiun-Yee Yen defended on October/23/2003

Neil Lundberg
Professor Directing Dissertation

John W. Winchester
Outside Committee Member

LeRoy Odom
Committee Member

James F. Tull
Committee Member

The office of Graduate Studies has verified and approved the above named committee members

ACKNOWLEDGEMENTS

Throughout the course of my doctoral program, I received help countless times from many individuals that help me in many aspects, both tangible and intangible. First and foremost, I would like to thank my advisor, Dr. Neil Lundberg, who is always positive and encouraging to talk to, and is always open-minded on ideas about research. Dr. Lundberg also provided financial support for field work, during which he was involved. His work ethic and keen observation in the field are extraordinary and have greatly contributed to this dissertation, directly and indirectly.

I would also like to thank my committee members, Dr. Roy Odom and Dr. James Tull, for supporting me with their advice and suggestions during all phases of this work. I would like to thank my outside committee member, Dr. John Winchester, who is passionate about science. Talking with him is always stimulating, and a conversation with him can easily lead to a published international opinion piece. I am also in debt to Dr. David Furbish, who opened my eyes to the more mathematical side of geology, which has become an important aspect of this research. I am extremely grateful to Dr. Charles Naeser, of the US Geological Survey, who provided much guidance and materials needed for the work on the fission-track project. His patience and attention to detail have greatly improved this project. The Central Survey of Taiwan provided a digitized geological map of the Hengchun Peninsula, which has been extremely useful during this project. Many thanks also go to Dr. Meg Streepey and Dr. Tom Janecek for their generosity in offering the use of equipment.

I am also very grateful to my many friends who provided different types of help. Michael and Erica Bizimis have been my first-hand source for American and Greek cultures. Mabry Gaboardi and Jon Spaniard, Simon Mudd and Robin Cathcart are extraordinary individuals, who are not only inspiring to talk with about their respective scientific fields, but are also great roommates. Chris Holm and Hongshen Cao also helped me at various stages during the course of my stay at FSU. Tami Karl and Mary Gilmore have been looking out for me during all the time I have been in Tallahassee and I cannot thank them enough.

Lastly, I thank my father who has been courageous throughout all his life in solving problems and is now bravely fighting to recover from the cancer, and my mother and sister who have been extremely supportive for what I have wanted to do. I would never have been

able to proceed, much less finish this project without all the wonderful emotional shelter they have consistently provided.

TABLE OF CONTENTS

LIST OF FIGURES

LIST OF TABLES

ABSTRACT

The Hengchun Peninsula (HCP) of southern Taiwan represents the newest emergent segment of the orogen built by the ongoing oblique collision between the Luzon arc and Eurasia continent. Newly recognized exposures indicate that a unit with the lithology of the Shihtzutou unit underlies the Lilongshan unit with a depositional contact. This discovery shows that Shihtzutou-type sands accumulated at least twice during the deposition of the Mutan Formation, and are in sedimentary contact with the Lilongshan unit. Fission-track analysis of detrital zircons reveals three age components from the samples analyzed from the HCP, which are 15, 34, and 66 Ma. These age components coincide with the thermal events of the opening of the South China Sea.

Uplift rates calculated from the pattern of horizontal motions observed by a network of GPS stations, coupled with the equation of conservation, indicate the need for the Fengkang fault to accommodate a significant differential in uplift rates north and south of this fault. To a first degree, predicted uplift rates agree with data available on uplift across Taiwan. The source terranes for the Miocene sedimentary sequences of the HCP likely formed by the following scenario. Rifting of the South China Sea (SCS) began in the Late Cretaceous, which created rift basins off the southeast coast of China. A second rift episode of the SCS during the Eocene then intersected the early rift basins and carried some rifted blocks of the continental margin farther from Asia, while at the same time creating new mafic crust that was later accreted into the forearc of the approaching Luzon arc. Between 10 Ma and 5 Ma the Manila trench encountered and accreted the rifted microcontinental blocks and blocks of young mafic crust, and raised them to a subaerial environment to provide eroded detritus including rounded pebbles to the HCP basin. These sediments were deposited into the HCP basin in different fan systems with different source terranes and paleoflow directions. From 5 Ma to the present, the HCP basin itself was incorporated into the accretioanry wedge and brought to its current position by the fast-moving Philippine Sea plate.

CHAPTER ONE
INTRODUCTION

Arc-continent collision is one of the mechanisms that operate to increase the landmass of continents. Although arc-continent collisions are often dwarfed by the scale of continent-continent collision, they are more abundant; they are also often short lived (Kearey and Vine, 1996). The transient nature of arc-continent collisions and the usual result of strongly deformed geologic terranes welded along continental margins make it difficult to establish the detailed processes of arc-continent collision from beginning to the end, especially in ancient examples. The study of modern and ancient arc-continent collisions has helped increase our understanding of mountain building processes along with the development of continental margins, processes that tectonically transform oceanic terrane into terrestrial area.

Because arc-continent collision is short-lived in nature, it may evolve from incipient stages to a fully mature collisional orogen in a shorter time than do continent-continent collisions. Active arc-continent collisions around the world are in different stages of development, providing us a series of snapshots through time of collision process that operate. By studying different cases at different stages of collision, we will be able to reconstruct mechanisms and processes involved during the course of mountain building and landmass growth. Arc-continent collisions are more numerous than continent-continent and offer a less complicated way to gain insight into collisional tectonism. Examples in different stages and tectonic settings provide varied insights. In Timor, the Indo-Australian plate is subducting northward along the Java trench to the west and the Timor trough to the east, and collided with the Banda arc (Cardwell and Isacks, 1978) in the late Miocene or early Pliocene. The subducting plate generates earthquakes as deep as 680km (Chiu et al., 1991). The development of Papua New Guinea records the collision between the overriding Bismarck plate and the northward-subducting Australian plate, beginning in the Pliocene (Abbott et al., 1994). The Finisterre Range is a volcanic arc complex made up of volcaniclastic and siliciclastic forearc turbidites, arc volcanoes and limestones. The Finisterre Range is juxtaposed against the New Guinea Highlands along the Ramu-Markham Fault, which acts as the suture zone. The New Guinea Highlands and Papuan fold-and-thrust belt represent the accretionary complex in this system. Abbott et al. demonstrated that the tectonic surface uplift rate in Finisterre Range is 0.8 to 2.1 mm/yr and this is caused by crustal thickening of the area that has a rate of 0.6 to 3.0 mm/yr (Abbott et al., 1997). During the formation of the Late Paleozoic supercontinent Pangea (Berzin et al.,

1996), the Magnitogorsk arc of southern Urals moved westward and collided with the East European craton during the Late Devonian (Alvarez-Marron et al., 2000; Brown et al., 2001). This collision is now represented by a tri-partite series of geologic terranes, comprising a foreland basin-accretionary complex-Magnitogorsk arc sequence, from west to east, all of which have been subjected to lower grade (greenschist facies) metamorphism. This setting shows a mature arc-continent collision in which compression ceased before the terranes were obliterated by tectonism or eroded by continental uplift. In Kamchatka, a change in subduction polarity is demonstrated by the collisional sequences. Here the Acaivayam-Valaginskaya arc collided with the Okhotsk microplate as the passive margin of the microplate subducted beneath the arc, at the end of the Paleocene to early Eocene. This collision propagated northward to the Olutorka region in the middle Eocene, when subduction changed its polarity to northwest-dipping and resulted in the formation of volcanic belts in the accreted margin in Eocene and Oligocene. The Kronotskaya arc collided with and docked onto Kamchatka during the Miocene, after which the subduction of the Pacific plate was established, forming the Eastern Kamchatka volcanic belt at around 5Ma (Gaedicke et al., 2000; Konstantinovskaia, 2001; Levin et al., 2002).

Most studies carried out on these arc-continent collisions have concentrated mainly on their tectonic histories. There are many global-scale problems involved in the processes of arc-continent collision such as controls on the geometry of the collisional mountain belt; how basal and internal friction affect tectonic proceses; fashion of fault propagation; provenance of the materials in the accretionary prism; sediment dispersal paths; ...etc. Some of these can be addressed by numerical modeling, yet others require comprehensive investigations of the materials and the interaction of the collision with its neighboring tectonic elements.

The nature of oblique collision in Taiwan makes this arc-continent collision an especially fruitful one to study. The collision started in the northern part of Taiwan, or even farther north, and the point of collision has propagated southward at an apparently steady pace. At the same time, the collided arc pushes the northern part of Taiwan into a more developed stage of collision. In other words, the oblique collision creates a situation of space-time equivalency, and one can see the older stages of collision in the north and increasingly younger ones progressively to the south. In order to decipher the history of the arc-continent collision, it is important to study the most recently emerging collision zone of the modern arc-continent collision. Then, by utilizing the fundamental geological principle "the present is the key to the past" and the space-time equivalency, a history of the arc-

continent collision can be established. The Hengchun Peninsula of southern Taiwan is the most recently emergent segment of the submarine accretionary prism, uplifted by the process of the collision to become the newest segment of the subaerial mountain belt. A thorough understanding of it is crucial to our understanding of both the ongoing modern collision and the ancient orogenic process of Taiwan. Obtaining the full picture of modern arc-continent collisions is also imperative for deciphering the tectonic histories of older collisional mountain belts.

Tectonic Setting of Taiwan

Taiwan is located on the southeastern periphery of the Eurasian plate and in the westernmost corner of the Philippine Sea plate (Figures 1, 2), and is part of two subduction systems, the Ryukyu subduction system to the northeast and the Manila subduction system to the south-southwest. To the northeast of Taiwan, the Philippine Sea plate is subducting toward the northwest in the Ryukyu subduction system. This subduction brings about the opening of the Okinawa trough in the upper (Eurasian) plate, which changes the shape of the ocean-continent boundary in this area. To the south, subduction of the South China Sea toward the east along the Manila trench produces the Luzon island arc. Between the two subduction systems, Taiwan marks the site of an ongoing oblique collision between the Luzon island arc and the passive continental margin of mainland China, with the island of Taiwan formed as an overgrown accretionary wedge (Suppe, 1984; Barrier and Angelier, 1986; Teng, 1990). Taiwan is morphologically asymmetric (Figures 3, 4), with Taiwan Strait on the west side and the Philippine Sea on the east. Taiwan also marks a site where the subduction polarity reverses. The Coastal Range of eastern Taiwan represents the northernmost segment of the north Luzon arc which has been colliding with the Eurasian plate, propagating southward at a rate of 45 mm/yr (Byrne, 1996) since mid- or late Miocene (12 to 5Ma) (Dorsey and Lundberg, 1988; Teng, 1990).

The southernmost tip of the island of Taiwan, the Hengchun Peninsula, can be regarded as the most recently emerged segment of the accretionary prism in this arc-continent collisional system. The Hengchun Peninsula is composed mainly of Miocene clastic sequences that are overlain (either depositionally or structurally) by the Kenting Formation, a chaotic unit generally interpreted as a mélange or an olistostrome. The Miocene clastic sequences of the Hengchun Peninsula do not resemble the age-equivalent strata found elsewhere on Taiwan, and their occurrence cannot be readily explained by the simple “bull

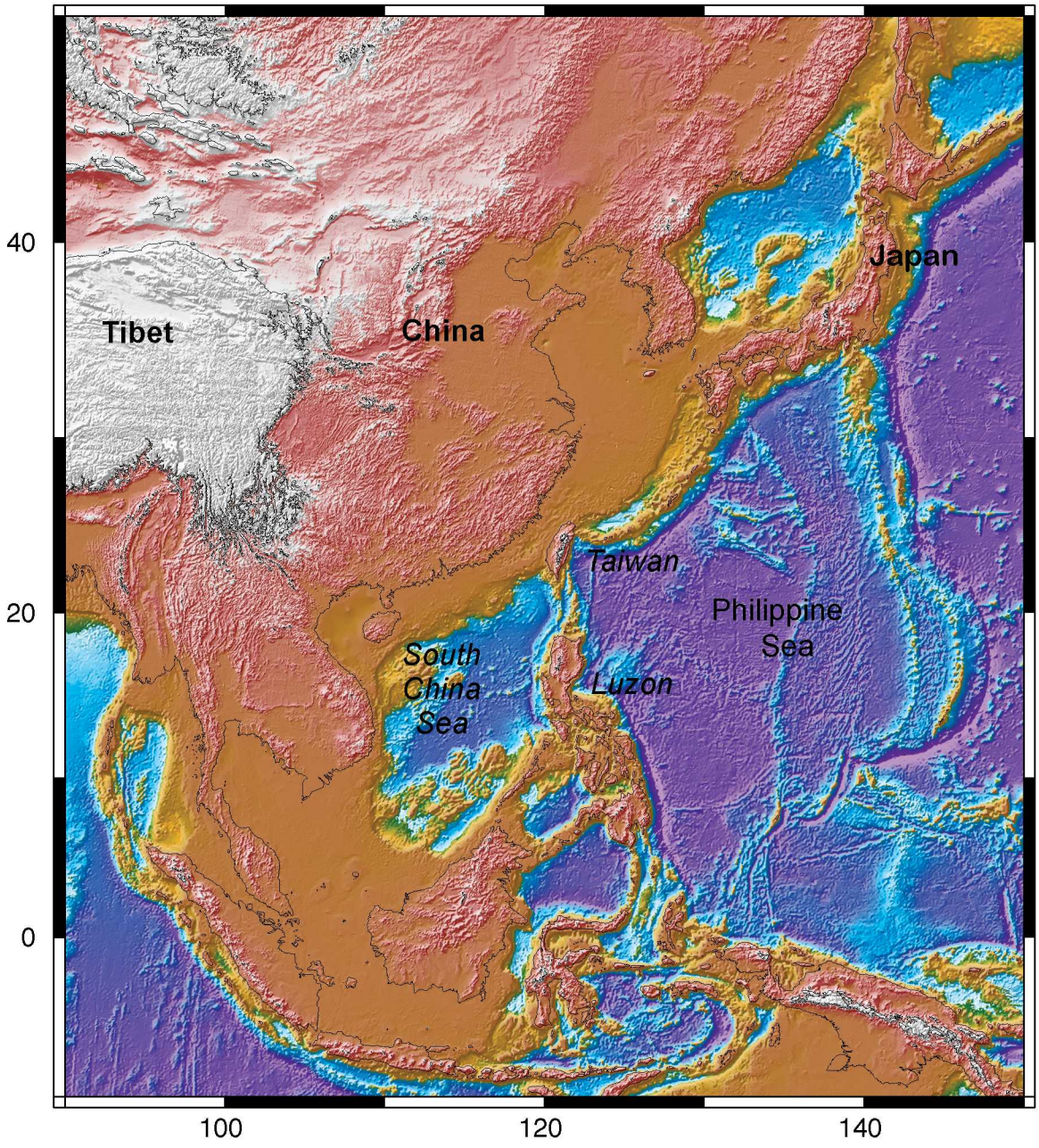

Figure 1 Topography, bathymetry, and coastlines of Southeast Asia. Etopo5 data from National Geophysical Data Center was used to create bathymetry.

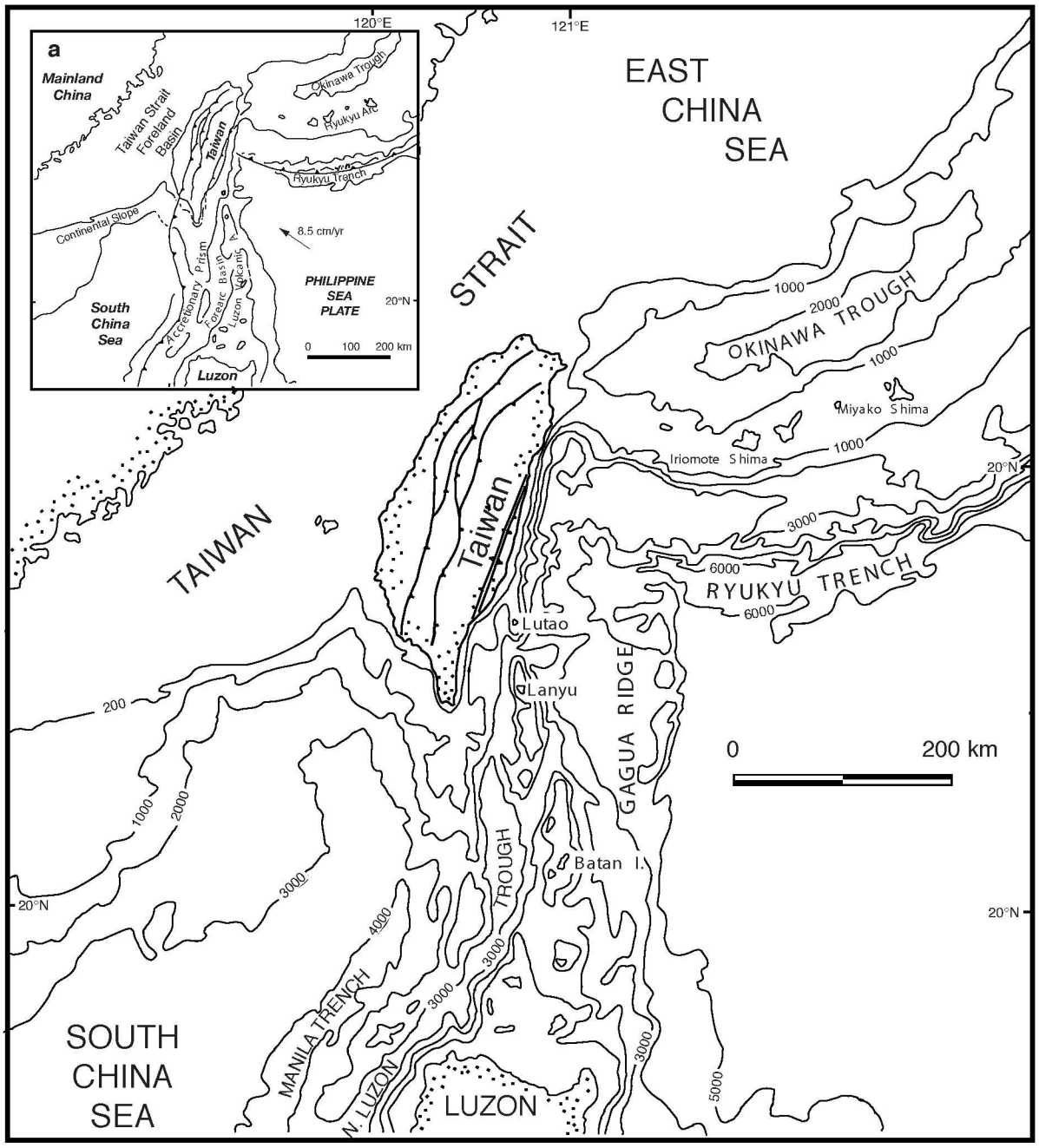

Figure 2. Tectonic map of Taiwan (modified after Lundberg and Dorsey, 1988)

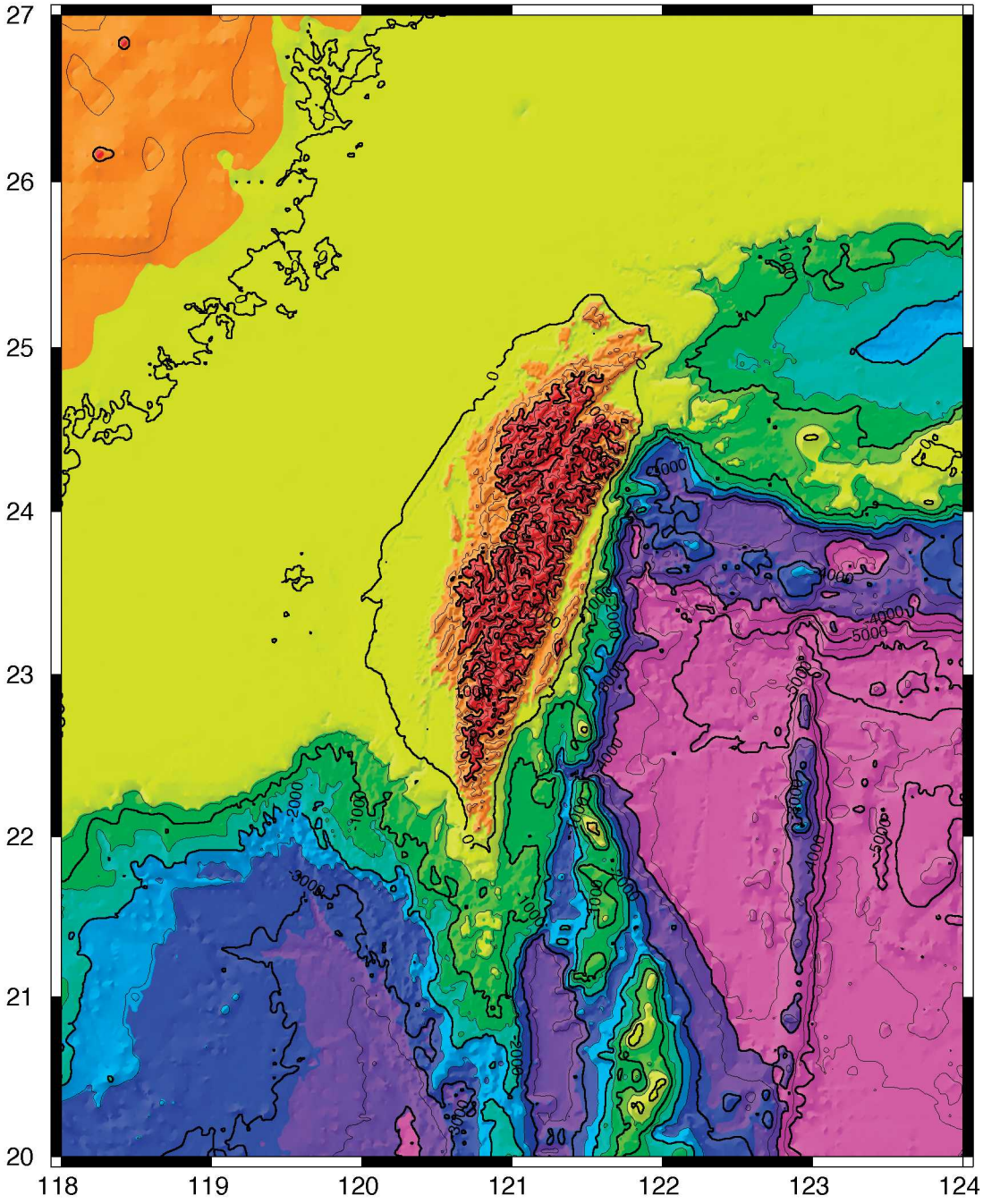

Figure 3. Topography of Taiwan and bathymetry of surrounding area. Etopo5 data from NGDC was used to create bathymetry. See Figure 4 for color explanation.

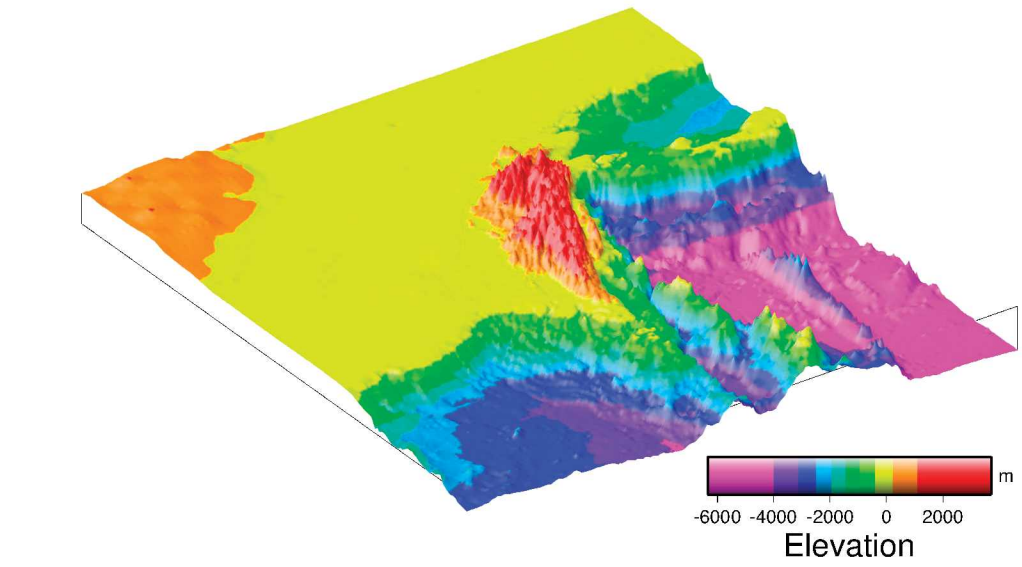

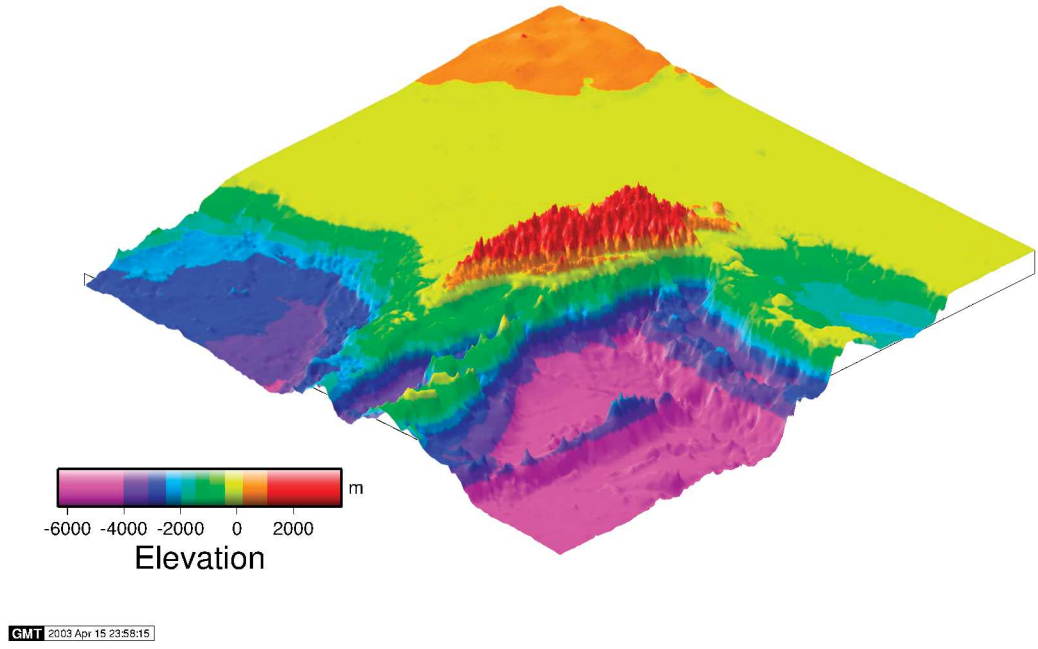

Figure 4. Three-dimensional views of topography of Taiwan and bathymetry of the surrounding area. Etopo5 bathymetric data from NGDC was used. The upper diagram is viewed from 225° of azimuth, and the bottom one from 135°.

dozer" model used successfully to explain most of Taiwan, in a modern analog widely used as a textbook example for arc-continent collision. Although there have been many previous studies of the geology of the Hengchun Peninsula, they mainly concentrate on the origin of the Kenting Formation (and its relationship to the Lichi Mélange of the Coastal Range, which has been interpreted as a sheared sediment sequence from deep within the forearc basin), or sedimentary environments of the Miocene clastic sequences, or local stratigraphy.

The Geology of Taiwan and its Southern Offshore

Taiwan is made up of four major north-south trending geologic provinces (Figure 5). From west to east, these are the western coastal plain, the western Taiwan foreland basin, the Central Ranges, and the Coastal Range. The western Taiwan foreland basin consists of Plio-Pleistocene orogenic deposits that overlie older Tertiary sequences of the passive Chinese continental margin. Along the eastern portion of the foreland basin, strata of both the upper collision-derived sequences and the underlying passive-margin deposits have been tectonically incorporated into the westward-advancing fold-and-thrust belt, forming the western foothills of the Taiwan mountain belt (Ho, 1982). Farther to the east, the western portion of the Central Ranges exposes low-grade metamorphosed Tertiary deposits (the Slate Formation), and the eastern flank of the Central Ranges exposes metamorphic complexes of the Yuli and Tailuko Belts, which include pre-Tertiary rocks (Figure 5). The rocks of the Central Ranges are complexly deformed and represent the northern extension of the accretionary wedge that lies east (arcward) of the Manila trench (Suppe, 1984). The easternmost geologic belt of the island of Taiwan is the Coastal Range, a narrow strip of volcanic and sedimentary rocks representing the accreted island-arc terrane and its cover sequence. Miocene volcanic rocks of the Tuluanshan Formation comprise basal flows and a plutonic complex covered by thick agglomerates and tuffs. This basement unit is overlain by Plio-Pleistocene sedimentary rocks of the Takangko Formation, deposited in a collisional basin that formed in a setting analogous to that of the forearc basin, similar to the present-day North Luzon Trough to the south. Separating the Central Range from the Coastal Range is a remarkably linear, NNE-trending valley, the Longitudinal Valley, which is generally taken to represent the modern onland suture zone between deformed rocks of the Chinese continental margin and the accreted Luzon arc (Ho, 1982; Lundberg and Dorsey, 1988; Huang et al., 1992a).

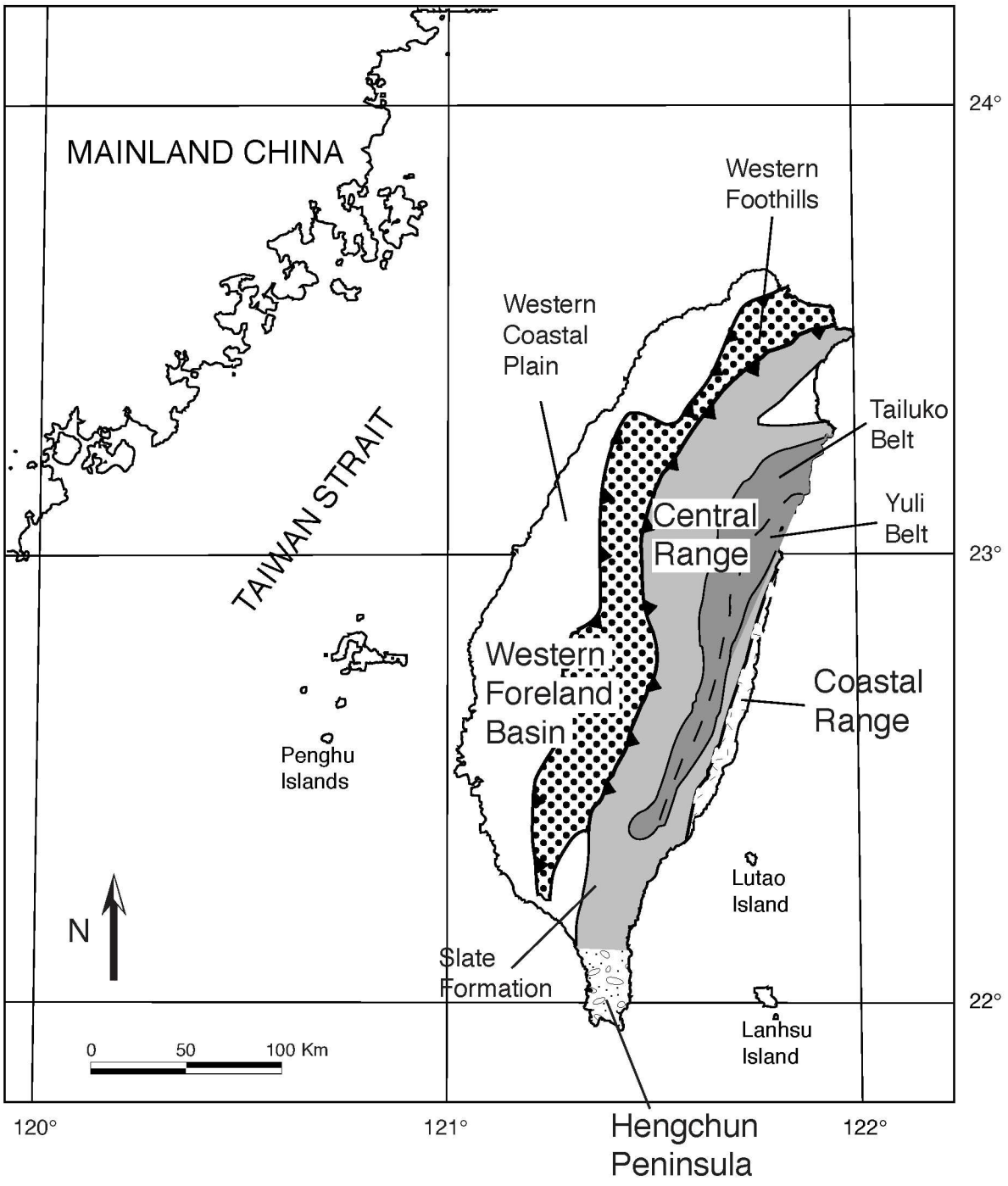

Figure 5. Major geologic provinces of Taiwan (modified after Lundberg and Dorsey, 1988).

There are many factors used to describe a collisional orogen. The orogeny can be expressed in four dimensions of length, width, height (depth), and time in a static state, or the change of length, width, and height in a more dynamic state. The first four factors describe the volume of an orogen at any given time and the latter three describe the rates of changes of volumetric components. The convergence rate of the two colliding plates is a fundamental factor that affects all aspects of the orogeny. The density of both plates and the relative portion of low-density materials on both plates will determine how the two plates interact with each other and with the mantle. The buoyancy of these converging materials becomes important in controlling the developing size and actual processes operating during collision and subduction. The coupled effect between erosion and tectonic uplift is currently a subject of great interest. In active collisional regions, the convergence rate controls the fundamental parameter of how much crustal material will be involved in the collisional process at any given time. The materials that are brought together along the convergent boundary then have to compete in density. The crustal material and the cover sequences undergo the process of subduction and collision with different "particle" paths (Beaumont et al., 1992). Those materials that do not subduct into the mantle will accumulate in the accretionary complex. The accretionary wedge will grow in a self-similar fashion (with similar aspect ratio but different in scale; Suppe, 1981; Dahlen and Suppe, 1988). The isostatic response of the mantle and the flexural response of the lithosphere will have negative effects on the growth of the accretionary prism. Nevertheless the size of the accretionary prism will typically grow as long as convergence is taking place, yet as the orogen grows, the newly built mountains are subject to increased erosion. The erosion removes material from the surface of the mountain belt and reduces the pressure within the accretionary prism. This in turn enhances the ability of the accretionary wedge to grow. The feedback mechanism is pronounced between erosion and uplift rates. Depending on the rate of convergence, angle of subduction, thickness of the cover sequence, and erosion rate, the growth rate of an accretionary prism and the paths taken by different particles will be different and will result in different unroofing patterns.

Many of these rates have been topics of active study in Taiwan by many researchers. The Philippine Sea plate is converging with Eurasia at 70 (Seno et al., 1993) to 86 mm/yr (Yu et al., 1997). Uplift of about 5 mm/yr has been established in several areas of Taiwan by many workers using different approaches to measure uplift over a spectrum of time scales. Radiocarbon dating of uplifted corals in eastern, southeastern, and western coastal areas as summarized by Peng et al. (1977) shows consistent uplift at 5.0± 0.7 mm/yr over the past 9 ka. Work on corals by Wang et al. (1989), integrating U-series and radiocarbon

dating with resurveying, suggests that Holocene uplift has been faster in eastern coastal areas (at 4 to 7 mm/yr) than in southernmost Taiwan (2 to 3 mm/yr). Lundberg and Dorsey (1990) obtained an average uplift rate of 7.5 and 5.9 mm/yr over the past 1 m.y. from a thick sequence of orogenic strata exposed in the Coastal Range, representing relative maxima in uplift in that region. Fission-track dating in the Central Range has yielded high cooling rates for the late Quaternary (Liu, 1982) and a denudation rate of 2.5 to 4.6 mm/yr that is equivalent to a cooling rate of 120°C/m.y. for the past 4 M.y. (Liu et al., 2000), rates that Barr and Dahlen (1990) have shown to be consistent with a denudation rate of 5.5 mm/yr (Li, 1976), on the basis of heat-flow constraints and thermal modeling of the mountain belt. In addition, unroofing rates of 4 to 5 mm/yr have been calculated by Dorsey (1988) for the ancestral Central Range of Taiwan during the Pliocene to earliest Pleistocene, on the basis of the first appearance (1.4 Ma) of orogenic detritus derived from biotite-grade rocks that were metamorphosed at 425±75°C and 4kbar (Ernst, 1983) during the ongoing collision. Repeated geodetic surveys from 1984 to 1987 by Liu and Yu (1990) reveal that the Coastal Range is being uplifted with respect to the Longitudinal Valley at a rate of about 30 mm/yr, although this rate is only found in a very confined region. They also concluded that the coast of eastern Taiwan is undergoing uplift at a rate ranging from 0 to 35 mm/yr. Liew and Lin (1987) used ^{14}C dating of coral fragments on marine terraces in Hengchun Peninsula and reported a Holocene uplift rate of 4.6 mm/yr east of Kenting.

In the region between Taiwan and Luzon, oceanic crust of the South China Sea subducts eastward beneath the Philippine Sea plate along the Manila trench. The active Luzon arc is colliding with the passive Chinese continental margin at an angle of 50°. Here, the andesitic Batan Islands represent active volcanoes of the Luzon arc. To the north, where the downgoing plate is made up of the Asian continent, subduction gives way to arc-continent collision at Taiwan (Biq, 1972; Suppe, 1988). The northern islands of the Luzon arc are Lanhsu and Lutao Islands. These two volcanic islands experienced eruptions most recently 1.4 m.y. and 0.5 m.y. ago, respectively (Yang et al., 1995). Further north, accreted arc rocks form the basement of the Coastal Range of easternmost Taiwan, with ages ranging from 8 to 16 Ma in the northern end of accreted arc and around 1.5 Ma in the southern end (Yang et al., 1995). The eastern boundary of the submarine accretionary prism south of Taiwan is marked by a steep, nearly linear scarp, approximately 2 km high, trending nearly north-south along 121°E. The western boundary of the accretionary prism is the Manila trench, in the south, and the northern extension of the associated western deformation front, which bulges westward at about the latitude of the southern tip of Taiwan (Figure 2, 3). Immediately

east of the accretionary prism and south of about 21°20' is the North Luzon Trough, a well-defined forearc basin. This deep (about 3500 m), narrow basin is closed structurally to the north at about 21°20' and dips gently to the south toward Luzon.

The Luzon arc initially collided with the Asian continental margin in the late Neogene (Chi et al., 1981; Teng, 1990) and has propagated southward. Seismic reflection profiles south of Taiwan show that the bulk of the submarine accretionary prism is west-verging, as the fold-and-thrust belt is onshore on Taiwan, but the steep rearward slope of the accretionary prism is dominated by east-verging structures. The forearc basin is being closed by thrusting of the accretionary prism over arc basement between north of 21°20' and Taiwan (Lieske et al., 1992; Lundberg et al., 1992; Reed et al., 1992; Lundberg et al., 1997). The area north of 21°N just southeast of the Hengchun Peninsula, where incipient arc-continent collision is taking place, comprises three geological regions. From west to east they are: the South Longitudinal Trough, which projects northward to the Longitudinal Valley of eastern Taiwan; the Huatung Ridge; and the northern extension of the Luzon arc; the latter two, separated by the Taitung Trough, project northward to the Coastal Range.

Geology of the Hengchun Peninsula

The Hengchun Peninsula, as previously described, represents the most recently emergent segment of the Taiwan arc-continent collision system. It is generally considered to be distinctly different from the strata exposed north of the peninsula and is bounded by the Fengkang Fault in most mapping studies. There have been many attempts to address the complexities of the stratigraphy of the Hengchun Peninsula (Ho, 1982; Chen et al., 1985; Chen et al., 1986; Mueller et al., 1986; Pelletier et al., 1986; Stephan et al., 1986; Sung, 1990; Chen, 1992); however, no general consensus has been reached on which stratigraphic system to adopt. Here we adopt the system proposed by Sung (1990, Figure 7) for it is one of the latest and most defensible systems, and a useful geological map has been published by the Geological Survey of Taiwan based on this scheme (Figure 6). The oldest sequence exposed on the peninsula is the early Miocene Chouchow Formation (Figure 7). Structurally overlying the Chouchow Formation is the Mutan Formation, which spans from the middle Miocene to the top of the Miocene. There are four distinct members within the Mutan Formation; they are the Shihmen, Loshui, Shihtzutou, and Lilongshan members. These four members are easily identifiable in the field in their type areas along the east and west coasts of the Hengchun Peninsula. They seem to lose their identities further inland, however,

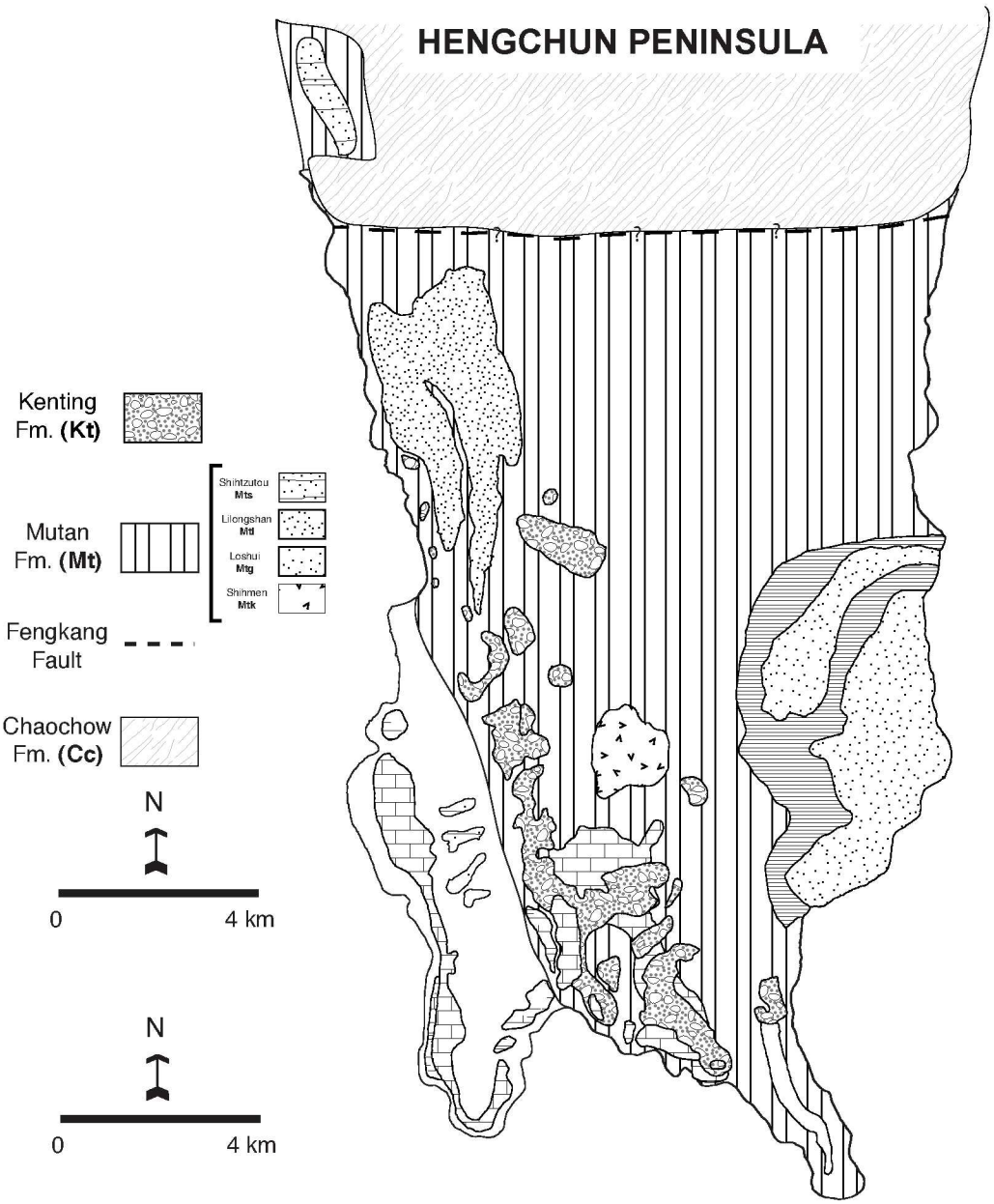

Figure 6. General geology of the Hengchun Peninsula (After Sung 1991).

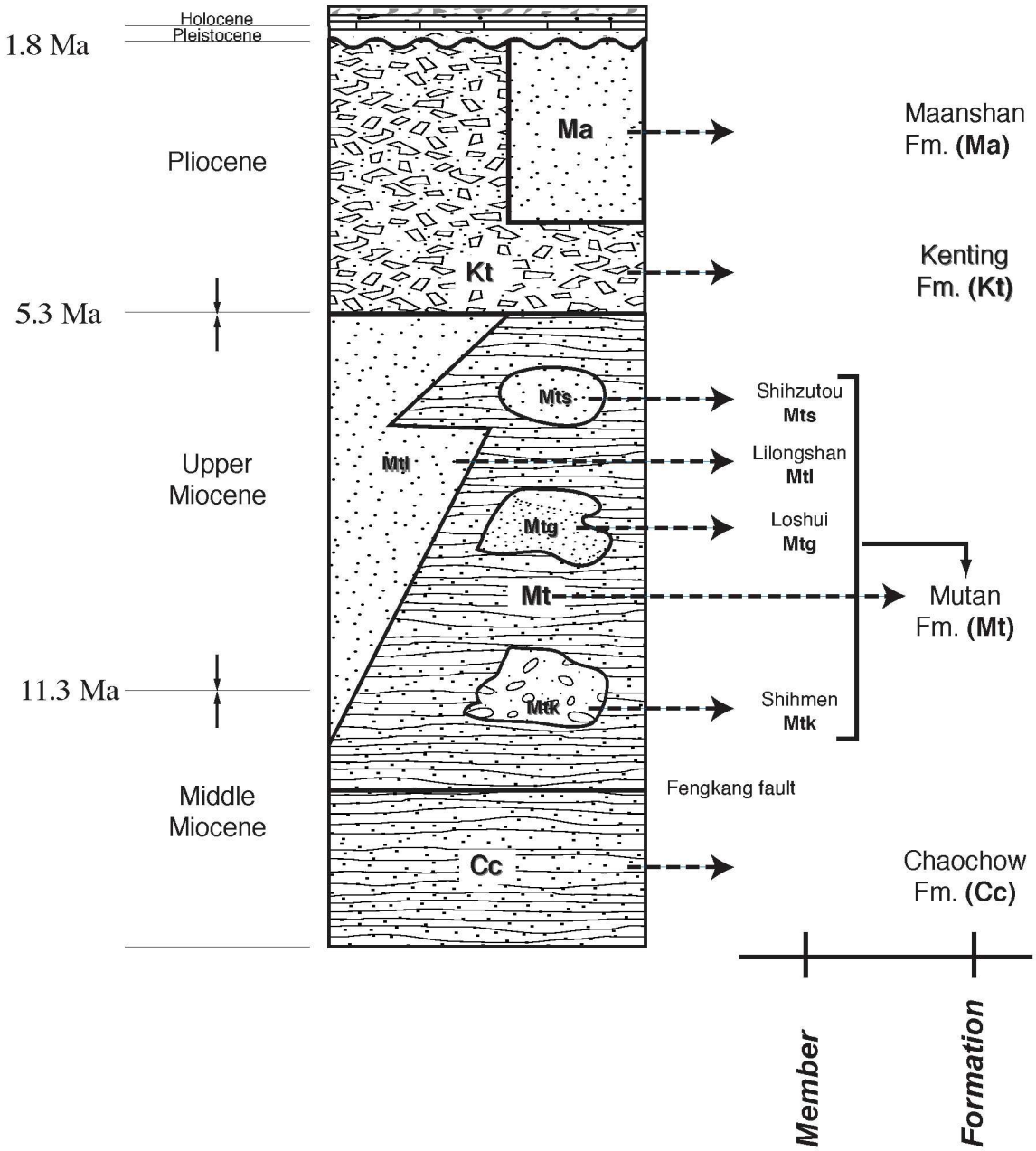

Figure 7. Stratigraphic column of Hengchun Peninsula (After Sung 1991).

creating confusion among researchers who have studied the area. The Kenting Formation structurally overlies the Mutan Formation along a thrust fault and is considered as mélange turned olistostrome (Page and Suppe, 1981; Page and Lan, 1983; Ho, 1984; Sung, 1991; Chen and 1991; Chen, 1992; Chung and Sun, 1992; Byrne, 1996; Byrne, 1998; Chang et al., 2000). Numerous blocks of different lithology ranging in size from millimeters to a kilometer are embedded in a mudstone matrix. Some parts of the mudstone matrix in the Kenting Formation have been highly sheared, yet in other outcrops there is no sign of structural disturbance.

Problems to be Addressed

The depositional environments and structural development of the sedimentary sequences in the Hengchun Peninsula have been studied extensively (Cheng et al., 1984; Ho, 1984; Chen et al., 1985; Chen et al., 1986; Mueller et al., 1986; Pelletier et al., 1986; Stephan et al., 1986; Suppe, 1988; Chen, 1992; Huang et al., 1992b; Huang et al., 1997; Chang et al., 2003;). The sequence is interpreted as a deep-sea fan system that may or may not be tied to the geological development of proto-Taiwan that existed at the time just north of this sedimentary basin (Chen et al., 1984). A long-standing controversy regards the interpretation of paleocurrent data from the Hengchun Peninsula. Many studies have cited paleocurrent indicators in the sandstones in the area (Cheng et al., 1984; Chen et al., 1985; Sung and Wang, 1985; Sung and Wang, 1986; Sung, 1990; Chang et al., 2003;), the results of which are intriguing (Figure 9). Sediment of the Mutan Formation, including all members but one, shows a SSE paleocurrent direction, whereas the Loshui member of the Mutan Formation exhibits a NNW paleocurrent direction. Because the paleocurrent directions are opposed, with no sign of gradual change, the Loshui unit has either been rotated about 180°, or the sediments must have come from a different source, southeast of its current location. Although most workers prefer the former hypothesis, a rotation of a geologic terrane by 180°, though not impossible, is not common. The latter hypothesis demands a source terrane southeast of the Hengchun sedimentary basin. A detailed examination of the area from the bathymetry map produced by Liu (1998) yields no obvious terrain in the area. This creates an "Atlantis problem," in which a landmass is missing yet left a trace. Another important aspect of the sedimentary sequence, the provenance, has largely been ignored in the previous studies. Suppe (1988) speculates that parts of the defunct spreading center of the South China Sea reached as far northeast as east of the present Taiwan island. It is also possible that a piece of rifted terrane caught in the Philippine Sea Plate provided the necessary

sediment source. The main question in this dissertation is therefore: how did the various Miocene stratigraphic elements of the Hengchun Peninsula form, come together, and then rise to form the leading tip of the Taiwan arc-continent collision system?

The arc-continent collision in Taiwan began at about 12Ma (Teng, 1990) to 5Ma (Dorsey, 1988), roughly equivalent to the age of most of the Miocene sedimentary units in Hengchun Peninsula. Therefore the Hengchun Peninsula preserves a record of deposition immediately before and during the initiation of the Taiwan orogeny. The contemporaneous nature of the deposition of the Hengchun strata and the span of the Taiwan collision make this sequence a valuable record of the history of the Taiwan collision.

To address the questions posed, I have used several disciplinary approaches to analyze the provenance and history of the Miocene strata of the Hengchun Peninsula. This dissertation comprises several chapters, each devoted to a disciplinary approach, as follows:

Chapter 2: Mapping, stratigraphy, and field relationships

Chapter 3: Modal analysis of sandstones

Chapter 4: Fission-track analysis of detrital zircons

Chapter 5: Neotectonics and morphotectonics

CHAPTER TWO
MAPPING, STRATIGRAPHY, AND FIELD RELATIONSHIPS

Mapping Issues

Many researchers have worked on the stratigraphic sequences in the Hengchun Peninsula, since early last century. The local stratigraphy was established by important surveying efforts by Tsan (1974), who also defined the Kenting Formation, interpreting it as an olistostromal unit produced by the convergence between the Philippine Sea plate and Eurasia plate. Biostratigraphy was largely established based on nannofossils by Chi (1982). Mueller et al. (1986) determined the age of ophiolitic blocks in the Hengchun Peninsula, and Pelletier and Stephan (Pelletier et al., 1986; Pelletier and Stephan, 1986; Stephan et al., 1986) determined that volcanic blocks within the Kenting Formation are about 12 to 20 Ma by potassium-argon dating.

Miocene sequences of sandstones and shales constitute the main body of the Hengchun Peninsula. Definition of the local stratigraphy and the geographic extent of each unit are still controversial and remain subjects of debate (Chen et al., 1985; Sung and Wang, 1985; Sung, 1990; Chen, 1992;). Most researchers agree, however, upon the distinct compositional nature of most of the geological units exposed on the Hengchun Peninsula. In this project, I initially adopted the stratigraphic system (Figure 7) and geologic map (Figure 8) of Sung (1991) published by the Central Geological Survey of Taiwan. The stratigraphy can be summarized, from oldest to youngest as: Chouchow Formation; Mutan Formation, including four named members of coarse-grained deposits (Shihmen, Shihtzutou, Loshui, and Lilongshan, roughly in order from oldest to youngest) embedded in it. Structurally overlying the Mutan Formation is the Kenting Formation of Pliocene to Pleistocene age, generally interpreted as a mélange or olistostrome (Tsan, 1974; Page and Lan, 1983; Ho, 1984; Chen, 1992).

A major problem in geological mapping in the Hengchun Peninsula is that although it is easy to identify the four named members of the Mutan Formation in their type localities (on or near the west and east coasts of the peninsula), it can be very difficult to identify to which group any given outcrop belongs in the large central region of the peninsula. The differences between units become less distinct in the central part of the peninsula. Therefore, many of the boundaries drawn on the geological map should be thought of as inferred; many workers have chosen to represent geological boundaries as dashed lines. A second major issue is whether or not the Fengkang fault really exists, much less represents a major boundary.

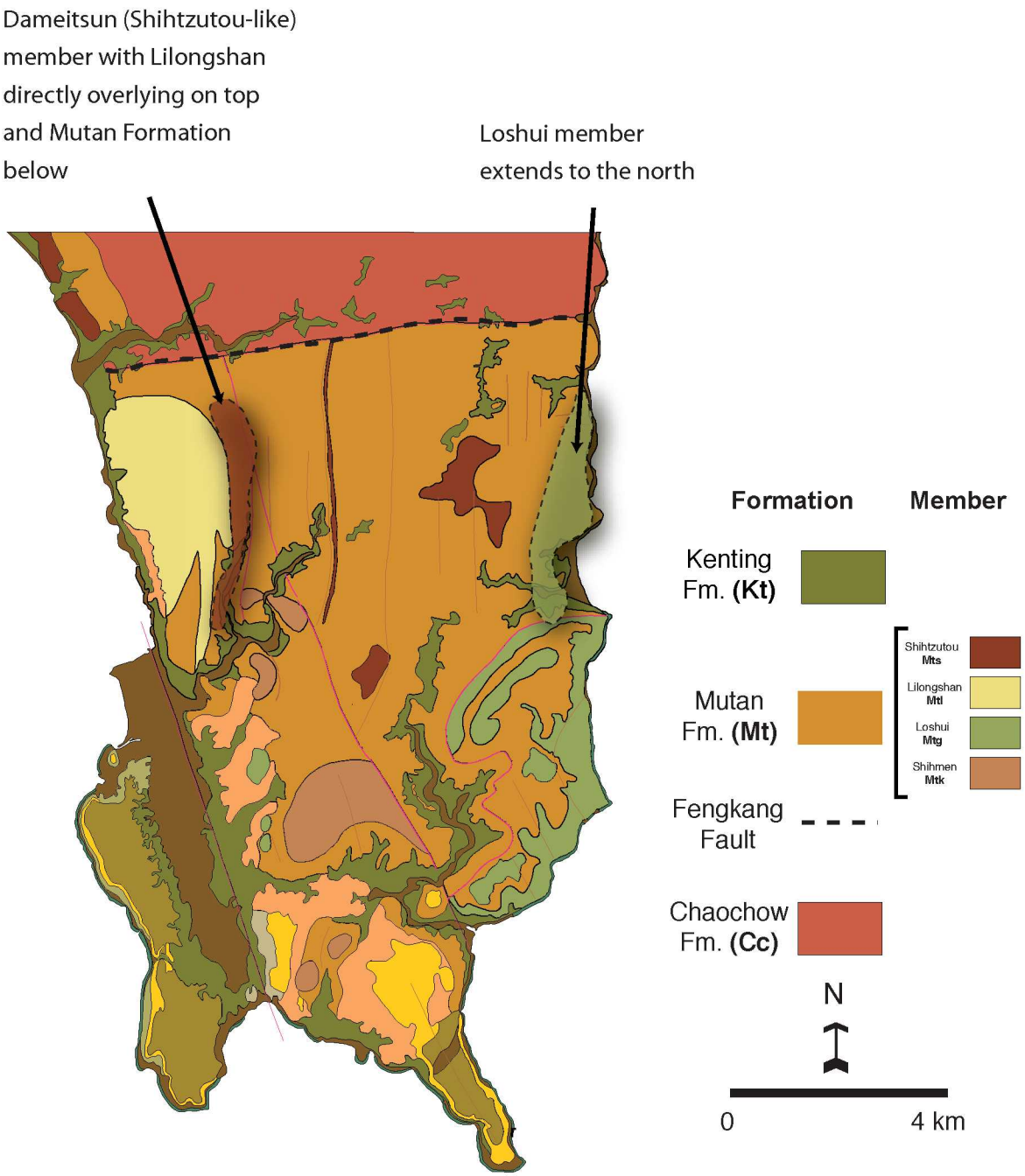

Figure 8. Geologic map of Hengchun Peninsula. Arrows indicate the areas in which stratigraphic units were previously misidentified. (After Sung 1991).

This fault marks the northern boundary of the Hengchun Peninsula, separating the main body of the Mutan Formation in the Hengchun Peninsula from rocks to the north, consisting mainly of the Chaochou Formation. This fault largely follows a major valley, and is not well exposed. Some researchers do not think the existence of the fault is necessary (Lin, 2003, personal communication).

The most controversial points are the origin of the Mutan Formation and its various coarse-grained members. Most models that have been proposed for the origin of the Mutan interpret these sedimentary sequences to represent deep-sea fan deposits of several different fan systems (Chen et al., 1985; Sung and Wang, 1985; Sung and Wang, 1986). In general, these members are believed to be independent from each other, because most of them are separated from each other by faults (for example: the Fengkang fault separates the Lilongshan and Shihtzutou units; a thrust fault has been mapped independently by several researchers between Loshui sandstones and the Mutan Formation). There is no coherent model to explain how these separate deep-sea units have been brought together to the same area, and where their sources were, respectively, if their origins are independent.

Paleoflow Direction

Many researchers have noted paleocurrent indicators in the sandstones in the area (Cheng et al., 1984; Chen et al., 1985; Sung and Wang, 1985; Sung and Wang, 1986; Sung, 1990; Chang et al., 2003). The results of paleocurrent are intriguing (Figure 9). The majority of the Miocene sequence in Hengchun Peninsula (i.e., the main body of the Mutan Formation) shows a south-southeast paleocurrent direction, whereas paleocurrents in the Loshui Member of the Mutan Formation are dominated by the north-northwest direction. (Most of the paleocurrent measurements were obtained from sole marks, with fewer measurements from ripple marks in turbidites). To have two paleocurrent directions as contradictory as are these two populations, without any sign of a gradual change in the paleocurrent direction, is striking. Either the Loshui unit was rotated significantly during emplacement, or sediments of the Loshui unit came from a source to the south and/or east of its current location, contrary to the rest of the Mutan Formation. The former hypothesis, which most workers have preferred, requires a rotation of nearly 180° of one stratigraphic unit. Although this is theoretically possible, it is not common. The latter hypothesis, however, requires a source terrane southeast of the Hengchun sedimentary basin.

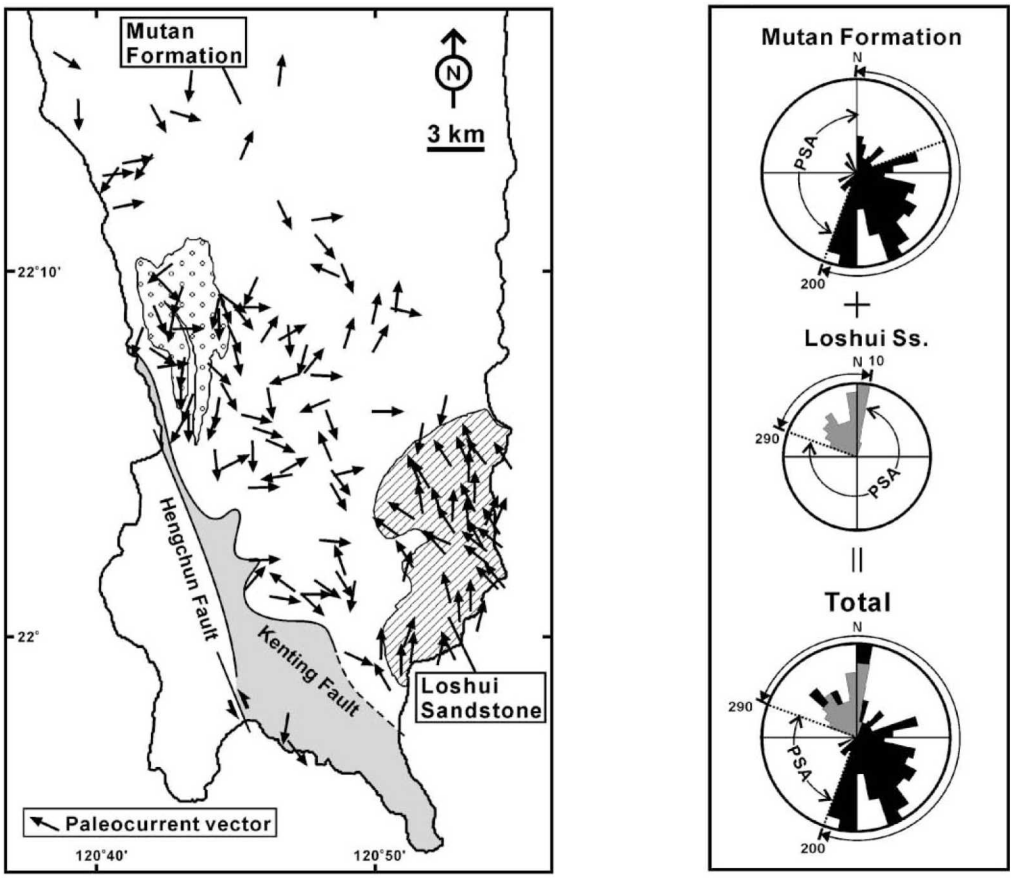

Figure 9. Paleoflow directions in Hengchun Peninsula (Chang et al. 2002). The paleocurrent directions of the Loshui unit differ markedly from those of all the other units.

New Findings

Two new observations made during field mapping for this project have major implications for the understanding of the structure and stratigraphy of the Hengchun Peninsula. One of these new observations concerns a newly recognized exposure of the Shihtzutou-like unit, and the other concerns the extent of the exposure of the Loshui unit. The Shihtzutou-like unit is easily identifiable in the field by the inclusion of locally abundant pebbles of sedimentary rock types (siltstone, argillite, and chert, plus vein quartz) and occasional large (several cm across) fragments of oyster shell in the sandstones. Contrary to the results of previous mapping, the Shihtzutou-like unit was recognized during this project to outcrop north of Dameitsun, south of the Fengkang fault and immediately east of the Lilongshan unit (Figure 8). I here name this the Dameitsun member of Mutan Formation. Previous mapping had shown the Shihtzutou lithology to outcrop mainly (1) immediately north of the Fengkang fault, along the west coast of Taiwan and (2) south of the Fengkang fault, as two isolated exposures that form hills (Ssulinkoshan and Mutanchihshan), and as a thin stratal layer extending south from the Fengkang fault over 10 km toward the center of the Hengchun Peninsula. In all these exposures, the Shihtzutou lithology is seen in contact only with the "background" strata of the Mutan Formation (not with other coarse-grained members). Along the thin stratal layer exposed in the central part of the Hengchun Peninsula, the Shihtzutou unit is stratigraphically underlain and overlain by "background" strata of the Mutan Formation.

The newly discovered exposure of the Dameitsun member is stratigraphically underlain by "background" Mutan Formation, but it is overlain by the Lilongshan unit, with no sign of a fault between the two members. This exposure of the Dameitsun unit follows along the eastern boundary of the only exposure of the Lilongshan unit, from the northern extent of the latter to nearly its southernmost extent. The Dameitsun unit in this exposure is relatively thin, probably less than 200 m. This is the first report of a depositional contact between any two of the four named members of the Mutan Formation. It is clear that in at least one locality, the Dameitsun unit lies stratigraphically between older "background" strata of the Mutan Formation and younger strata of the Lilongshan unit. Just north of the Fengkang fault, the Shihtzutou unit is overlain depositionally by "background" strata of the Mutan Formation, although because the units are both overturned, the Shihtzutou overlies the background Mutan beds structurally.

On the east side of the Hengchun Peninsula, the Loshui unit is readily identifiable in the field, with sandstone beds considerably thicker and more abundant than in the background strata of the Mutan Formation, but without the conglomerate horizons that are common in the Shihtzutou, Shihmen, and Lilongshan units. In some layers, shale rip-up clasts ranging in size from mm's to 10's of cm across can be found. The Loshui unit is also characterized by distinctive sedimentary structures, with common sole marks, such as flute casts, groove casts, and loading features, and paleocurrent direction indicators show flow overwhelmingly toward the northwest. Field results previous to this study have mapped the Loshui unit of the Mutan Formation on the east side of the Hengchun Peninsula, north of Chialeshui and south of Chiupengtsun village. The Loshui unit is bounded to the west by the Manchou fault, generally identified as a low-angle thrust fault (Cheng et al., 1984; Chen et al., 1985; Sung and Wang, 1985). However, during the current investigation, the Loshui unit was mapped considerably further north of the previously known outcrop, reaching to Hsuhaitsun village on the eastern coast of the Hengchun Peninsula, just south of the Fengkang fault. Here in the north, the newly discovered exposure of the Loshui unit extends westward from the east coast as far as about 5 km to Mutantsun village, where the "background" Mutan Formation appears rather abruptly. The "background" Mutan Formation is on top of the Loshui unit, with a possible fault contact in between. The exact width of the exposure of the Loshui unit and the nature of the contact with background Mutan strata were not directly observed in the field.

Implications

The discovery of the Dameitsun (Shihtzutou-like) unit south of the Fengkang fault and depositionally below the Lilongshan unit paves a way to reconciling the difficulty in correlating the stratigraphy between the areas north and south of the Fengkang fault.

The Loshui unit extends much farther north than indicated in the map published by the Central Geological Survey of Taiwan, although the exposure narrows in its northernmost extent. The southern part of the Loshui exposure has been mapped as bounded by the Manchou fault, and seems to comprise stratigraphic intercalations of Loshui strata with background strata of the Mutan Formation. The bedding orientations measured are complex, especially in the northern region that had not previously been mapped as Loshui. The structures inferred from the attitudes measured suggest east-west trending fold axis within the Loshui unit. Although it is certainly possible that a small amount of rotation about a vertical axis has affected this unit, the elongate, narrow outline of the exposure of the Loshui unit, particularly including its newly recognized northern extension, make it extremely unlikely

that it has been rotated 180° (Cheng et al., 1984; Sung and Wang, 1985; Sung and Wang, 1986; Sung, 1990; Chang et al., 2003) while being transported along a thrust fault.

The Dameitsun unit is clearly depositionally overlain by strata of the Lilongshan unit, in addition to outcrops in several other localities on the Hengchun Peninsula. In particular, rocks similar to the Shihtzutou unit must have been deposited at two distinct times during basin development. This indicates that the named stratigraphic members of the Mutan Formation are not all depositionally independent from each other, and it suggests that these units were probably not distant and unrelated, concurrent sedimentary systems that were later brought together by structural means. A more likely scenario is that the named members of the Mutan Formation each represent a specific type of coarse sediment influx to a basin, likely diluting the normal "background" sedimentation that produced the main body of the Mutan Formation. The coarse-grained members are restricted in time and space, but may recur or alternate temporally rather than simply being stacked structurally one on top of another.

From the stratigraphic columns (Sung, 1991), the Shihtzutou and Lilongshan units are both as young as about 5 Ma (NN16 for the Shihtzutou unit, and NN15 to NN17 for the Lilongshan unit), but the Lilongshan also extends relatively far back, almost as old as the oldest strata of the Mutan Formation (Sung, 1990). Along the northwest coast of the Hengchun Peninsula, the Lilongshan unit strikes north-south and dips toward the west, younging westward. Hence, the discovery of the Shihtzutou unit depositionally beneath the Lilongshan unit creates a problem, in that this Shihtzutou unit must be older than the entire Lilongshan unit must. The only way this is possible would be that the newly discovered Shihtzutou unit is actually older than the oldest strata of the Lilongshan unit, and should be properly named as a new member. This newly defined Dameitsun member is likely derived from the same source as the Shihtzutou unit. Other outcrops of the Shihtzutou unit may belong to a younger sequence.

There may be recurring changes of alternate source areas in a rather small sedimentary basin. This suggests the possibility of several small deep-sea fans or fan lobes, co-mingling or in part coalescing to fill a basin. So the different units may represent deposition at somewhat different times, with different source areas, in slightly different areas within the basin. Some of the source areas might have experienced recurring tectonic rejuvenation, producing repetitive depositional units of distinctive lithologies.

CHAPTER THREE
MODAL ANALYSIS OF MIOCENE SANDSTONES

Sandstones from Miocene sequences of Hengchun Peninsula are generally in the size of fine sand to very fine sand with some exceptions in which large pebbles are embedded in the sandstones, and they are rather altered in many outcrops. Sandstones are generally coarser on the east and west sides of the Peninsula and finer in the central region. Angularity of grains in sandstones varies from unit to unit but most sandstones are sub-angular to sub-rounded. The amount of matrix also varies between units but is generally not very high.

Thin sections were stained for feldspars, preserving half of each section unetched for detailed textural studies and for improved lithic identification. Samples were point-counted using the Gazzi-Dickinson convention (Dickinson, 1970) in order to minimize effects of grain-size variation on sand composition (Ingersoll et al., 1984). At least 300 grains were counted in each sample. Table 1 presents the classification of grain types used in this research. Conventions for grain recognition followed those of Dickinson (1970), Graham et al. (1976), Ingersoll and Suczek (1979), and Dorsey (1988). Data collected by Sung and Wang (1985) were combined to perform further statistics. Modal sand compositions were plotted on standard ternary diagrams (QtFL and others) in order to evaluate the nature of sediment source terranes.

Further statistical analyses were performed to obtain the insight of the relationships among the samples, stratigraphy, and source terranes. In order to classify the samples to their natural groupings, cluster analysis was performed, and discriminant function analysis was used to verify the natural grouping of samples and the stratigraphic sequences. Lastly, principal component analysis was performed to trace the possible dispersal paths of the sediments.

Petrology

Except for samples from the Shihmen unit, most of the sandstones studied are generally rich in quartz, and they are generally low in feldspar and lack higher-grade metamorphic lithic fragments (Lm_2; Dorsey, 1988). This is in sharp contrast to the modern offshore sediments (Yen, 1998) and sedimentary rocks in the Coastal Range of eastern Taiwan (Dorsey, 1988; Lundberg and Dorsey, 1988). This indicates that the sedimentary basin of the Hengchun Peninsula did not have an unroofing terrane that was actively eroding higher-grade

Table 1. Recalculated sandstone modal parameters used in this study.

---

1. Primary parameters (after Graham et al., 1976; Dickinson and Suczek, 1979)

Qt = Qm + Qp, where
- Qt = total quartzose grains
- Qm = monocrystalline quartzose grains
- Qp = polycrystalline quartz grains, including chert grains

F = P + K, where
- F = total feldspar grains
- P= plagioclase feldspar grains
- K= potassium feldspar grains

L = Ls + Lv + Lm = Lsm + Lvm = Lt - Qp, where
- Ls = sedimentary lithic fragments, mostly mudstones and shales
- Lv = volcanic lithic fragments
- Lm = metamorphic lithic fragments
- Lsm = sedimentary and metasedimentary lithic gragments
- Lvm = volcanic, hypabyssal, metavolcanic lithic fragments
- Lt = total aphanitic lithic fragments

2. Secondary parameters (after Dickinson, 1970)
P/F = plagioclase / total feldspar grains
Lv/L = volcanic / lithic fragments

---

metamorphic rocks. Grain shapes vary between contrasting grain types. Shale fragments are more elongated and sub-rounded. Quartz, feldspar and volcanic lithic fragments are more angular. Alteration is moderate and usually affects heavy minerals but is not significant in other grains. (Figure 10-13)

Petrographic Data

QtFL plot(Figure 14): Sandstones from the Shihmen member plot close to the lithic fragment pole and their mean plots within field of "magmatic arc" provenance (Dickinson, 1985). Sandstones from the Lilongshan member plot closer to the Q-L line than other samples, and their mean plots within the field of "Type 3" sandstones defined by Teng (Teng, 1979), which resemble lithic arenite. Samples from the other three units cluster together in field of "recycled orogen" although Shihtzutou and Loshui means are clearly inside the field and the meaen of the Mutan sandstones is closer to the border of the field.

QmFLt plot (Figure 15): Most of the samples plot in a very concentrated region in this ternary diagram, off the central region toward the lithic fragment pole. The mean composition of Shihmen sandstones falls in the field of "magmatic arc" provenance and close to the field of Type 1 sandstones defined by Teng (Teng, 1979), which is volcanic-rich sandstone. The mean detrital mode of sandstones from the Lilongshan unit is on the border between "recycled orogen" and "magmatic arc" fields. All the other group means plot in the field of "magmatic arc" provenance.

QpLvmLsm plot (Figure 16): These components serve to discriminate the various Miocene units of the Hengchun Peninsula. Samples cluster well in stratal units. Shihmen sandstones plot close to the Lvm pole and their mean plots close to the field of "mixed magmatic arc and rifted continental margins" provenance, in this case implicating the influence of a mafic igneous body close by at the time of deposition. The other four groups of samples have low volcanic lithic content, and plot near the Qp/Lsm join. The samples of individual groups cluster together quite well, as can be seen in Figure 16. From Qp pole to Lsm pole, they are Shihtzutou, Loshui, Mutan, and Lilongshan. Shihtzutou and Loshui sandstones, which are located on opposite sides of the peninsula, have higher affinity to each other than to geographically neighboring units.

LsLvLm plot (Figure 17): Shihmen sandstones plot toward the Lv pole, away from other units. Most samples contain a considerable amount of slightly metamorphic grains,

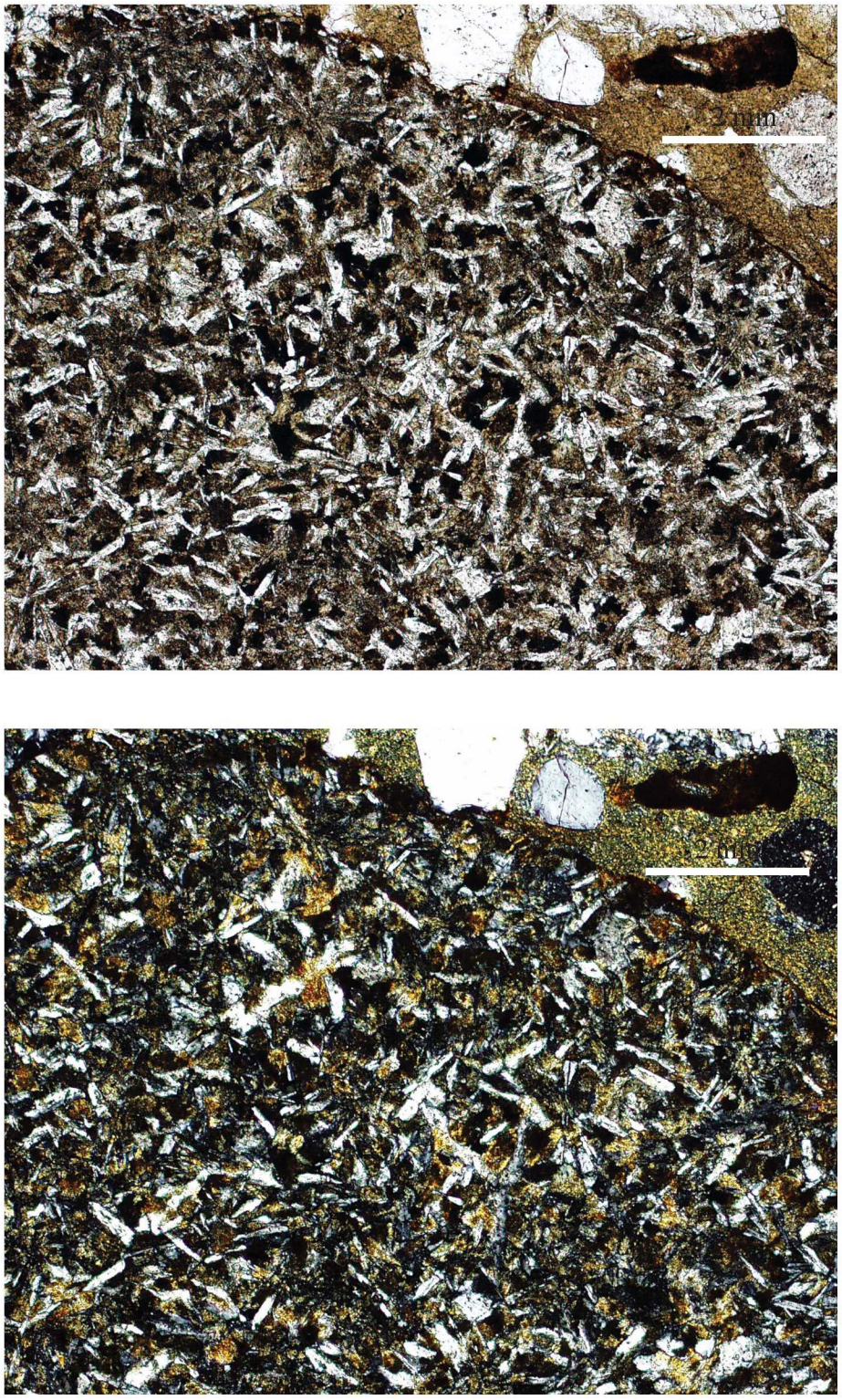

Figure 10. Photomicrographs of petrographic thin section of Shihmen sandstone with plane-polarized light (upper) and cross-polarized light (lower). Sample from Shihmen unit.

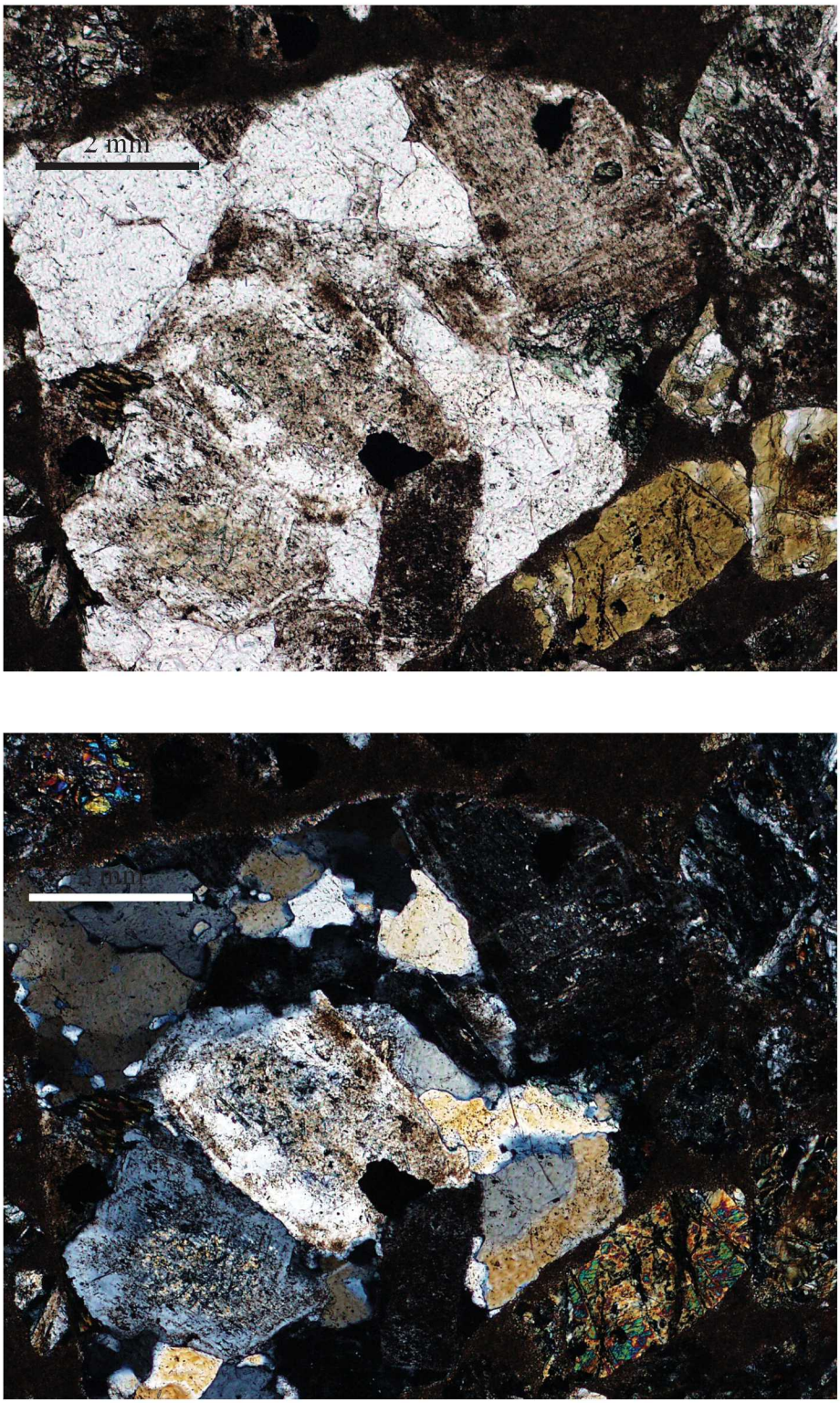

Figure 11. Photomicrographs of petrographic thin section of Shihtzutou sandstone with plane-polarized light (upper) and cross-polarized light (lower).

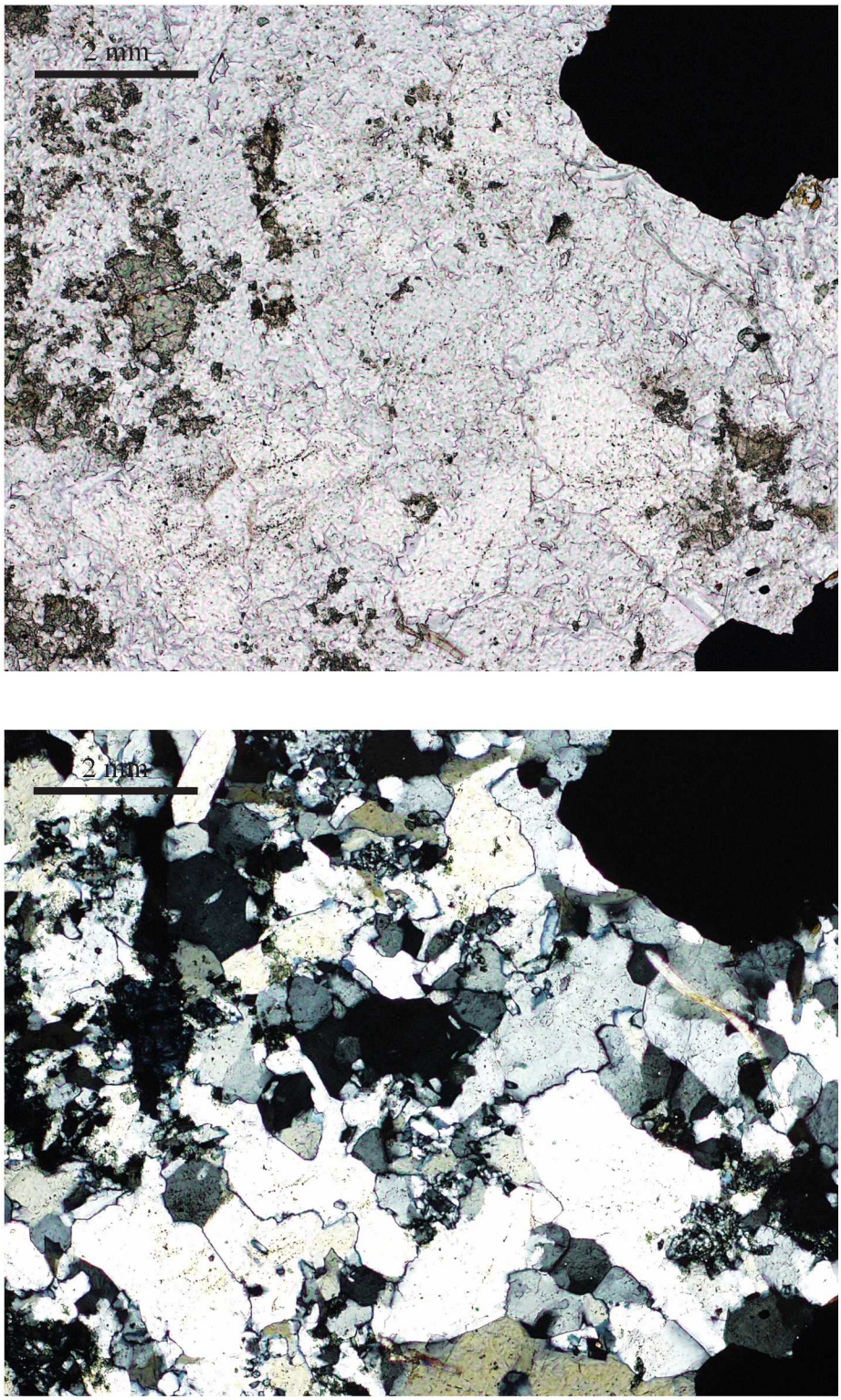

Figure 12. Photomicrographs of petrographic thin section of Shihtzutou sandstone with plane-polarized light (upper) and cross-polarized light (lower).

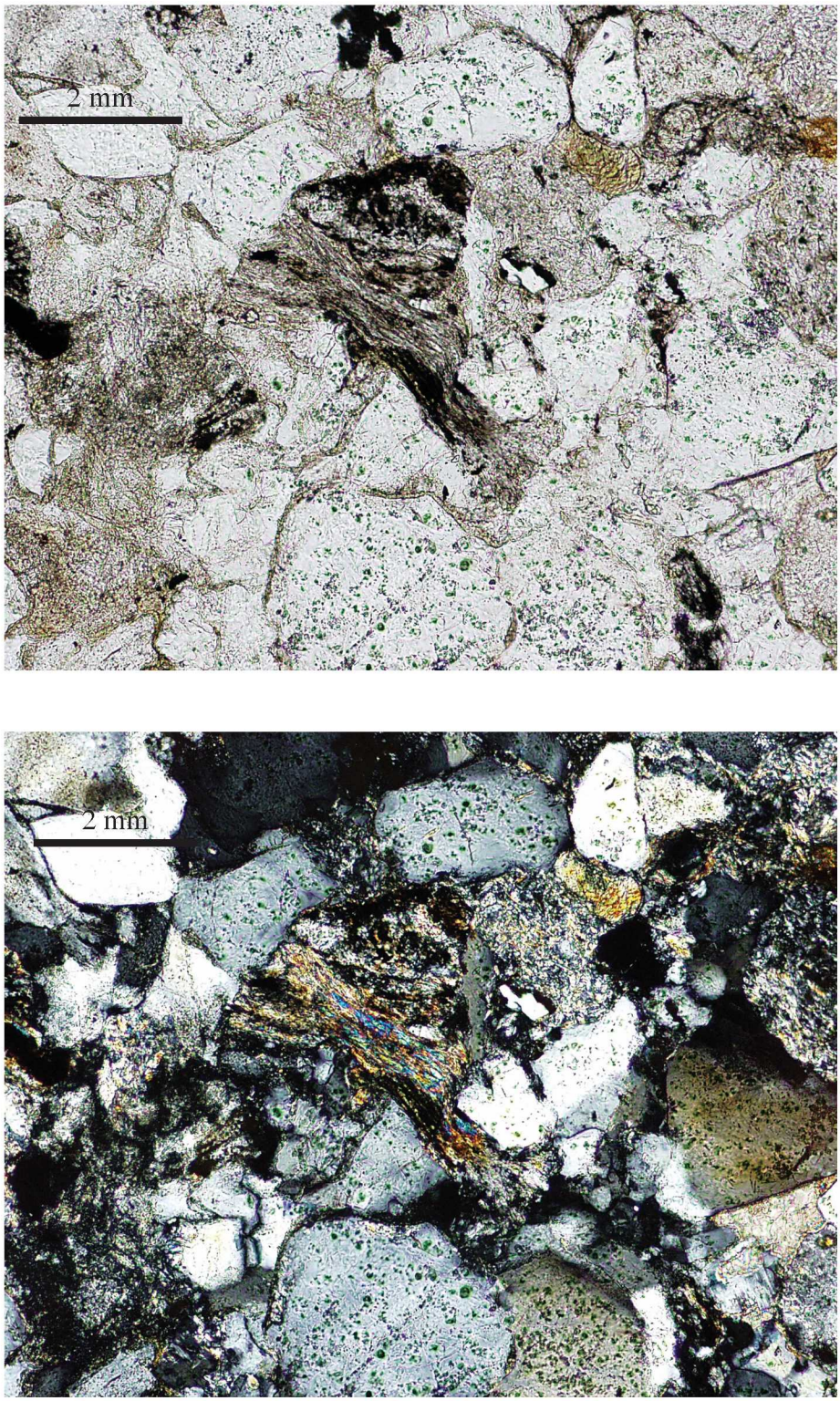

Figure 13. Photomicrographs of petrographic thin section of Loshui sandstone with plane-polarized light (upper) and cross-polarized light (lower).

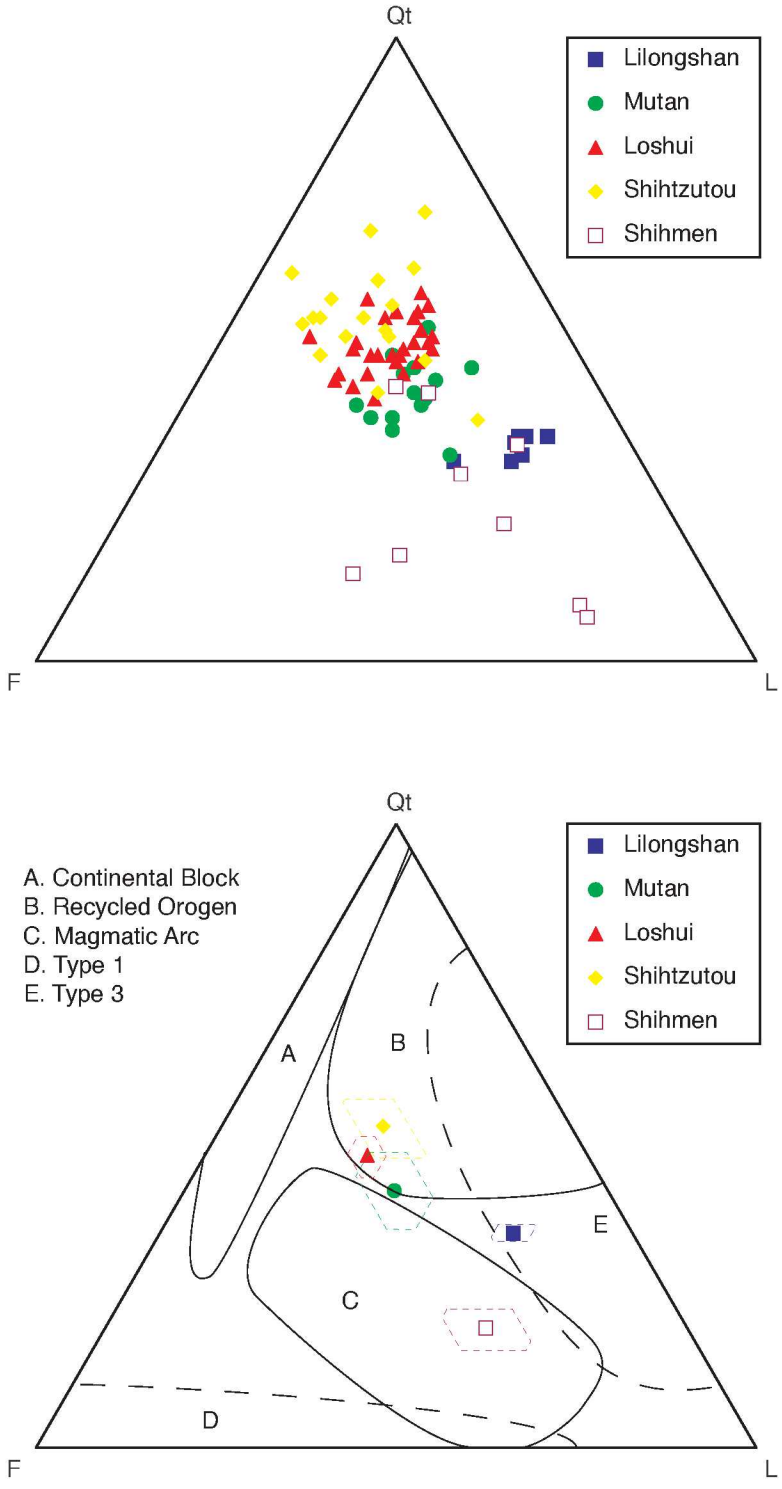

Figure 14. Q-F-L ternary diagram of Miocene sandstones from Hengchun Peninsula (Provenance fields are from Dickinson,1979, Ingersoll and Suczek,1979, and Teng, 1979.)

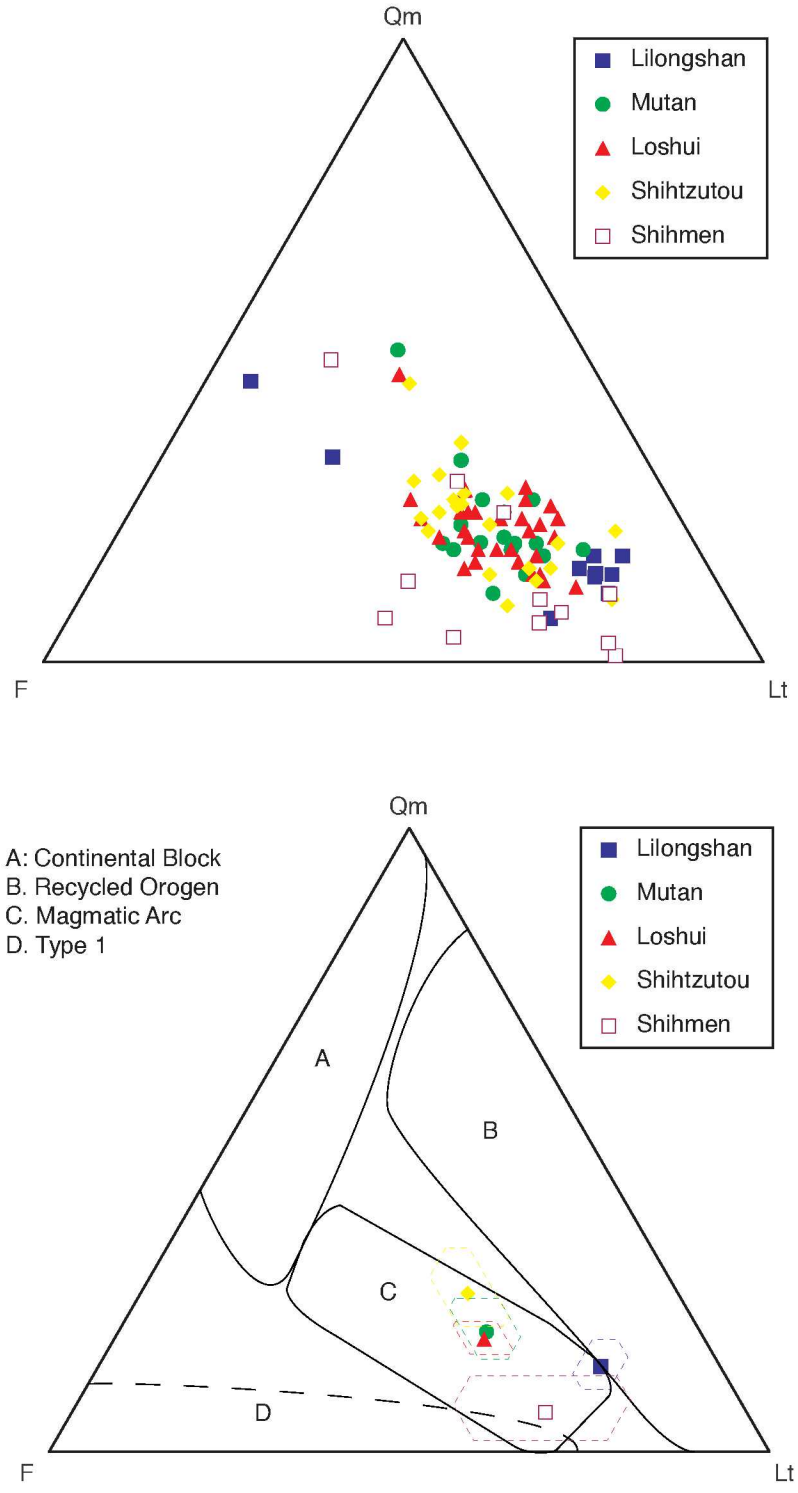

Figure 15. Qm-F-Lt ternary diagram of Miocene sandstones from Hengchun Peninsula (Provenance fields are from Dickinson,1979, Ingersoll and Suczek,1979, and Teng, 1979.)

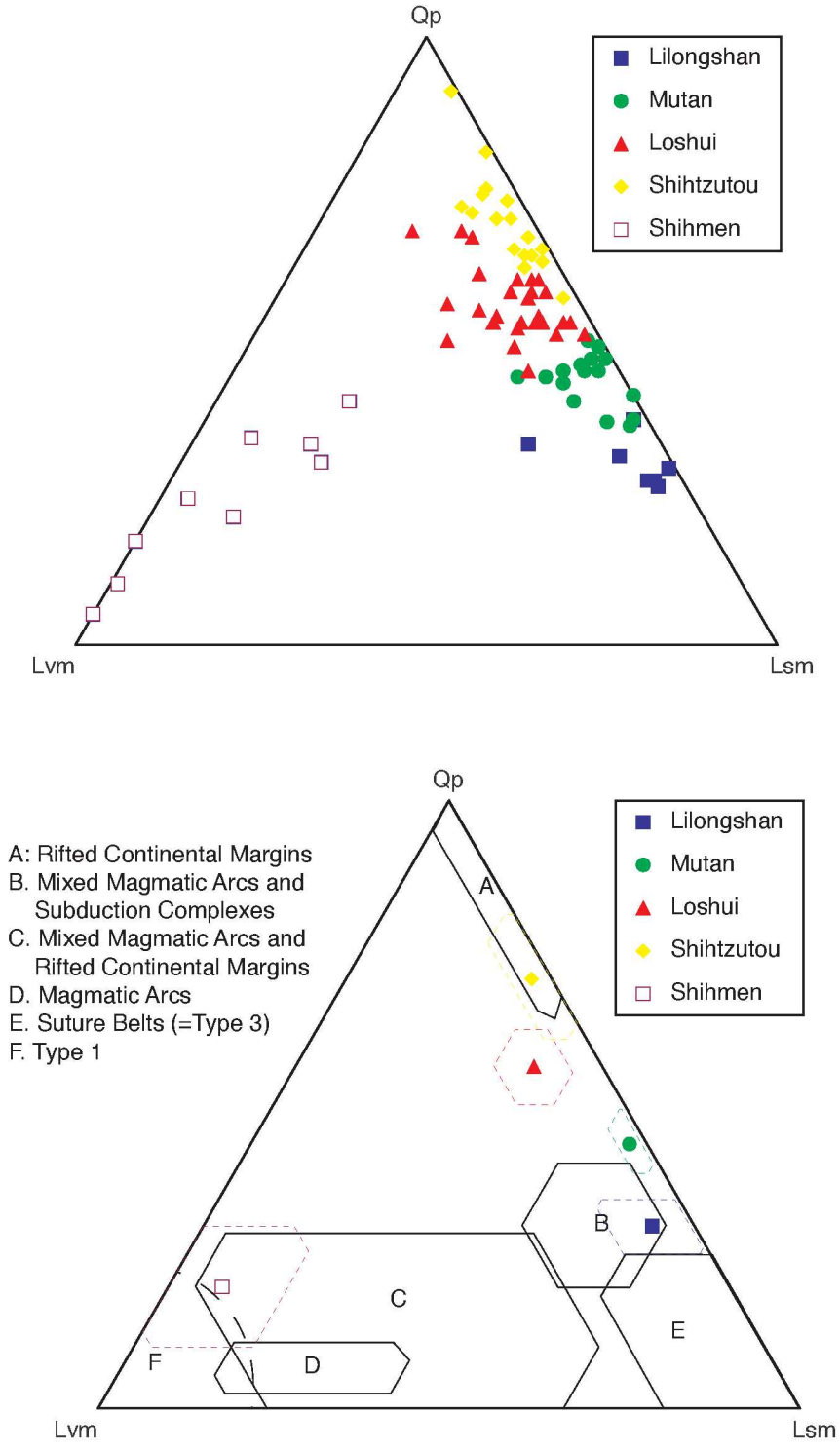

Figure 16. Qp-Lvm-Lsm ternary diagram of Miocene sandstones from Hengchun Peninsula (Provenance fields are from Dickinson,1979, Ingersoll and Suczek,1979, and Teng, 1979.)

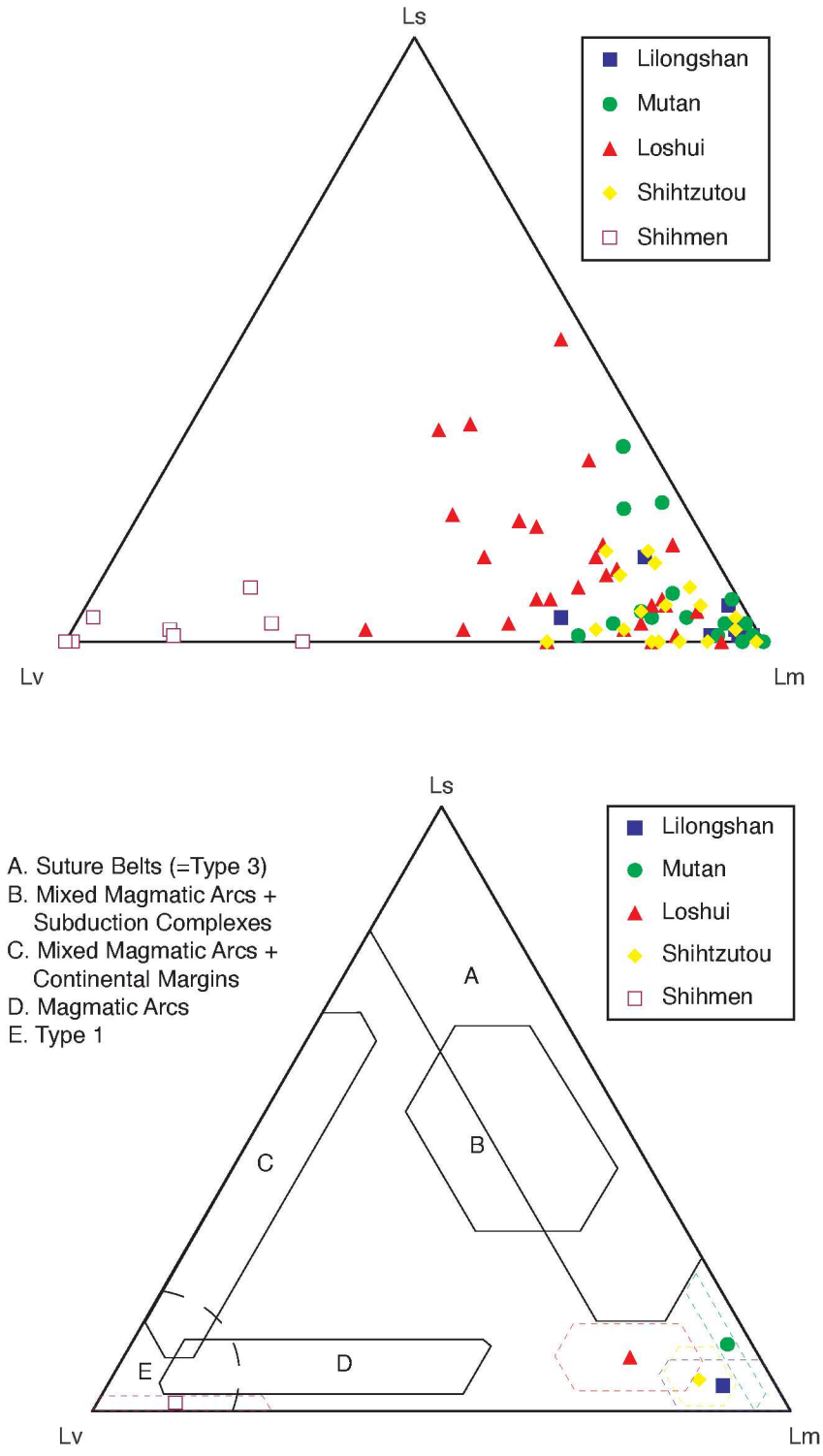

Figure 17. Ls-Lv-Lm ternary diagram of Miocene sandstones from Hengchun Peninsula (Provenance fields are from Dickinson,1979, Ingersoll and Suczek,1979, and Teng, 1979.)

which cluster them together near the Lm pole, near enough that their means all fall outside all defined provenance fields.

Summary Of Each Stratigraphic Unit

Sandstones from the Shihmen unit differ consistently from those of other units. The mean of Shihmen sandstones generally falls into the fields of magmatic-arc provenance (QtFL, QmFLt), mixed-magmatic arc and rifted-continental-margin provenance and volcaniclastic "type 1" (QpLvmLsm), and "magmatic arc" provenance and volcaniclastic "type 1" (LsLvLm). The analysis clearly indicates that Shihmen sandstones have a high affinity to "magmatic arc" provenance and may have a slight influence from "rifted continental margin" provenance.

The Lilongshan unit includes a distinctive upper layer of conglomerate and very coarse sandstones that contains abundant altered mafic material. In this analysis, however, the mean of the Lilongshan sandstones shows more affinity to lithic arenite "type 3" provenance (QtFL, Figure 14), "recycled orogen" provenance and "magmatic arc" provenance in QmFLt (Figure 15), "mixed magmatic arcs and subduction complexes" (QpLvmLsm, Figure 16). These sand are rich in sedimentary and metasedimentary lithic fragments, and do not resemble the very coarse materials that stand out in the field in the uppermost part of the Lilongshan unit.

The mean of Shihtzutou sandstones plots in the field of "rifted continental margin" provenance on a QpLvmLsm plot, but shows contradictary affinities in other plots ("magmatic arc" in a QmFLt plot, "recycled orogen" in a QtFL plot). These latter ternary plots are not capable of discriminating the sandstone compositions of this unit from most others.

The compositions of Loshui sandstones are generally very close to those of the Shihtzutou sandstones. The mean compositions of both these units fall into the "recycled orogen" field in the QtFL plot and "magmatic arc" provenance in the QmFLt plot but fall outside of all defined fields in QpLvmLsm and LsLvLm plots.

Mutan sandstones show affinity to "recycled orogen" provenance in QtFL and "magmatic arc" provenance in QmFLt plot, while plotting close to "mixed magmatic arcs and subduction complex" provenance in QpLvmLsm and to "suture belt" in LsLvLm plots.

THE FLORIDA STATE UNIVERSITY

COLLEGE OF ARTS AND SCIENCES

PROVENANCE OF MIOCENE SEDIMENTARY SEQUENCES IN HENGCHUN PENINSULA, SOUTHERN TAIWAN, AND IMPLICATIONS FOR THE MODERN TAIWAN OROGEN

BY

JIUN-YEE YEN

A Dissertation submitted to the
Department of Geological Sciences
in partial fulfillment of the
requriements for the degree of
Doctor of Philosophy

Degree Awarded:
Fall Semester, 2003

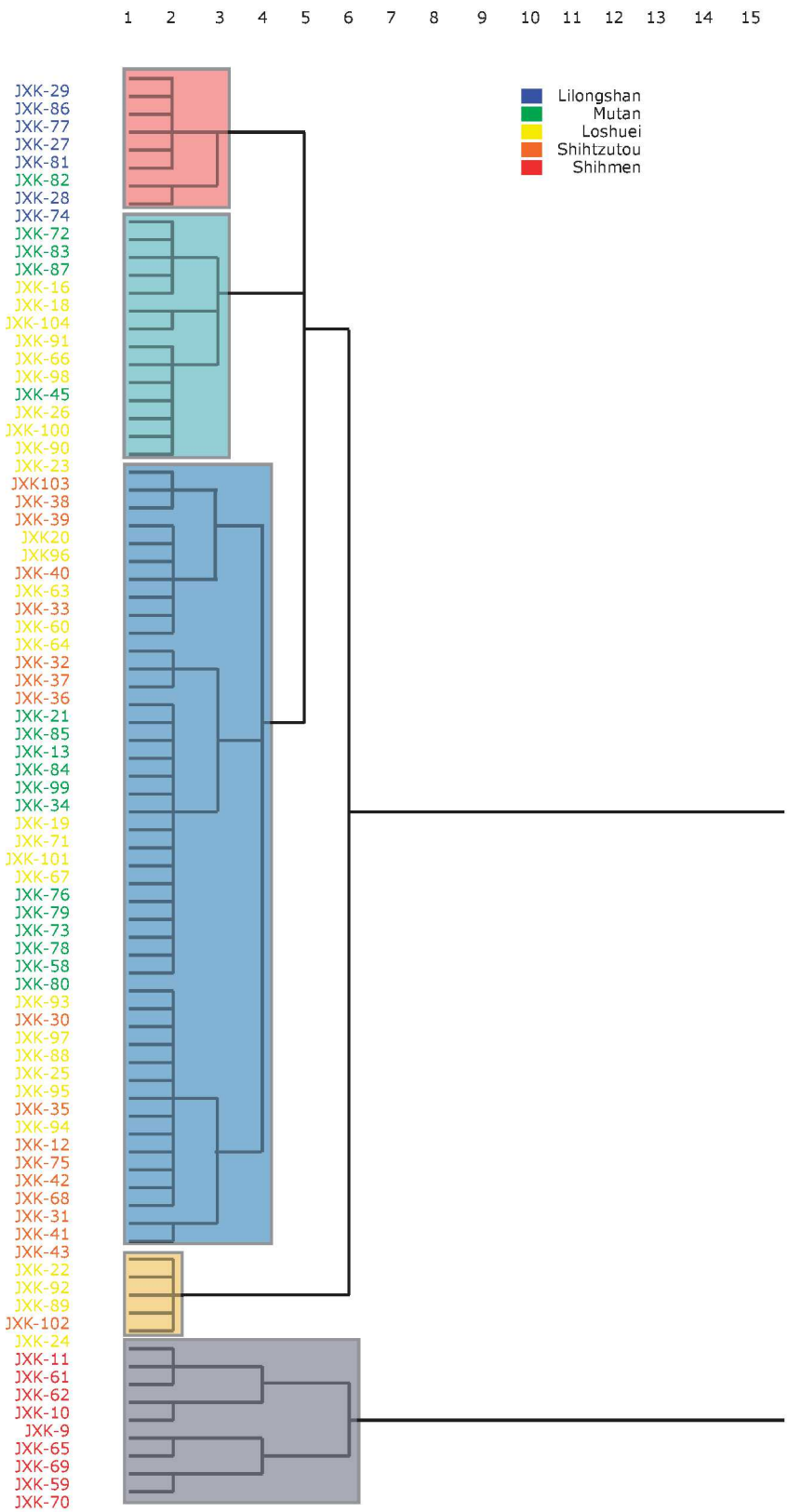

Figure 18. Dendrogram derived from cluster analysis performed on sandstone modal data.

and Loshui units, which reside on opposite sides of the peninsula, are compositionally nearly indistinguishable.

Factor Analysis

Some parameters in modal analysis may vary with other parameters. For example, the amount of volcanic lithic fragments and the amount of feldspar are often positively related. Consequently, using any single parameter to infer the sediment dispersal path will result in under-utilizing the information embedded in the modal analysis data. On the other hand, it would be tedious to plot every single parameter on a map, and many of them may not contain any meaningful information. In order to extract the maximum information from the data and to reduce the number of parameters requred, Q-mode principal component analysis was performed on the data set.

The goal of principal component analysis is to discover meaningful patterns in complex numerical data by reducing the complexity (Imbrie and van Andel, 1964). More specifically, principal component analysis is used on a set of compositional data to resolve samples into a small number of "components," each component representing an end member (a theoretically distinct sample). By applying principal component analysis to the compositional data set, we reduce the number of geological significant variables (for example, to three components or theoretical end members) and we can denote each sample in terms of the relative contributions from each end-member. A real sample can then be represented by a linear combination of components extracted. By plotting the contribution of each end member for each sample, we can evaluate significant variation patterns in a complex data set.

Q-mode principal component analysis was conducted on the results of modal analysis. Four components extracted from the dataset represent 99% of variations in the dataset and 97% of variation can be explained by using only three components. In Q-mode principal component analysis, "loading" can be regarded as the similarity of a sample to the extracted component. Higher loading means high similarity and vice versa. The extracted components can be decomposed to show their relationships to the modal analysis parameters, and the relationships between each component and the parameters are factor scores. The component loadings of the four components extracted are listed in Table 3 and factor scores are listed in Table 4.

Table 2. Canonical discriminant function coefficients and correlation between each variable.

Canonical Discriminant Function Coefficients				
	Function1	Function2	Function3	Function4
P/F	0.007	0.114	0.098	0.166
Lv/L	-0.09	-0.067	0.177	-0.058
Qp	0.131	0.199	-0.48	-0.003
Lvm	0.042	0.223	-0.245	0.051
(Constant)	-5.631	-19.138	-4.865	-10.31

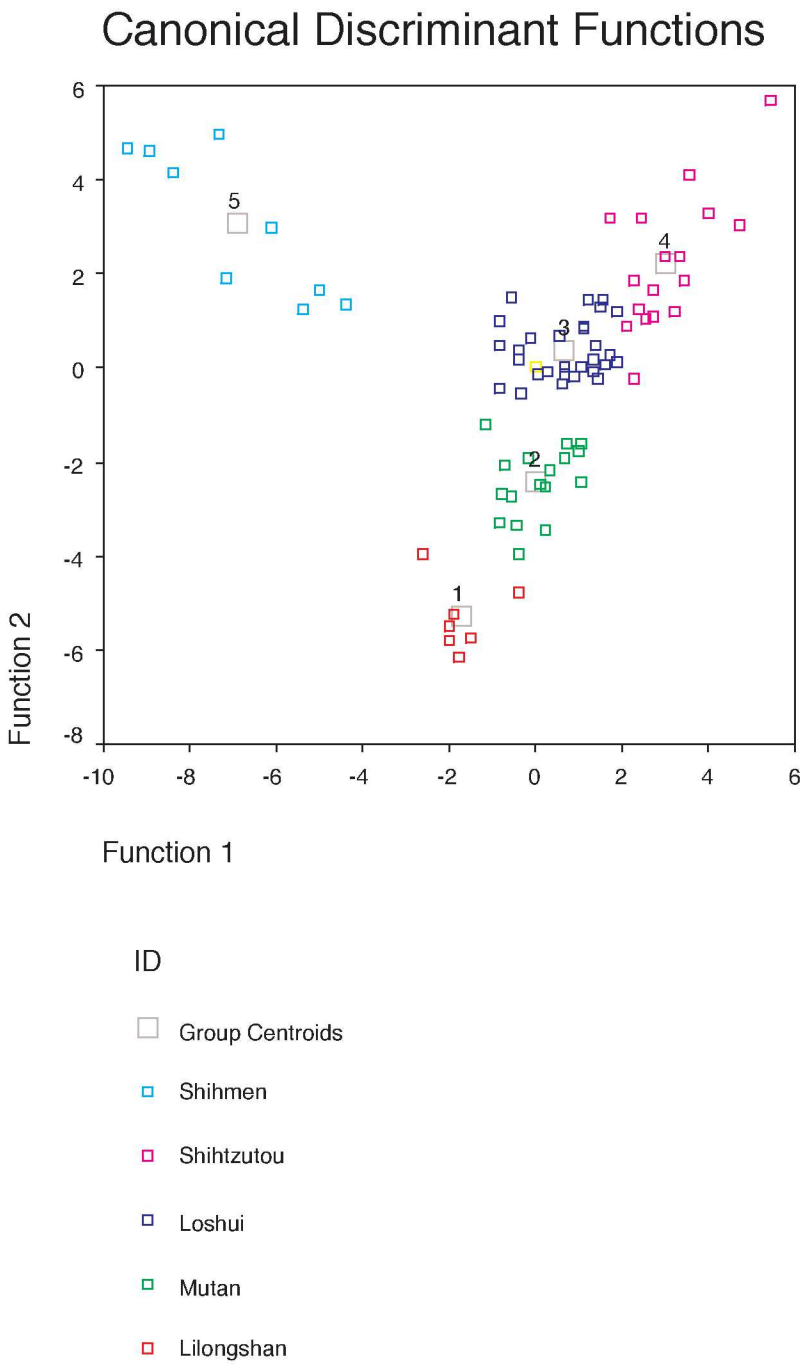

Figure 19. Distribution maps of the canonical discrimminant function evaluated for the samples taken from Hengchun Peninsula.

Table 3. Rotated component matrix. Component loading is the similarity between component and the individual sample.

Strata	sample	comp1	comp2	comp3	comp4
Lilongshan	JXK-27	0.953	0.246	-4.38E-02	0.112
Lilongshan	JXK-28	0.871	0.294	0.331	9.88E-02
Lilongshan	JXK-29	0.959	0.238	-6.75E-02	9.29E-02
Lilongshan	JXK-74	0.941	0.218	-1.45E-02	0.189
Lilongshan	JXK-77	0.945	0.256	-0.107	0.142
Lilongshan	JXK-81	0.91	0.37	-5.06E-02	7.55E-02
Lilongshan	JXK-86	0.959	0.247	-1.52E-02	0.103
Loshui	JXK-100	0.615	0.727	1.40E-02	0.292
Loshui	JXK-101	0.656	0.733	-2.50E-02	0.126
Loshui	JXK-104	0.244	0.711	9.84E-02	0.645
Loshui	JXK-16	0.472	0.496	5.34E-02	0.704
Loshui	JXK-18	0.49	0.439	-0.246	0.706
Loshui	JXK-19	0.752	0.628	-6.71E-02	0.173
Loshui	JXK-20	0.497	0.825	0.219	7.43E-02
Loshui	JXK-22	0.398	0.774	0.47	8.46E-02
Loshui	JXK-23	0.527	0.777	0.159	0.189
Loshui	JXK-24	4.39E-03	0.809	0.535	7.47E-02
Loshui	JXK-25	0.557	0.8	-3.18E-02	0.198
Loshui	JXK-26	0.657	0.716	0.108	0.208
Loshui	JXK-60	0.678	0.686	0.158	0.161
Loshui	JXK-63	0.66	0.694	5.09E-02	0.254
Loshui	JXK-64	0.596	0.624	-5.62E-02	0.456
Loshui	JXK-66	0.623	0.667	0.148	0.368
Loshui	JXK-67	0.747	0.632	2.03E-02	0.201
Loshui	JXK-71	0.748	0.644	-9.81E-02	8.65E-02
Loshui	JXK-88	0.667	0.723	-5.67E-02	4.83E-02
Loshui	JXK-89	0.138	0.968	7.88E-02	0.137
Loshui	JXK-90	0.641	0.69	-5.42E-02	0.289
Loshui	JXK-91	0.251	0.847	0.201	0.346
Loshui	JXK-92	0.534	0.734	0.396	7.24E-02
Loshui	JXK-93	0.633	0.744	-0.132	9.85E-02
Loshui	JXK-94	0.658	0.734	1.84E-02	8.17E-02
Loshui	JXK-95	0.675	0.685	-0.133	0.181

Table 3 (continued). Rotated component matrix. Component loading is the similarity between component and the individual sample.

Strata	sample	comp1	comp2	comp3	comp4
Loshui	JXK-96	0.471	0.804	0.213	0.176
Loshui	JXK-97	0.612	0.77	-0.154	7.49E-02
Loshui	JXK-98	0.607	0.654	0.172	0.406
Mutan	JXK-13	0.857	0.472	-0.176	5.81E-02
Mutan	JXK-21	0.789	0.553	-0.211	0.126
Mutan	JXK-34	0.766	0.591	-0.217	4.03E-02
Mutan	JXK-45	0.758	0.602	0.214	9.11E-02
Mutan	JXK-58	0.82	0.558	1.69E-02	0.126
Mutan	JXK-72	0.814	0.395	-0.212	0.318
Mutan	JXK-73	0.85	0.508	-1.92E-02	9.39E-02
Mutan	JXK-76	0.826	0.529	-3.18E-02	9.95E-02
Mutan	JXK-78	0.797	0.589	7.29E-02	8.31E-02
Mutan	JXK-79	0.829	0.529	-5.12E-02	0.143
Mutan	JXK-80	0.841	0.506	3.80E-02	0.13
Mutan	JXK-82	0.913	0.379	-6.97E-02	8.50E-02
Mutan	JXK-83	0.791	0.39	-0.282	0.301
Mutan	JXK-84	0.751	0.601	-0.218	3.64E-02
Mutan	JXK-85	0.798	0.574	-0.149	8.16E-02
Mutan	JXK-87	0.674	0.493	-0.346	0.341
Mutan	JXK-99	0.797	0.556	-0.145	4.59E-02
Shihmen	JXK-10	-8.72E-02	0.314	0.92	0.133
Shihmen	JXK-11	0.149	0.135	0.967	6.42E-02
Shihmen	JXK-59	-0.3	-8.65E-02	0.904	-0.131
Shihmen	JXK-61	0.202	0.175	0.961	1.57E-02
Shihmen	JXK-62	-2.54E-02	-7.73E-02	0.994	-3.12E-02
Shihmen	JXK-65	-2.32E-02	-0.164	0.971	-9.08E-03
Shihmen	JXK-69	-7.68E-02	-0.245	0.949	-6.83E-02
Shihmen	JXK-70	-0.17	1.28E-03	0.958	3.14E-02
Shihmen	JXK-9	-0.341	0.164	0.848	-8.61E-02
Shihtzutou	JXK-102	0.3	0.934	0.143	5.96E-02
Shihtzutou	JXK-103	0.482	0.842	-7.00E-02	6.47E-02
Shihtzutou	JXK-12	0.484	0.845	-0.187	8.66E-02
Shihtzutou	JXK-30	0.553	0.808	-0.141	7.49E-02
Shihtzutou	JXK-31	0.344	0.899	-9.78E-02	0.209
Shihtzutou	JXK-32	0.663	0.736	1.04E-02	9.19E-02

Table 3 (continued). Rotated component matrix. Component loading is the similarity between component and the individual component.

Strata	sample	comp1	comp2	comp3	comp4
Shihtzutou	JXK-33	0.584	0.755	6.02E-02	0.248
Shihtzutou	JXK-35	0.562	0.782	-0.151	0.214
Shihtzutou	JXK-36	0.752	0.624	-7.04E-02	7.19E-02
Shihtzutou	JXK-37	0.651	0.733	-7.60E-02	0.11
Shihtzutou	JXK-38	0.475	0.818	6.90E-02	0.142
Shihtzutou	JXK-39	0.511	0.777	0.212	0.201
Shihtzutou	JXK-40	0.542	0.817	1.49E-02	3.06E-02
Shihtzutou	JXK-41	0.388	0.862	-5.42E-02	1.80E-03
Shihtzutou	JXK-42	0.414	0.858	-0.254	0.114
Shihtzutou	JXK-43	0.689	0.592	-0.216	-8.34E-03
Shihtzutou	JXK-68	0.432	0.864	-0.148	8.40E-02
Shihtzutou	JXK-75	0.584	0.766	-0.17	0.173

Table 4. Factor scores of the 4 components. Matrix shows the relationship between the components and the variables used in the petrographic study.

Variables	Component1	Component2	Component3	Component4
Qt/QFL	-.48442	1.12550	-.54333	.33924
Qm/QFL	-.75527	-.20866	-1.14454	-.62057
F/QFL	-.59090	.03636	-.66599	-.75326
L/QFL	.86015	-1.39035	.22599	-.44806
Lt/QFL	1.11430	-.15321	.86554	.76581
P/F	.56597	.84424	.89906	1.78106
Lv/L	-.97055	-.19933	1.41358	-.53738
Qp/Qt	.70677	.62525	.88052	.55217
Qp	-.87362	1.91479	-.63436	.02777
Lvm	-.58703	-1.00360	.62980	-1.09524
Lsm	1.23259	-1.24016	-.94437	.46326
Lm	1.83459	1.00604	-.90115	-1.65218
Lv	-.98747	-.20720	1.38493	-.53860
Ls	-1.06512	-1.14967	-1.46568	1.71599

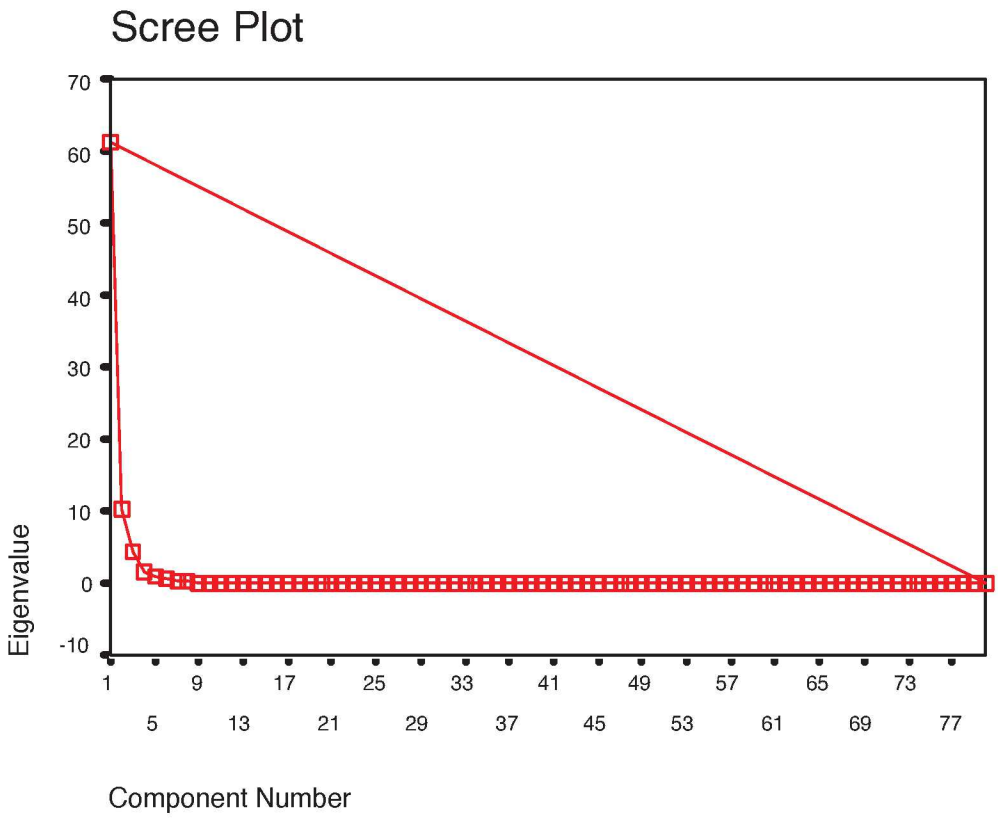

Figure 20. The scree plot show that only the first four factors have significant information.

The four components represent four possible types of sand compositions, probably related to different sediment sources.

Component 1 shows high component loadings (0.8 and higher) exclusively from the Lilongshan and Mutan units. From the factor score it is clear that component 1 has a high lithic content, and is particularly high in metamorphic lithic fragments, and generally has negative affinity to volcanic and sedimentary lithic fragments.

Component 2 is associates with samples from the Loshui and Shihtzutou units. The factor score indicates that component 2 has a high affinity to quartz content, specifically to polycrystalline quartz. It has relatively low lithic fragments, especially sedimentary lithic fragments.

Component 3 is a combination of high volcanic lithic fragments, polycrystalline quartz and total lithic fragments. The samples with high component loading of component 3 are usually from the Shihmen unit.

Component 4 is high in sedimentary lithic fragments and very low in metamorphic lithic fragments. Samples from the Loshui and to a lesser degree Shihtzutou units have high component loadings of component 4.

The scree plot in figure 20 indicates that these four components contain more than 99% of the information in the whole dataset. Therefore, instead of tracking all the parameters in modal analysis, more than 99% of the information can be explained by linear combinations of these four components.

Geostatistical Representation

Among the ternary diagrams plotted, it is clear that the lithic fragment categories Qp, Lvm, and Lsm (Figure 16) are the best parameters to discriminate the compositions of the sandstones analyzed. In order to exploit the sediment dispersal path as an indication of the possible paleo-source areas, a density map is needed, showing the location of high and low values of various parameters. To interpolate this dataset, with its limited areal distribution of data coverage, to a full two-dimensional grid, kriging, a geostatistical technique, is performed on the parameters of the sandstones modal analysis. The data were then piped to the Generic Mapping Tool developed and maintained by Wessel and Smith of *University of Hawaii at*

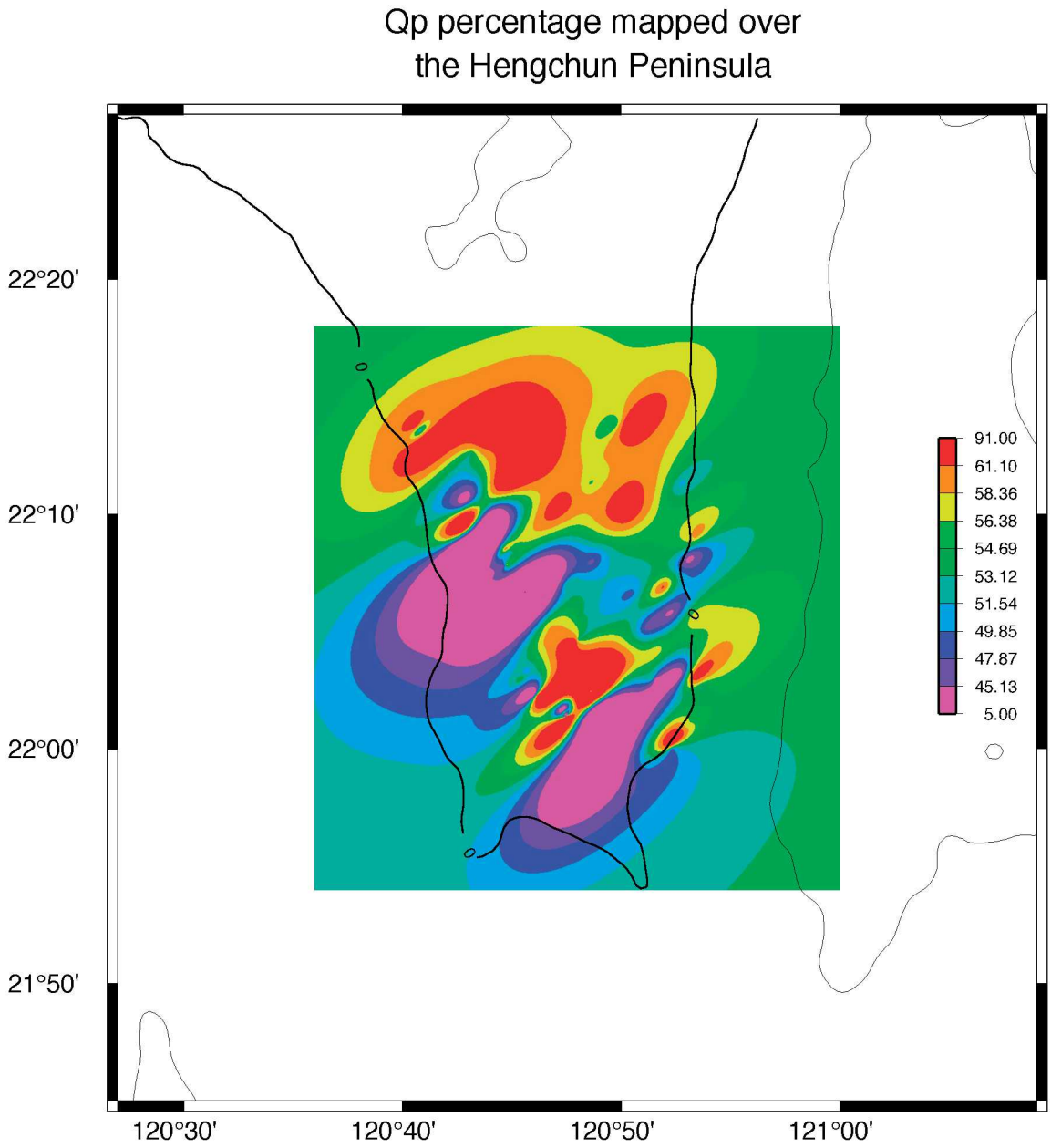

Figure 21. Qp percentage plot. The relative amount of the Qp is overlain on top of the studied area, indicating the higher concentration of Qp in the north of Hengchun Peninsula, and lower in the south.

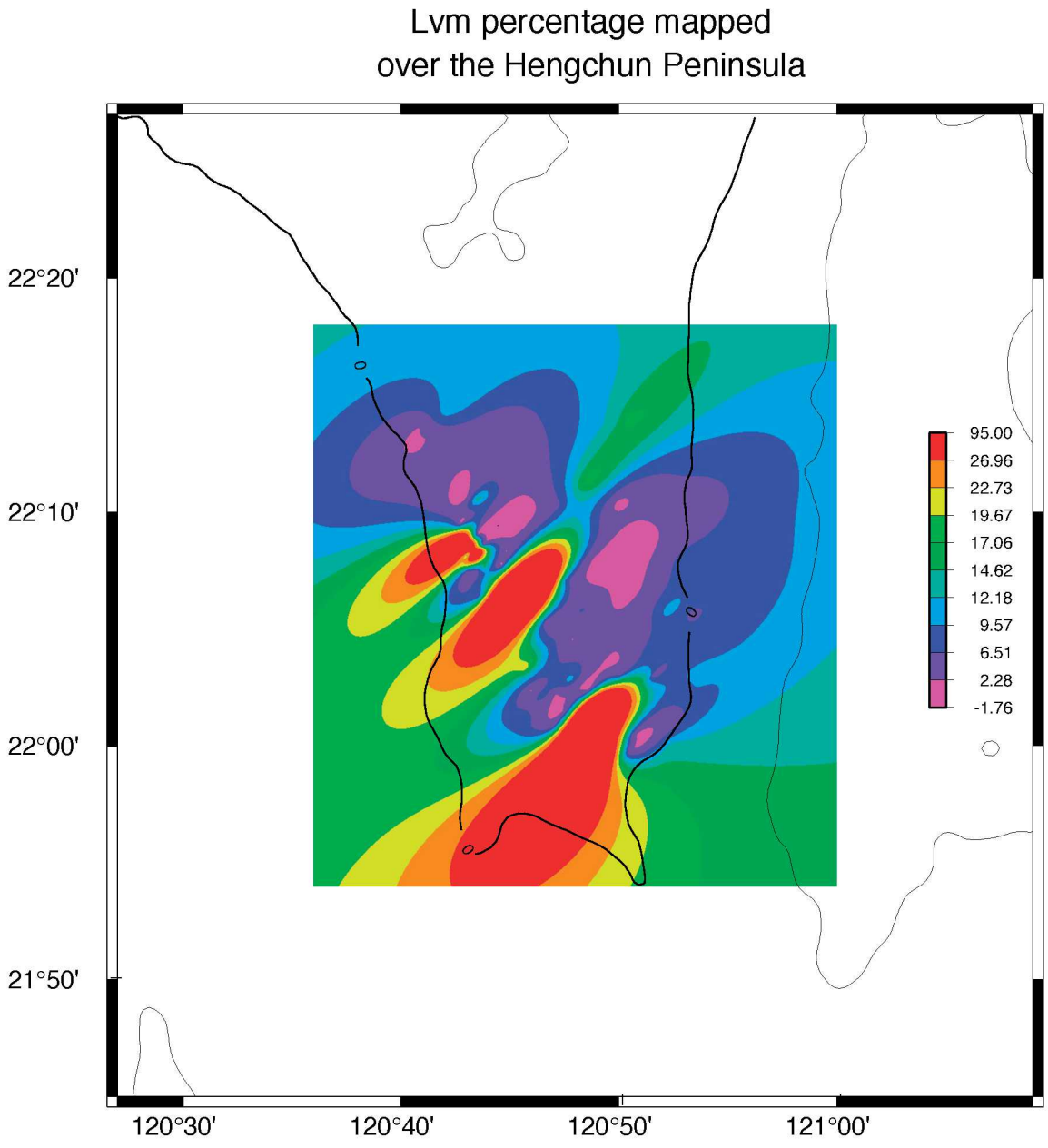

Figure 22. Lvm percentage plot. There is higher concentration of volcanic lithic fragments in the west side of the Hengchun Peninsula compared to the east.

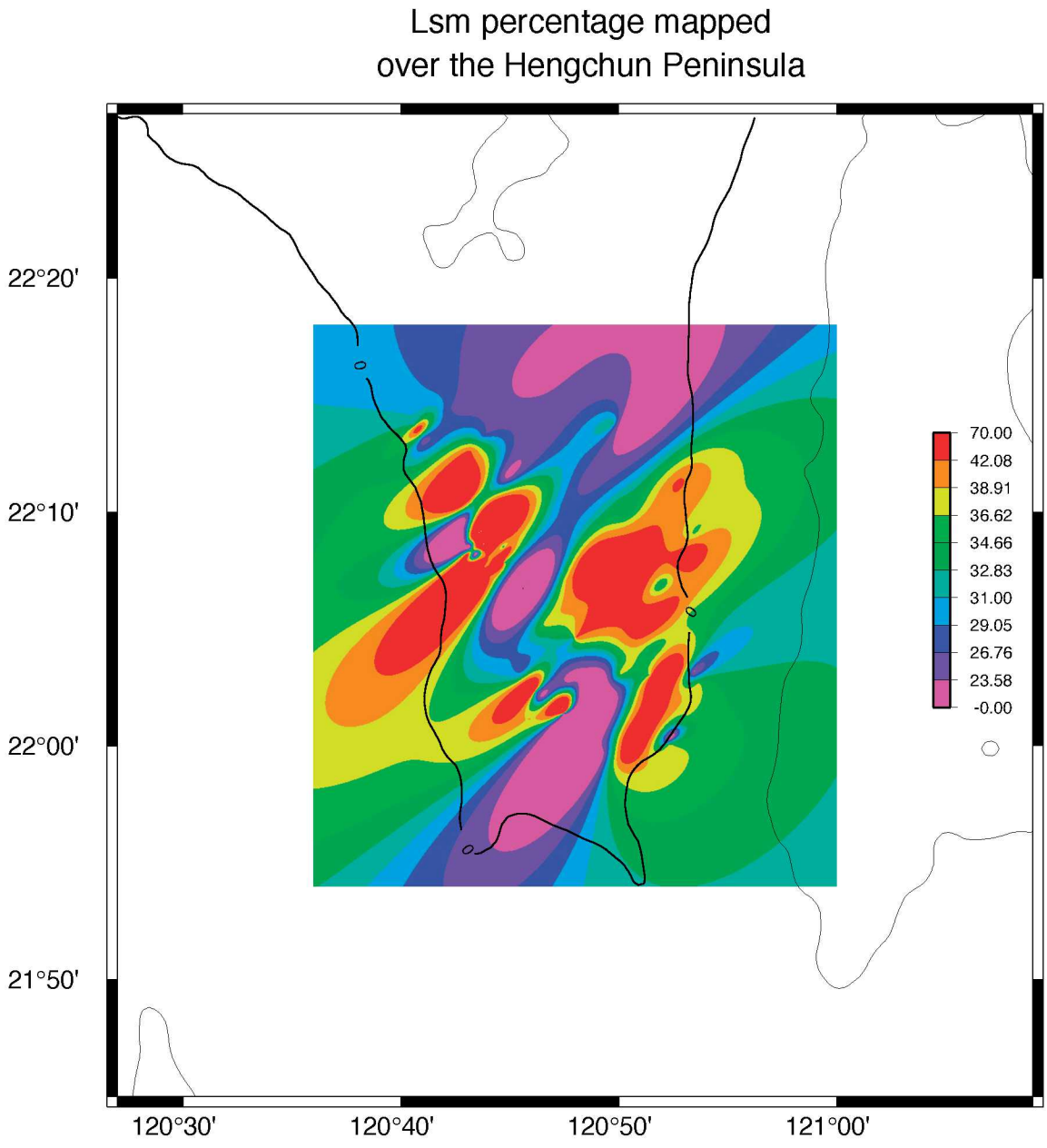

Figure 23. Lsm percentage plot. The sedimentary lithic fragments are more concentrated on the western and eastern coast of the Hengchun Peninsula and less concentrated on the central part.

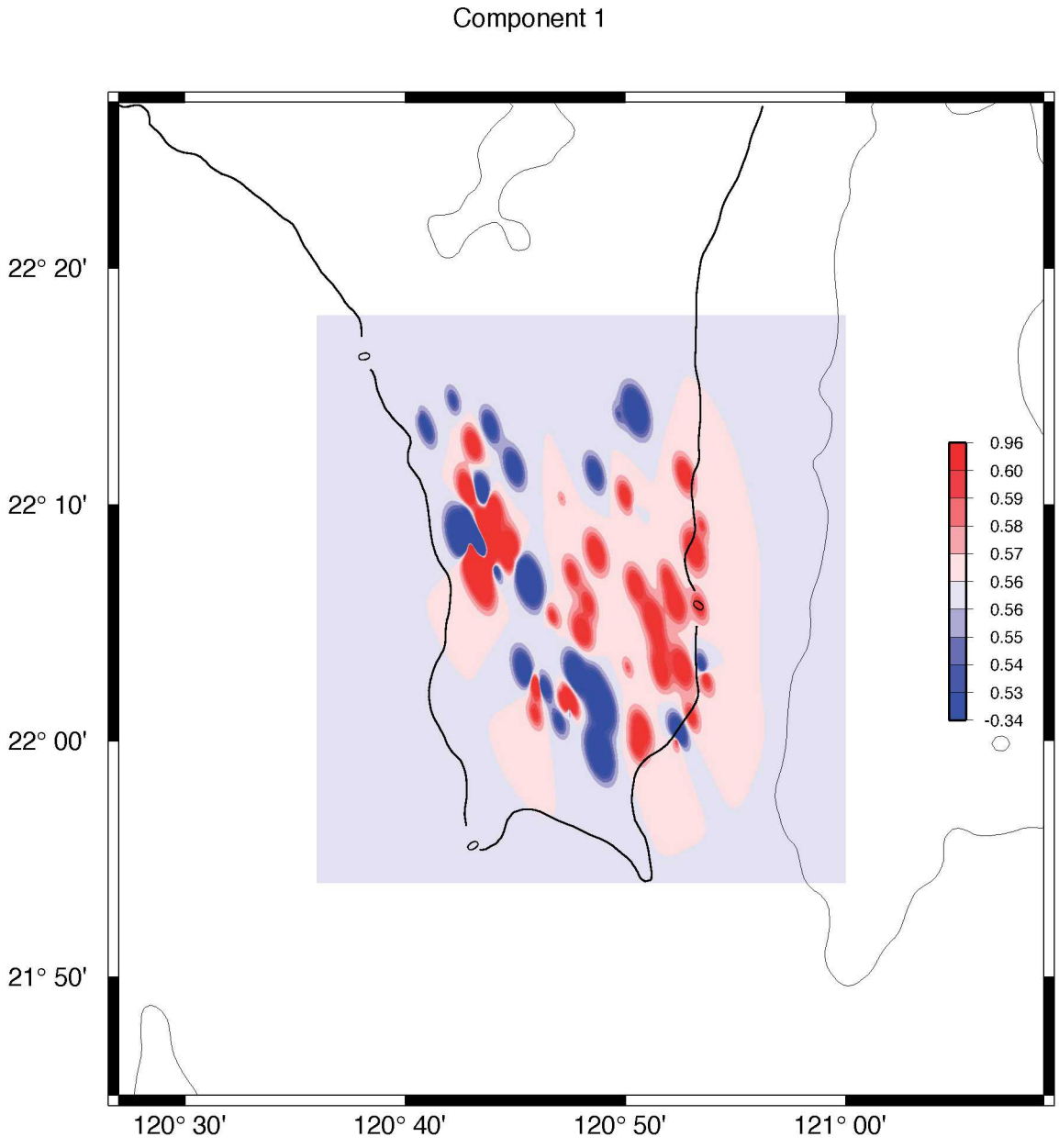

Figure 24. Component loadings of Component 1 plotted across the Hengchun Peninsula. Component 1 is associated with the Lilongshan and Mutan units and does not show a strong geographic trend.

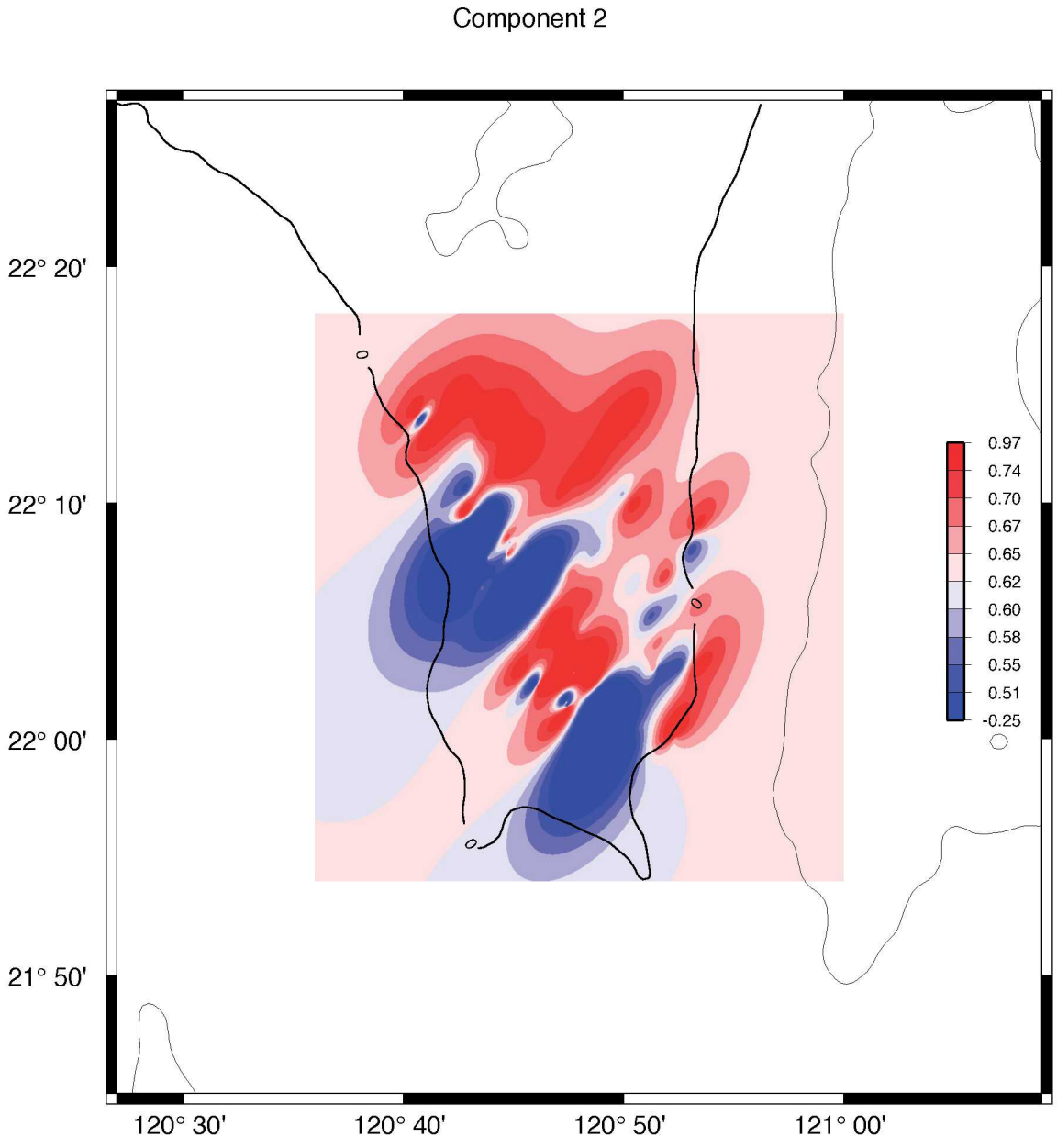

Figure 25. Component loadings of Component 2 plotted across the Hengchun Peninsula. Component 2 is associated with the Loshui and Shihtzutou units and has higher values in the north, suggesting a southward sediment dispersal path.

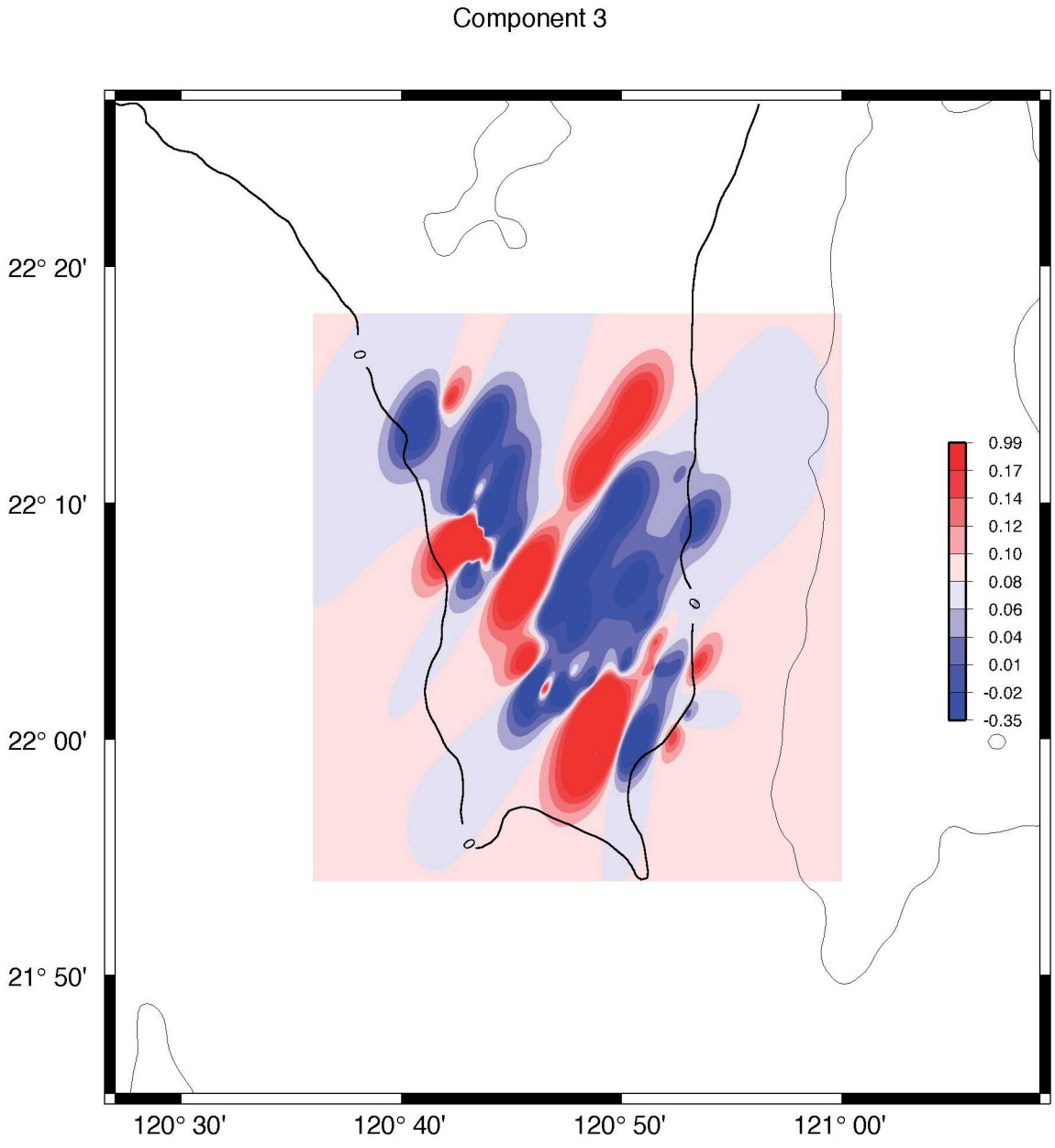

Figure 26. Component loadings of Component 3 plotted across the Hengchun Peninsula. Component 3 is associated with the Shihmen unit and has higher values in the west and northeast corner of the peninsula, suggesting an eastward sediment dispersal path.

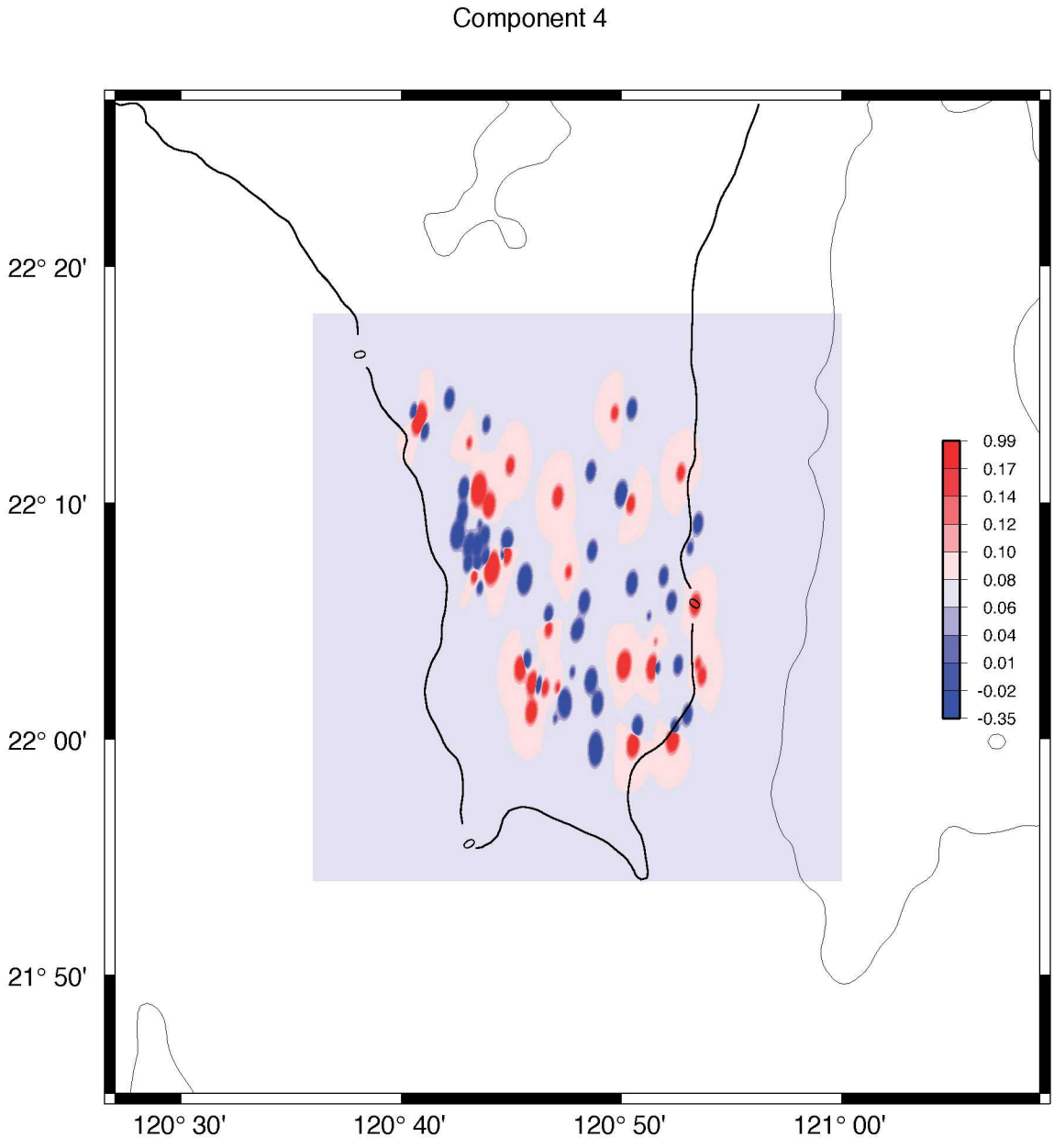

Figure 27. Component loadings of Component 4 plotted across the Hengchun Peninsula. Component 4 is similar to component 1 but contains a lot less information. Component 4, similar to component 1, does not show a strong trend.

Manoa, and the results are plotted and overlaid as maps (Figures 21, 22, and 23 for Qp, Lvm, Lsm respectively; details of the kriging techniques are described in the methodology section of Chapter 5). The parameters Qp, Lvm, and Lsm imply that the sandstones derive from three different types of source terranes, one rich in metamorphic rocks, one rich in volcanic rocks, and one rich in sedimentary rocks.

The Qp map indicates that the northern part of the Hengchun Peninsula is very high in Qp, and this composition generally decreases southward, albeit with local fluctuation (Figure 21). From the QpLvmLsm ternary diagram, we know that high Qp value means higher affinity to the Loshui and Shihtzutou units, implying a south-propagating sediment dispersal path for the Loshui and Shizetou units. On the other hand, Lvm shows the highest concentration on the western flank of the peninsula, and lower values on the eastern half of the study area (Figure 22). This is indicative of the Shihmen unit and its possible dispersal path. Lsm shows yet another trend, quite different from the previous two parameters, and is high on both the east and west sides of the peninsula and very low in the central part of the region (Figure 23). This implies that a sedimentary source (or sources) provided detrital materials for these two areas. This parameter has a high affinity to the Lilongshan and Mutan units.

Kriging was also applied to the values of component loading of the four components from the result of principal component analysis, and is plotted geographically as were the modal analysis parameters (Figures 24, 25, 26, and 27 for components 1, 2, 3, and 4 respectively).

Component 1, which is associated with abundant metamorphic lithic fragments, and usually with the Lilongshan and Mutan units, does not show a very clear trend (Figure 24). There seems to be a long axis along the east side of the peninsula that has a high component loading. And there is another high area of component loading in the northwest corner of the peninsula. Overall the values of the component loading are high, and only a few places have very low component loadings. This is an indication that most samples exhibit the influence of this component, and this component is distributed rather evenly throughout the whole region.

Component 2 is associated with high content of polycrystalline quartz and metamorphic lithic fragment, and the high component loadings are usually associated with the Loshui and Shihtzutou units. The distribution of this component (Figure 25) shows a very dramatic high

concentration in the northern part of the Peninsula and decreases southward, with a low value on the central western coast of the peninsula and another low on the southeastern tip of the peninsula.

Component 3, associated with the Shihmen unit, represents volcanic lithic fragments and polycrystalline quartz. This component is very high in the western flank of the study area and decreases east- northeastward (Figure 26). There is a tongue of high component loading that extends from the center of the western flank toward the northeast.

Component 4 is shown for the sake of completeness (Figure 27) but is judged meaningless. This component by itself includes less than 2% of the overall information of the sandstone compositions in the samples analyzed.

Interpretation

From the petrographic data, cluster analysis, and discriminant function analysis it is clear that sandstones from the Shihtzutou and Loshui units are very similar in composition, and sandstones from the Mutan and Lilongshan units are close in composition also. Although the field aspects of these units are distinct in their type localities, their compositions are very similar.

From the geostatistical representation of petrographic parameters and component loadings, it appears that volcanic clastic materials in the Hengchun Peninsula came from the west side and were only transported eastward for a short distance. This trend is indicated in the Lvm plot (Figure 22) and component 3 plot (Figure 26). Sandstones of the Shihtzutou and Loshui units are from the north and dispersed southward as implied by Qp plot (Figure 21) and component 2 plot (Figure 25). Component 1 extracted is associated with the Mutan and Lilongshan units, as is parameter Lsm. However the density plot of component 1 and density plot of Lsm show very different patterns. In the Lsm density plot, the high values are located on both sides of the peninsula and are slightly higher in the north than in the south, while the central longitudinal axis of the peninsula has a relatively low value of Lsm. This seems to indicate a slight trend of southward transport of this materials. On the other hand, the density plot of component 1 shows no clear trend and no obvious clustering of low values other than on the very southern end of the peninsula. The explanation of this might be that the principal component analysis extracted the common composition of the samples into component 1, and these "common compositions" are particularly high in the Lilongshan

and Mutan units. This seems to imply that there is a "background" type of sediment that is pervasive throughout the whole region, and which is included in most of the sandstones regardless of their stratgraphic units. Although at times influx of coarse sediment could dilute the "background" sediment, this particular composition exists in most of the samples.

CHAPTER FOUR

FISSION TRACK ANALYSIS OF DETRITAL ZIRCONS

Principles

Fission tracks, formed by natural fission of ^{232}Th, ^{235}U and ^{238}U, are damage zones in crystal lattices (Figure 28). The decay constants of the first two isotopes are so small that, for all practical purposes, all fission tracks are derived from fission of ^{238}U (Andriessen, 1995). The spontaneous fission-track (FT) density is proportional to the time elapsed and the uranium content. The latter parameter is determined by irradiation of the sample with thermal neutrons causing the ^{235}U-isotope to fission. A new set of induced fission tracks is thus made and counted and the induced FT density is proportional to the amount of uranium, because the ^{235}U /^{238}U ratio is taken to be constant (Faure, 1986).

Charged particles can travel in the solid medium of a crystal lattice and will leave a trail of damage by transferring kinetic energy. In the natural environment, the tracks are caused by particles resulting from the fission of ^{238}U, which produce large mass fragments that carry high energy (200 MeV). Fission-track analysis is the study of these natural tracks produced over geological periods of time.

Price and Walker (1962) first discovered these tracks in natural samples of mica. They proposed that the density of fission tracks can be used for dating, given that etched fission tracks can be easily observed with a petrographic microscope under high magnification, and that the U fission process is statistically random and operates at a constant rate. Fission track can be used to date minerals. The only contrast with other isotopic dating methods is that the fission tracks replace the role of daughter products analyzed in other methods.

To obtain a fission-track age, it is required to estimate the abundance of ^{238}U and spontaneous tracks in the mineral to be dated. One can easily obtain the density of spontaneous tracks by observing the tracks revealed by etching. In order to determine the abundance of ^{238}U, it is necessary to irradiate the sample with low-energy thermal neutrons that induce fission in ^{235}U. This fission will create artificial tracks in a similar fashion as the production of spontaneous tracks. As long as we know the neutron flux, the number of induced tracks is related to the abundance of ^{238}U, and because the ratio $^{238}U/^{238}U$ is constant in nature, we can estimate the abundance of ^{238}U in the sample (Gallagher et al., 1998).

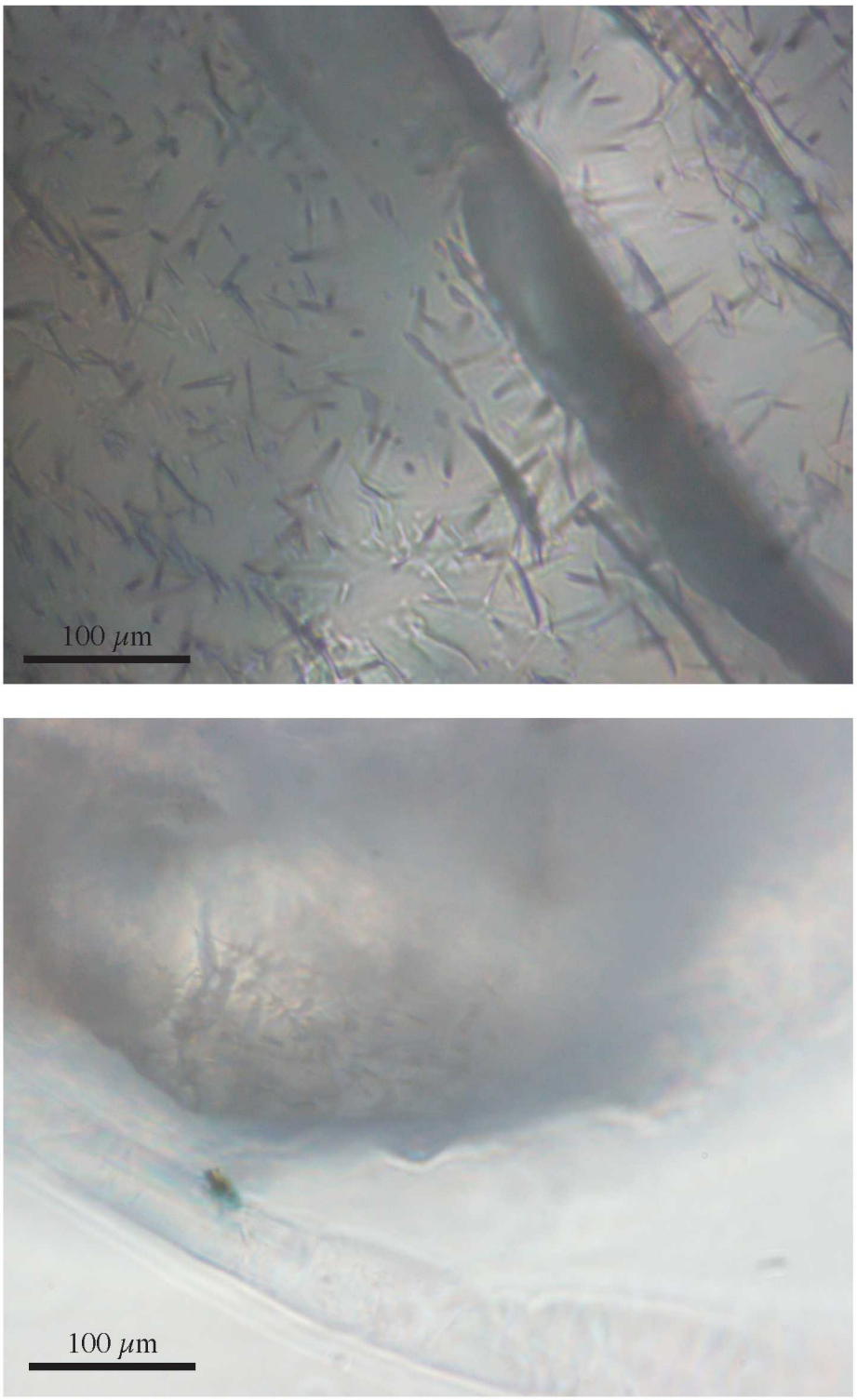

Figure 28. Zircon fission tracks in samples 060201-1 from the Loshui unit (top) and 050802-1 from the Shihtzutou unit (bottom).

The general age equation as used in fission track dating is:

$$t_{unk} = \frac{1}{\lambda_\alpha} ln[1 + \frac{\rho_s}{\rho_i} \frac{\lambda_\alpha}{\lambda_f} \phi \sigma I]$$

Where t is the age; ρ_s and ρ_i are the spontaneous and induced track densities; λ_α is the alpha decay constant of ^{238}U (Faure, 1986.)

I adopt the zeta calibration method first proposed by Hurford and Green (1982), and followed by many others. For the external detector ζ method, the fission track age equation is written as:

$$t_{unk} = \frac{1}{\lambda_\alpha} ln[\frac{\rho_s}{\rho_i} \lambda_\alpha \zeta g + 1]$$

$$\zeta = \frac{(e^{\lambda_\alpha t_{std}} - 1)}{\lambda_\alpha (\rho_s / \rho_i)_{std} \rho_d}$$

ρ_d is track density in the dosimeter; g is known as the geometry factor (which allows for the fact that the spontaneous tracks intersecting the surface of observation represent a sample from twice the effective volume as that represented by the induced tracks); and ζ is a constant of proportionality made up of other parameters, including the fission decay constant and neutron-capture cross section. The value of ζ can be obtained by calibrating with a known source (in our case, zircon from Fish Canyon Tuff generously provided by C. Naeser) with the dosimeter, and then the ζ value can be applied to the analyses of the unknown samples to solve for their age and eliminate uncertainty in the etching, radiation, and counting procedures.

Provenance Study with Fission Track Analysis

Clastic sedimentary rocks are lithified sediments derived from erosion of pre-existing rocks, and therefore heavy minerals in clastic sequences contain the fission tracks that accumulated during the history the original source rocks. Provided that the quasi-stable fission tracks in the heavy minerals were not reset and annealed during burial, they will contain age information related to the original source rocks. The higher-temperature (around 250°C depends on the cooling rate) stability and the resistance to physical and chemical weathering of zircon means it is better suited for tracking the provenance (Gallagher et al.,

1998; Carter, 1999). In particular, if enough single grains are analyzed, several discrete age components may be recognized in the samples.

The results of the fission-track analysis can be considered in various ways. The most commonly used method is the graphical estimate of the different component ages in an overall age distribution using a probability-density plot. One problem with this method is that overlapping peaks are generally affected and shifted toward the higher-amplitude peak, and low-amplitude peaks can be masked (Brandon, 1992, 1996).

The grain age estimates from fission-track analysis often have different precisions and the often-used one-dimensional histogram does not preserve the precision information, which may be important in interpreting the obtained age. A radial plot was introduced to retain the precision information of the grain analyses and for easier extraction of age components from fission track data collected using the external detector method (Galbraith, 1981, 1998). The radial plot is an x-y scatter plot with $x_j=1/\sigma_j$, and $y_j=(z_j - z_0)/ \sigma_j$; where z_j is the grain age of the j^{th} grain, σ_j is the associated standard error, and z_0 is the central age.

Previous studies (Liu et al., 2000; Liu et al., 2001) show that zircon grains collected from the main body of the island of Taiwan have grain ages that range from younger than 1 Ma to 216 Ma, with the majority of the age dates ranging between 1 Ma and 100 Ma. The oldest dates (>150 Ma) generated in the analysis were from samples collected from the very northern part of Taiwan. Most samples collected from the Central Range produce very young FT age dates, clustering around 1 Ma, whereas zircons collected from the Western Foothills, immediately west of the Central Range, have greater FT ages, from several 10's of M.y. old to around 100 Ma. An eastward-younging trend can be seen in central ages of the grains plotted according to their sampling locations. The authors suggested that the samples in the Central Range have been reset by the modern Penglai Orogeny, and the samples to the west have been partially reset to varying degrees. This is consistent with thermal modeling of the Taiwan mountain belt (Barr and Dahlen, 1989, 1990; Willett, 1999).

Methodology

Many of the sample preparation procedures are well established and have been described in the literature (Crowley et al., 1989; Garver, 2000). The procedures are followed carefully to ensure inter-laboratory compatibility. In this project, sandstone samples were reduced in

size first by jaw-crusher and then further by pulverizer in the lab. These samples were then sieved into different size fractions, retaining the fraction between 3ϕ to 4ϕ. This fraction was then poured into a separatory funnel filled with tetrabromoethane of density 2.95 g/cm^3. The heavy fraction was passed through a Frantz magnetic separator with 1 Amp, 8° inclination and 2° tilt for multiple passes to further concentrate zircon.

Zircon samples were mounted in teflon. Zircon grains were pressed into incipient melting teflon by heating to 310°C on a hotplate. The mounts were then ground and polished to 0.5 micron, and carefully examined under the microscope to make sure the surfaces appear smooth under high magnification.

Zircon mounts were etched with potassium hydroxide (8g) and sodium hydroxide (11.2g) melted eutectically at 228°C in an oven with an attached thermocouple wire thermometer. Zircon mounts were placed face-down in the hydroxide flux in a teflon container. I used an etch time of 24 hours. The appropriate time of etching can be determined by examining the developing tracks under a microscope.

I used muscovite as an external detector for zircon, apatite, and a glass standard (SRM963a) that was obtained from National Institute of Standards and Technology. The muscovite I used has approximately 5 to 10 tracks per square centimeter. The muscovite is heated to 550°C to anneal the spontaneous tracks. Muscovite sheets are cut into pieces 1.5cm by 1.5cm and cleaned with alcohol and allowed to dry. These muscovite sheets were then taped together with zircon and apatite mounts and the glass standard. I also included some annealed mica sheets in the sample batch for irradiation in order to obtain the background track density (Figure 29). Muscovite sheets were etched after irradiation with 48% HF for 15 minutes to reveal induced tracks (Faure, 1986; Crowley et al., 1989; Garver, 2000).

I used the program BINOMFIT developed by M. Brandon (Brandon, 1996) based on Galbraith and Green's algorithm (Galbraith and Green, 1990; Galbraith and Laslett, 1993) to process the data and extract age components from the fission-track age data.

Results and Data Analysis

The results of zircon fission-track analysis are listed in Table 5 and shown in Figures 30-36. The pooled age and central age of all samples analyzed from the Hengchun Peninsula

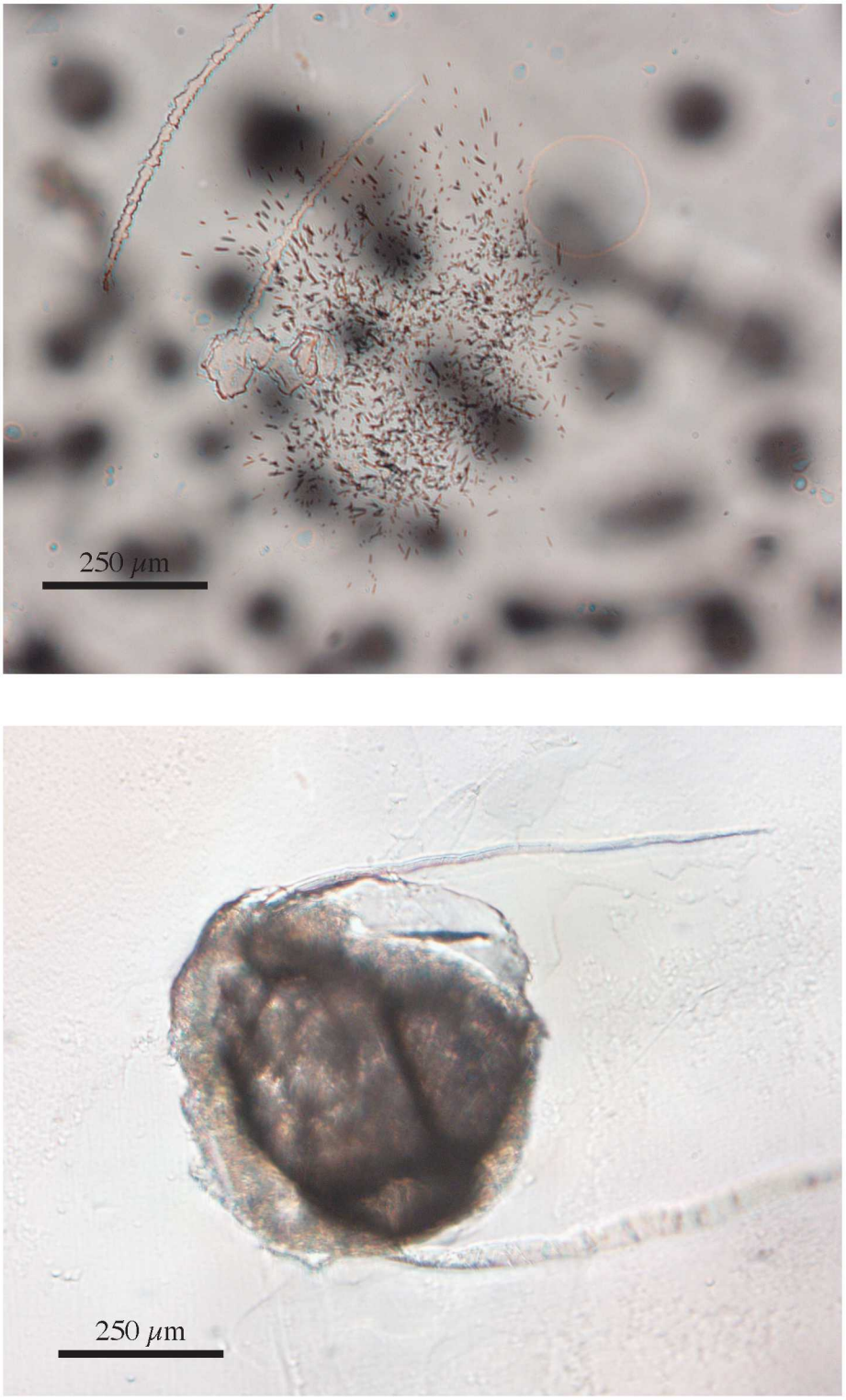

Figure 29. Fission tracks obtained from external mica detector that covered the zircon on the grain in the lower picture. Sample 050802-1, from the Shihtzutou unit.

Table 5. Fission track ages of detrital zircon grains analyzed

July 31 2003 18:02 BinomFit for Windows ver.1.0 Page 1
Datafile: C:\WINNT\Profiles\yen.000\Desktop\FissionTrack HC only\FissionTrack HC only.ftz
Title: Hengchun sandstones

NEW PARAMETERS - ZETA METHOD

EFFECTIVE TRACK DENSITY FOR FLUENCE MONITOR (tracks/cm^2): 1.06E+04
RELATIVE ERROR(%): 4.95
EFFECTIVE URANIUM CONTENT OF MONITOR (ppm): 0.82
ZETA FACTOR AND STANDARD ERROR (yr cm^2): 7648.35 2544.06
SIZE OF COUNTER SQUARE(cm^2): 7.13E-08

GRAIN AGES IN ORIGINAL ORDER

Grain no.	RhoS cm^-2	Ns	RhoI cm^-2	Ni	Squares	U+/-2s	Grain Age	Age (Ma) --95% CI--
1	2.10E+07	27	3.74E+07	48	18	2899 881	22.9	13.6 37.7
2	2.38E+07	107	2.05E+07	92	63	1588 366	47.1	34.7 63.9
3	4.91E+07	63	5.61E+07	72	18	4349 1109	35.5	24.5 51.1
4	1.05E+07	36	2.22E+07	76	48	1721 429	19.3	12.4 29.3
5	1.10E+07	63	2.42E+07	138	80	1875 369	18.6	13.3 25.6
6	3.53E+07	181	3.82E+07	196	72	2960 514	37.4	29.7 47.1
7	4.23E+07	190	3.87E+07	174	63	3003 543	44.2	35.0 55.8
8	2.65E+07	51	3.01E+07	58	27	2336 653	35.7	23.7 53.5
9	3.43E+07	66	2.81E+07	54	27	2174 627	49.5	33.6 73.1
10	2.14E+07	55	2.81E+07	72	36	2174 554	31.0	21.1 45.2
11	1.61E+07	110	2.43E+07	166	96	1880 346	26.9	20.5 35.1
12	1.54E+07	88	2.35E+07	134	80	1821 362	26.7	19.8 35.7
13	2.92E+07	100	4.33E+07	148	48	3352 643	27.4	20.7 36.2
14	3.68E+07	118	2.37E+07	76	45	1836 458	62.7	45.9 86.2
15	2.61E+07	67	1.40E+07	36	36	1087 376	75.0	48.9 117.1
16	4.01E+07	103	1.79E+07	46	36	1389 430	90.2	62.4 132.2
17	3.00E+07	77	8.88E+07	228	36	6886 1138	13.7	10.3 18.2
18	2.81E+07	36	3.43E+07	44	18	2658 839	33.2	20.5 53.3
19	2.13E+07	41	1.66E+07	32	27	1289 470	51.8	31.6 85.8
20	7.01E+06	18	5.61E+07	144	36	4349 842	5.1	2.9 8.4
21	2.81E+07	96	5.90E+07	202	48	4575 787	19.3	14.7 25.2
22	3.27E+07	84	2.03E+07	52	36	1570 461	65.2	45.1 95.2

POOLED 2.51E+07(1777) 3.23E+07(2288) 994 2503 269 31.5 28.0 35.3
CHI^2 PROBABILITY (%): 0.0

POOLED AGE WITH	68% CONF. INTERVAL(Ma):	31.5, 29.6	-- 33.4 (-1.8 +1.9)
	95% CONF. INTERVAL(Ma):	28.0	-- 35.3 (-3.5 +3.8)
CENTRAL AGE W/ 68% CONF. INTERVAL(Ma):		33.1, 23.2	-- 47.2 (-9.9 +14.1)
	95% CONF. INTERVAL(Ma):	16.5	-- 66.4 (-16.6 +33.3)
	AGE DISPERSION (%): 53.0		

Table 5. (continued) Fission track ages of detrital zircon grains analyzed

FIT OPTION: Best-fit peaks using the binomial model of Galbraith and Green

INITIAL GUESS FOR MODEL PARAMETERS (number of peaks to fit = 3)

Peak #.	Peak Age	Theta	Fraction(%)	Count
1.	31.50	0.437	22.1	4.86
2.	45.00	0.527	26.5	5.82
3.	63.70	0.612	18.4	4.04

Total range for grain ages:	5.2 to 89.8 Ma
Number of active grains:	22
Number of removed grains:	0
Degrees of freedom for fit:	17
Average of the SE(Z)'s for the grains:	0.17
Estimated width of peaks in PD plot in Z units:	0.2

PARAMETERS FOR BEST-FIT PEAKS

*Standard error for peak age includes group error

*Peak width is for PD plot assuming a kernel factor = 0.60

#.	Peak(Ma)		68%CI	95%CI		W(Z)	Frac(%)	SE(%)	Count
1.	15.1	-4.4	+6.2	-7.4	+14.4	0.18	24.0	9.5	5.3
2.	34.4	-9.9	+13.9	-16.7	+32.5	0.17	52.2	13.1	11.5
3.	66.3	-20.0	+28.6	-33.6	+67.6	0.20	23.8	11.8	5.2

Log-likelihood for best fit:	-111.917
Chi-squared value for best fit:	25.199
Reduced chi-squared value:	1.482
Probability for F test:	2%
Degrees of freedom for fit:	17
Condition number for covar matrix:	12.46
Number of iterations:	14

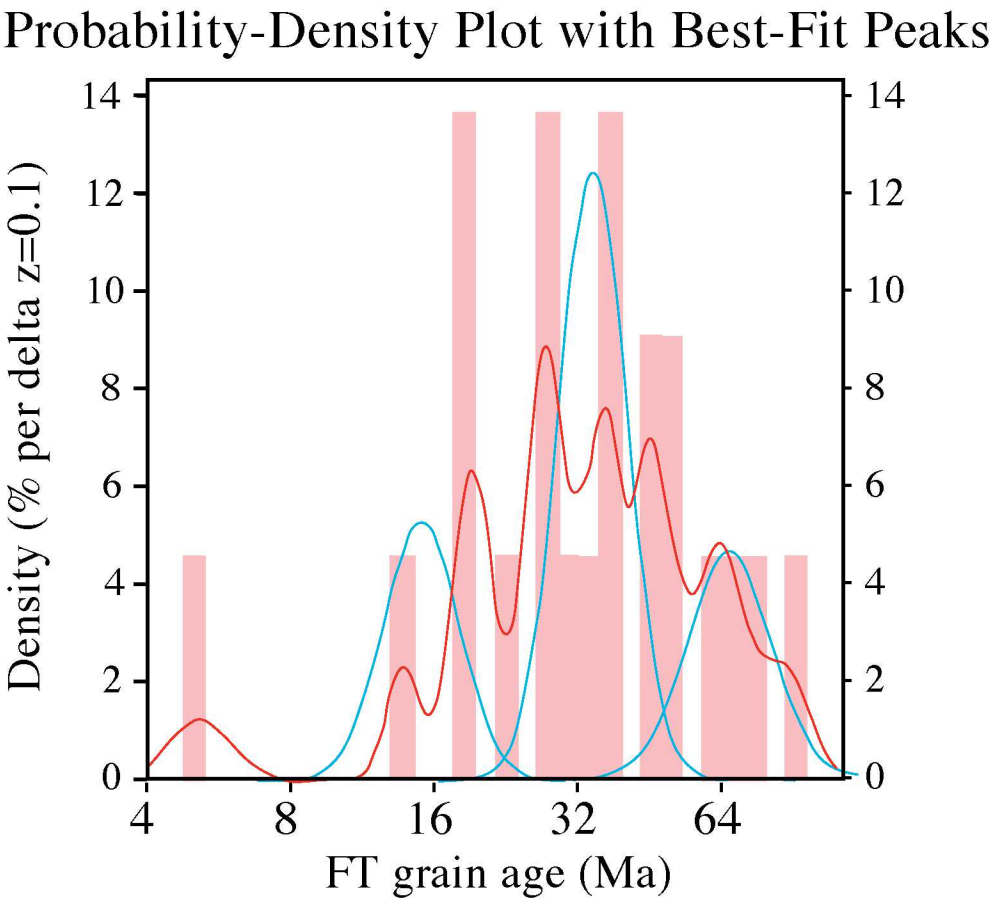

Figure 30. Fission track age probablility-density plot of the detrital zircon grains analyzed. Red color curve is the density plot of the peaks, blue color curves are the best-fit peaks.

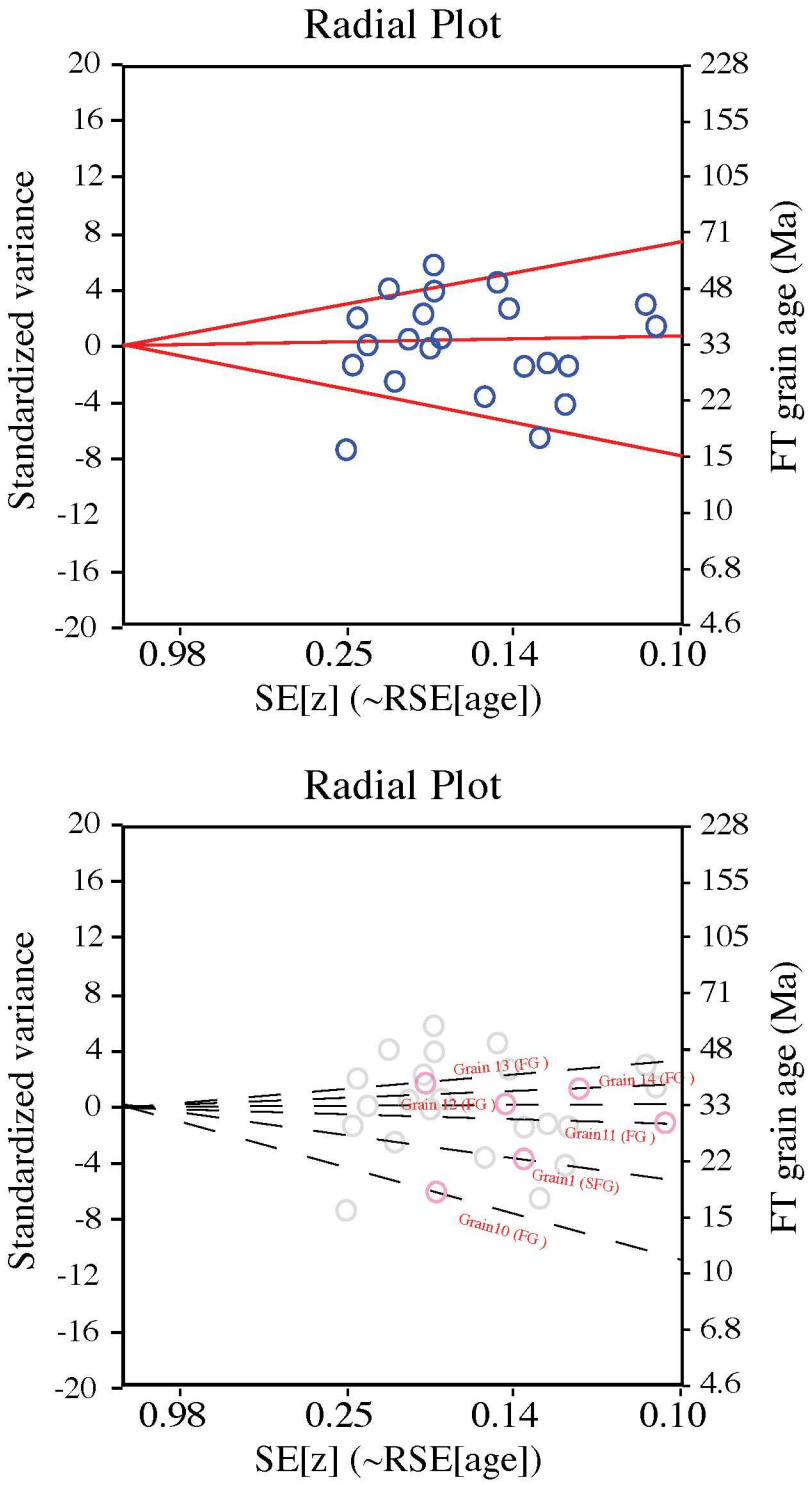

Figure 31. Radial plot of detrital zircon grains from Hengchun Peninsula (top), showing three age components of 15, 34, and 66 Ma. The lower diagram shows the grain ages of Fugan sandstones (FG) and Shanfugee sandstones (SFG)

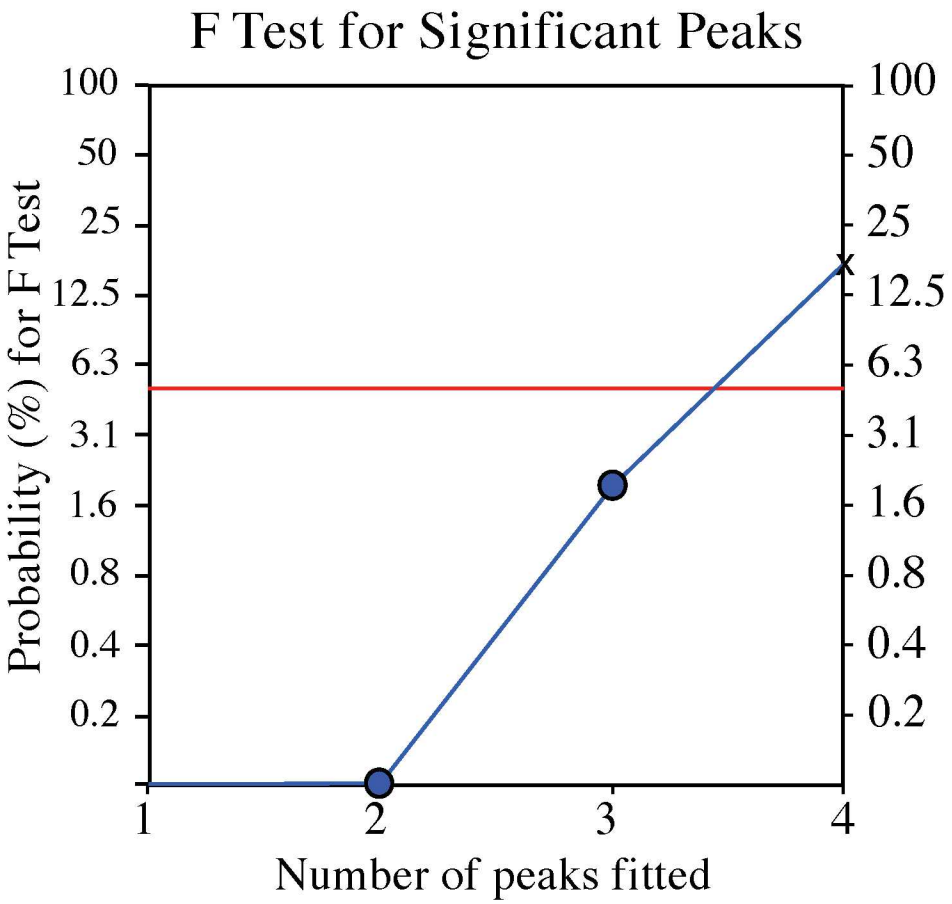

Figure 32. F-test for numbers of peaks fitted. There are only three significant peaks in the age data.

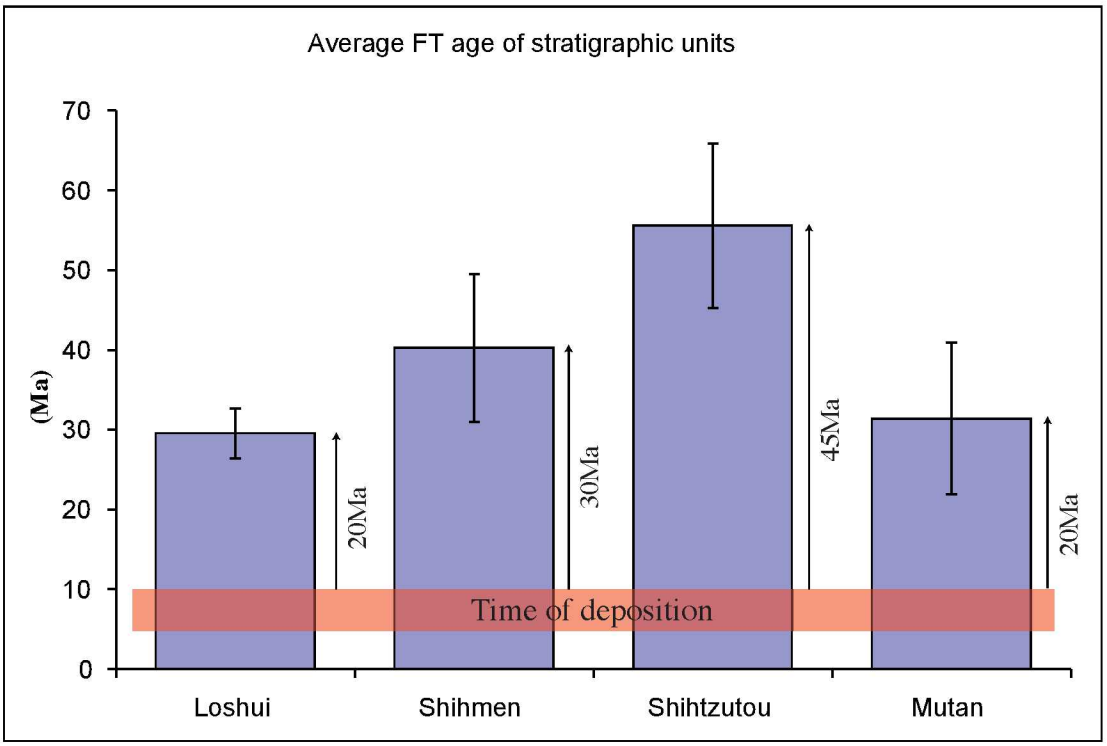

Figure 33. Average ages of the grains from the stratigraphic unit with standard error indicating the precision. The arrows on the side of each individual bar represent the "lag time" of the unit. The lag time is the age of the grains when they were buried.

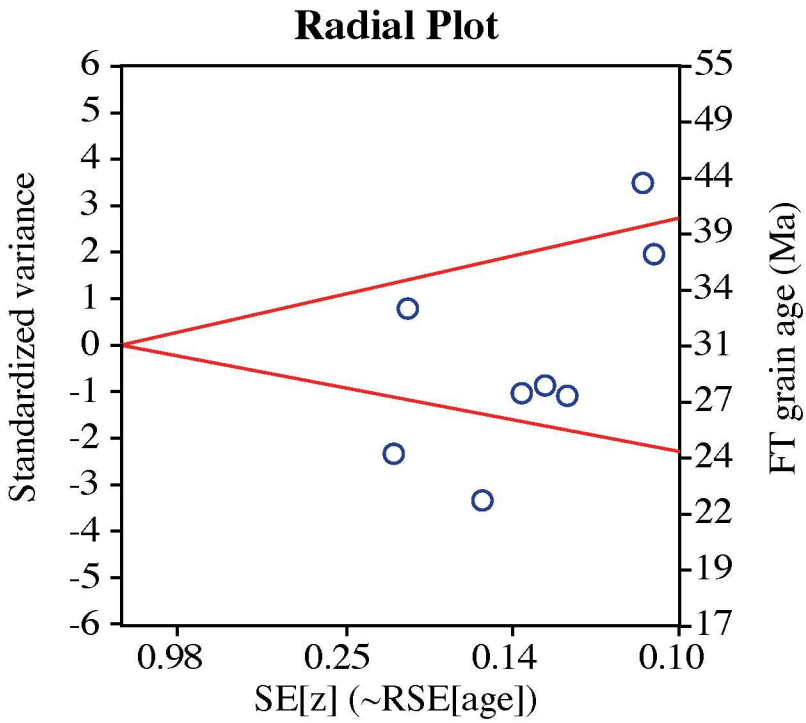

Figure 34. Radial plot of Loshui unit showing two age components of 24 Ma and 40 Ma.

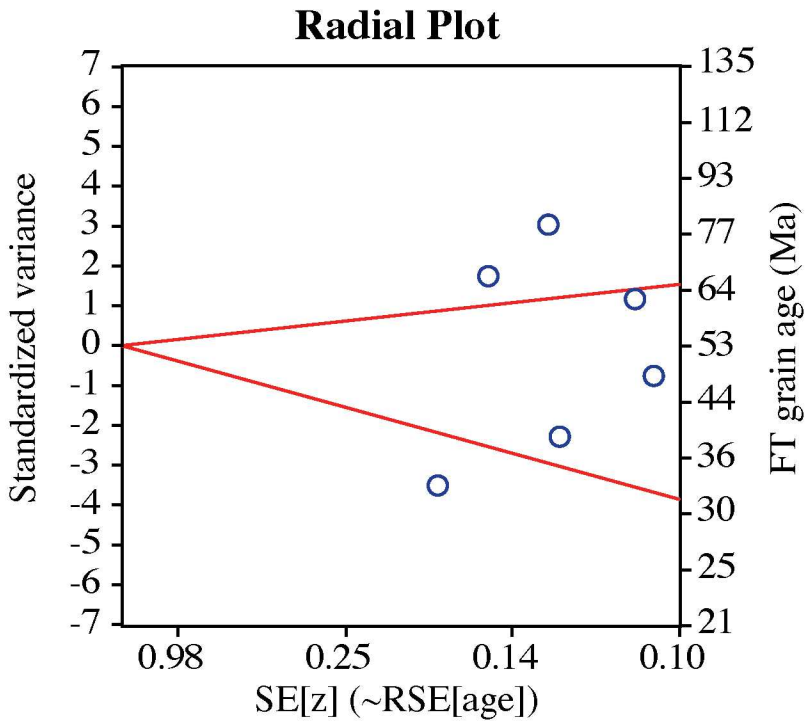

Figure 35. Radial plot of Shihtzutou unit showing two age components of 31 Ma and 64 Ma.

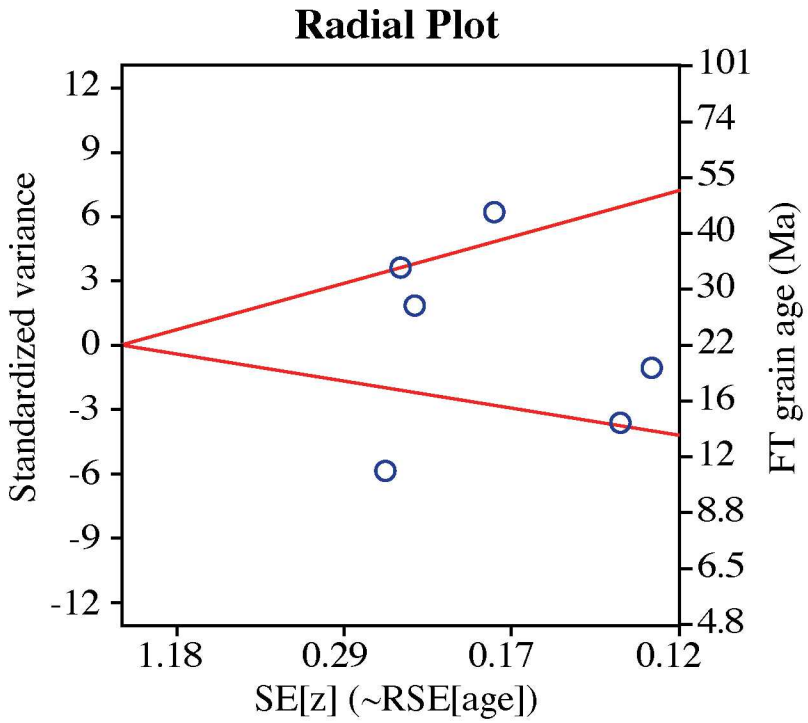

Figure 36. Radial plot of Mutan unit showing two age components of 51 Ma and 14 Ma.

are 31.5 Ma and 33.1 Ma respectively. The pooled age is simply calculated from the sum of all spontaneous tracks divided by the sum of all induced tracks, whereas the central age is essentially the weighted mean of the log-normal distribution of single grain ages, and is preferred (Gallagher et al., 1998). The central ages of the Mutan, Shihtzutou, Loshui, Shihmen units are 25.2 Ma, 50.6 Ma, 28.9 Ma, and 40.3 Ma (mean), respectively (Figure 33). Samples from the Loshui unit can be further resolved to two age components of 24.5 and 40.0 Ma, and the Shihtzutou unit has two age components of 31.4 and 61.3 Ma. The three age components extracted from all samples analyzed from the Hengchun Peninsula are 15.1, 34.4, and 66.3 Ma.

The lag time is defined as the difference between the depositional age and the age components determined (generally using the youngest or second-youngest peak), which indicates the FT age of the grains when they were deposited. The depositional ages of all these sandstones (late middle Miocene to late Miocene, or ~11 to 5 Ma) is younger than the minimum age of the age components extracted from the fission-track analysis. The lag times for the individual stratigraphic units are: Loshui unit, 20 Ma; Shihmen unit, 30 Ma; Shihtzutou unit, 45 Ma; and Mutan unit, 20 Ma.

Also analyzed were zircons separated from two stratigraphic units from elsewhere in Taiwan that are essentially age-equivalent to the upper Miocene units of the Hengchun Peninsula. Zircons from the Fugang Sandstone, exposed at the southern tip of the Coastal Range in eastern Taiwan, and from the Shanfugee Sandstone from northern Taiwan are also plotted on a radial plot (Figure 31). The FT age of zircons from the Shanfugee Sandstone is 19.6 Ma ; the central FT age of zircons from the Fugang Sandstone is 28.8 Ma. The sample of Shanfugee Sandstone taken from central-northern part of Taiwan was collected from the western Taiwan foothills, in an area that is reported to record partially reset zircon FT ages (Liu et al., 2001).

The individual stratigraphic units of the Mutan Formation have a common age component of around 30-40 Ma, while the Shihtzutou unit has a much older age component of around 64 Ma. This is one of the three age components showing in the overall samples. In fact the grain ages of the older cluster of the Shihtzutou unit are 62.7, 75, and 90.2 Ma. The southeastern border of the Chinese continent is made up of a series of accreted terranes. The outermost (the very southeastern part that borders China) is about 70-140 Ma (Jahn et al., 1990). Therefore this cluster of samples seems to have been derived directly

from the Chinese continent or from a terrane rifted from it. Dates from the Shihmen unit seem to cluster around 40 Ma, and zircons from the rest of the units cluster around 30 Ma. According to Liu's hypothesis, these samples may be explained by being partially reset during the Penglai orogeny that has generated the island of Taiwan. The age components extracted from sandstones of the Hengchun units are compatible with those samples from the unmetamorphosed Western Foothills on the main island of Taiwan (Liu et al., 2000; Liu et al., 2001), and structurally the Hengchun Peninsula is the southern extension of the Central Range. However, the sedimentary sequences exposed on the Hengchun Peninsula do not appear to be metamorphosed. Furthermore, there does not appear to have been a heating event that could have caused an in-situ partial reset during the Penglai orogeny, because many of the samples still retain the "signature" old age similar to those of the southeastern border terrane of the Chinese continent. Although the similarity in ages between samples from the Western Foothills and those from the Hengchun Peninsula suggests that the sources of these sedimentary rocks were similar, closer inspection indicates that the answer is not so simple. The Hengchun Peninsula is an emerging accretionary prism, and the exposed strata in the peninsula are expected to represent a rather shallow level of the accretionary prism. These strata should have undergone very little metamorphism, and should not have experienced temperatures high enough to have reset zircon fission-track ages. Another suggestion is that the sedimentary rocks of the Hengchun Peninsula were derived from erosion of materials from the northern part of the Taiwan orogen. However, the general consensus on the timing of collision initiation is between 12 and 5 Ma (Teng, 1990), and emergence of proto-Taiwan postdates the depositional age of the main sequences of interest in Hengchun Peninsula. Furthermore, the eroded detritus needs to have had an FT age of around 20 M.y. old at the time of deposition, which should not have been available at the time, because the reset is regarded as a product of the modern orogeny. This excludes the possibility of self-recycling orogeny in this case. Willett reports an anomalous apatite fission-track date in the Hengchun Peninsula with an age of 2Ma (personal communication, 2002), younger than the depositional age of the sample, and Willett suggests a hot oceanic basin is a possible cause of this post-depositional reset. This does not seem to explain the zircon ages either, because the event is rather young and does not have an universal effect on all the materials on the peninsula.

A possible scenario is that a terrane rifted from the continental margin was heated by later rifting of the South China Sea during its expansion. The multiple stages of SCS expansion with different orientations of successive spreading centers make it possible to heat

a large area in the SCS basin. Mafic materials in the Shihmen unit could easily have formed in the South China Sea at around 40 Ma, and all these elements could then have been later accreted to the approaching Manila trench – Luzon arc system during the closing of the South China Sea basin.

CHAPTER FIVE
NEOTECTONICS AND MORPHOTECTONICS IN TAIWAN

Uplift Predicted from Horizontal Motions, and Implications for the Hengchun Peninsula

The rates of uplift and erosional denudation are among the most valuable parameters for geologists who study the processes of orogeny, whether active or ancient. These rates are important in the sense that they represent the duration of time that a specific volume of orogenic material takes to "cycle through" an orogenic system. In other words, these rates, the basin evolution, and the P-T-t paths followed by specific rock volumes are mutually dependent. Rates of uplift and denudation can be estimated in a variety of ways over various time spans, and with varying precision. Real-time techniques for measuring rates of uplift and horizontal motions include global positioning system (GPS) networks, and satellite radar interferometry. Among these technologies, GPS has been widely accepted and utilized by academia. The fundamental theory behind the global positioning system is rather straightforward. The precise positions of the satellites that send out signals for the global positioning system are known at any specific time. The satellites send out signals that are encoded with the satellite's identity and a time code. The ground unit, upon receiving the signal, compares the time code received to its internal clock to obtain a lag time. This lag time then can be converted to calculate the distance. With three or more satellite visible to the GPS unit, a precise location can be determined. The relatively small size and affordability of GPS units and the relatively short time of required operation and relatively good precision have made GPS a popular method for geodetic surveys.

Convergence between the Philippine Sea plate and the Eurasia plate near the island of Taiwan generates an enormous amount of deformation and produces frequent earthquakes in the area. Thus there is a long-standing need for good geodetic surveying to monitor the relatively rapid deformation.

GPS Network in Taiwan

In 1989 the Institute of Earth Sciences of Academia Sinica in Taiwan established a large-scale Taiwan GPS network. This network is composed of 140 stations and covers the island of Taiwan (Yu et al. 1997). Several of these sites are located on apparently stable parts of the Eurasian plate, and several sites sit on the northwestern Philippine Sea plate

(Yu and Chen 1994; Yang et al. 2001). Survey data collected (Figure 37) show that the velocity of the Philippine Sea plate relative to the Eurasia plate is 87 mm/yr at 307° with a sudden drop in the velocity immediately west of the Longitudinal Valley and the gradual decreases in magnitude of the velocity vector westward. Most of the island has a westward net velocity with respect to the stable Eurasia plate. Between sites of two islets that reside on the northwestern Philippine Sea plate and the eastern side of the Coastal Range (northern extension of Luzon arc), there is a difference of about 10-20 mm/yr, showing strong deformation within the colliding arc and forearc of the Philippine Sea plate. About 30 mm/yr of difference is observed across the Longitudinal Valley. The velocity field derived from the GPS survey shows a fan-shaped distribution of the relative-motion vectors, which is consistent with other data (Yu and Chen 1994; Yu et al. 1997; Lacombe et al. 2001; Yang et al. 2001; Yu and Kuo 2001).

A notable shortcoming of GPS surveys is that they are much less precise in the vertical measurement, therefore very few surveys to date have reported the vertical velocity of crustal movement. Yet, the vertical component of crustal motion is one of the most sought-after aspects for researchers who study active collision. In a constrained system, however, if we make some simple assumptions to simplify the problem, we can turn the problem around and predict the vertical crustal motion by the observed horizontal motion, using mathematical manipulation of the equation of conservation.

Methodology and Mathematical Derivation

There are two assumptions needed for this calculation. The first is that the rheology of the rock can be ignored, in other words, that the material behaves as a continuum without rheology involved. The second is that the vertical motion is smaller than horizontal motions. This is typically true in a convergent plate boundary, where horizontal motions are generally an order of magnitude greater than vertical motions. The assumption is that the volume of the study area is conserved without increase or decrease, and the change in the thickness/height of the area of interest will be represented by a change in topography. In reality, however, the density of the rock will change under different conditions during deformation, and isostacy may partially compensate the topography. Therefore, the calculated result should be viewed as the maximum possible uplift rate at each point.

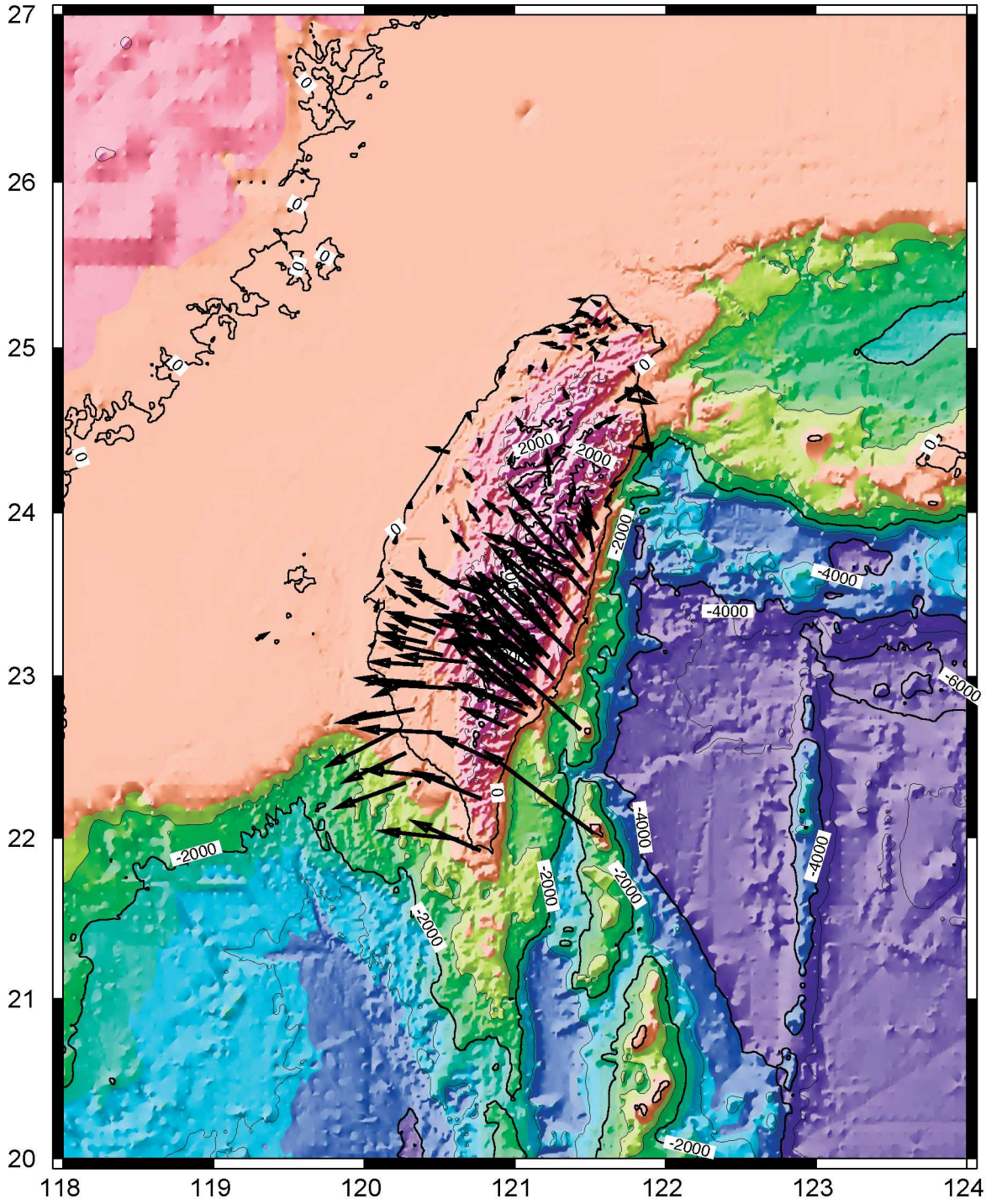

Figure 37. Locations of GPS stations and the associated vector of horizontal motion. (Yu et al., 1997; data collected during 1990-1995, 1997)

The conservation equation is:

$$\nabla V = 0 \ \ (V = (u, v, w)) \qquad \text{----------(1)}$$

If w<< u and v;

$$\frac{\partial u}{\partial x} + \frac{\partial v}{\partial y} + \frac{\partial w}{\partial z} = 0 \qquad \text{----------(2)}$$

We can now integrate the above equation with respect to depth:

$$\frac{\partial}{\partial x}(\xi u) + \frac{\partial}{\partial y}(\xi v) = -\frac{d\xi}{dt} \qquad \text{----------(3)}$$

And substitute with finite difference form:

$$h_{x,y}^{t+1} = h_{x,y}^{t} - \Delta t(h_{x,y}^{t}\frac{u_{x+1,y}^{t} - u_{x,y}^{t}}{\Delta x} + u_{x,y}^{t}\frac{h_{x+1,y}^{t} - h_{x,y}^{t}}{\Delta x} + h_{x,y}^{t}\frac{v_{x,y+1}^{t} - v_{x,y}^{t}}{\Delta x} + v_{x,y}^{t}\frac{h_{x,y+1}^{t} - h_{x,y}^{t}}{\Delta x}) \qquad \text{----------(4)}$$

Now the equation has three variables, which are v_x, v_y, and h. We can then use a finite difference scheme to solve this equation for velocity data measured in Taiwan.

The values of v_x, v_y variables can be obtained from the original vector data. The vector dataset are resolved to x and y directions to be used in the equation utilized by the finite difference method. The GPS stations in Taiwan, although they cover a large area, are generally geographically scattered and locally clustered. There are more stations in areas of interest such as the Longitudinal Valley, the Coastal Range, and the eastern part of the Central Range, where high rates of differential horizontal motion are suspected. In general, they are clustered in areas with high seismic activity. To solve the problem with a finite difference scheme, however, requires gridded data over the whole area of interest. To circumvent this, kriging was used as the means to interpolate the clustered dataset to produce two-dimensional square grids that cover the entire area. I used Surfer 7.0 on a PC to carry out the kriging process. A variogram is generated from the original dataset, fitted with an exponential model. By running the kriging processes with different parameters, the results are shown not to be sensitive to the various model variograms used; the results are, however, sensitive to the magnitude and the direction of anisotropy. Anisotropy of the model is limited

to a ratio of 2, to prevent distortion of the interpolation resulting from extreme anisotropy, and the direction of long axis of anisotropy was adjusted to an azimuth of 10°, which fits the major structural and topographical trend in Taiwan. By feeding the values of grided v_x and v_y into the finite difference conservation equation, we can calculate the v_z component, which is the predicted uplift rate.

The core of the software to solve the equation in finite difference form is written in ANSI C++ code on a Mac OS X platform and compiled with GCC 3 compiler. Graphical representations (scientific visualizations of the generated data) were created using GMT (Generic Mapping Tools) and GNUPLOT, which are freely available.

Results

Figures 38 and 39 show the x and y components of the velocity field. These components are obtained by interpolating the original x, y components over a mesh of 251 by 201 grids over the study area using a kriging scheme. The x component of the velocity field represents the east-west velocity component of the original velocity vector and the y velocity component represents the north-south component. These two figures reveal that the southern part of the Coastal Range, along with Lutao and Lansu volcanic islands and the Hengchun Peninsula, are moving at about 60 mm/yr westward and approximately 30 mm/yr toward the north relative to Eurasia. This is in sharp contrast to many other parts of the island of Taiwan, which are moving around 10 mm/yr to the west and about 20 mm/yr to the north. Figure 40 is the calculated result of the z component plotted over the study area. The predicted uplift rate along the Coastal Range is around 40 mm/yr, rising sharply from near zero immediately east of the Coastal Range in the Philippine Sea plate. The magnitude of this predicted motion is in general agreement with the observed values in Taiwan, around 44.6 mm/yr along the Longitudinal Valley and 30.2 mm/yr along the coastal highway east of the Coastal Range (Hwang and Hwang, 2002). Repeated geodetic surveys during 1984 to 1987 by Liu and Yu (1990) revealed that the Coastal Range is being uplifted with respect to the Longitudinal Valley at a rate of about 30 mm/yr, although this rate is only found in a very confined region. They also concluded that the coast of eastern Taiwan is currently undergoing uplift at a rate ranging from 0 to 35 mm/yr. However, using ^{14}C dating on the paleo-shoreline on the east coast, Vita-Finzi and Lin (1998) found that during the Holocene, the uplift rate in the Coastal Range is 3mm/yr to 5 mm/yr, this is one magnitude lower than the predicted uplift rate along the Coastal Range from this study (which is around 30 to 40 mm/yr). On the Hengchun Peninsula, Liew and Lin (1987) used ^{14}C dating of coral fragments

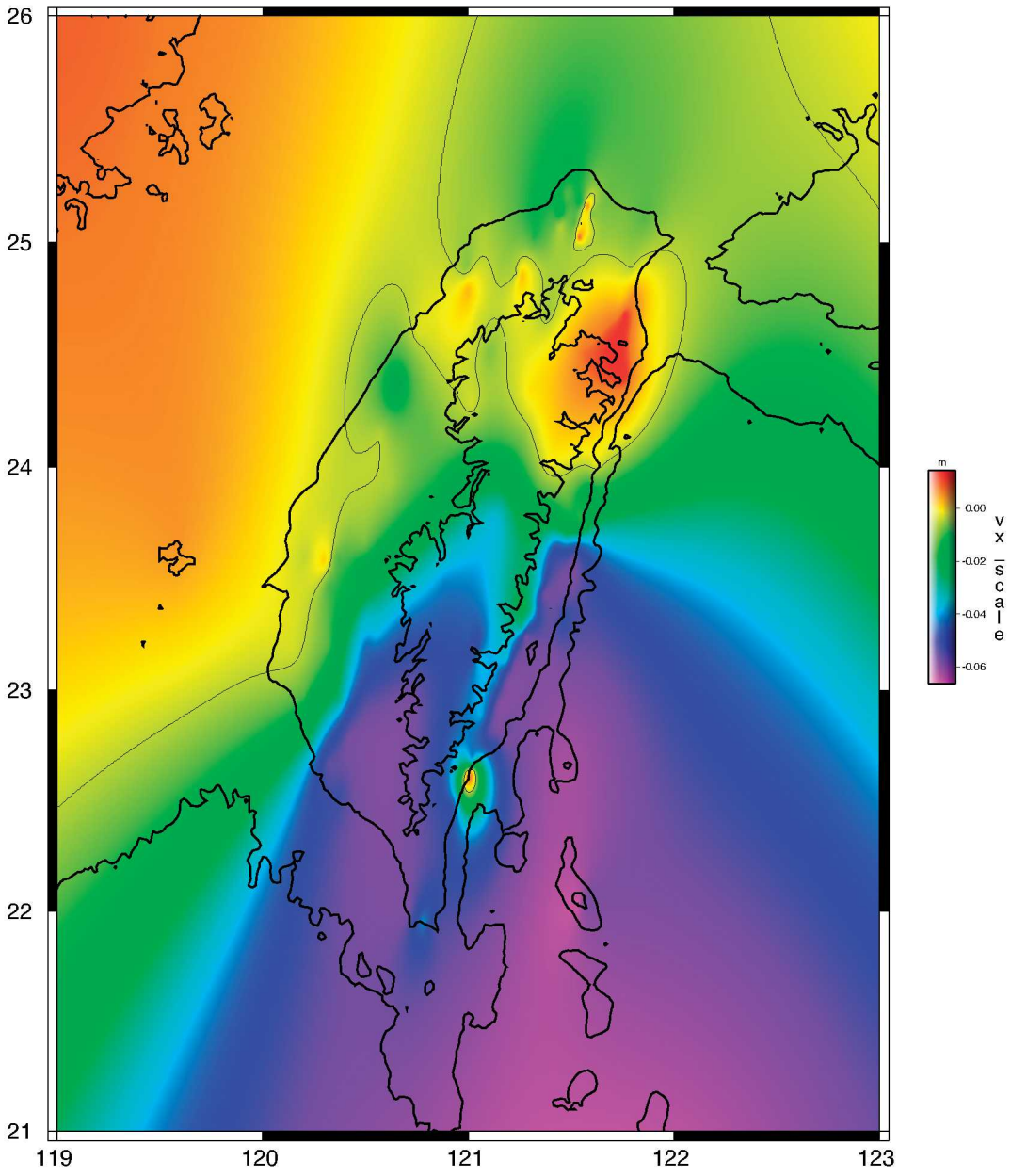

Figure 38. Crustal velocity field in the east-west direction (x component). The velocity field has a positive number for eastward motion, negative for westward motion.

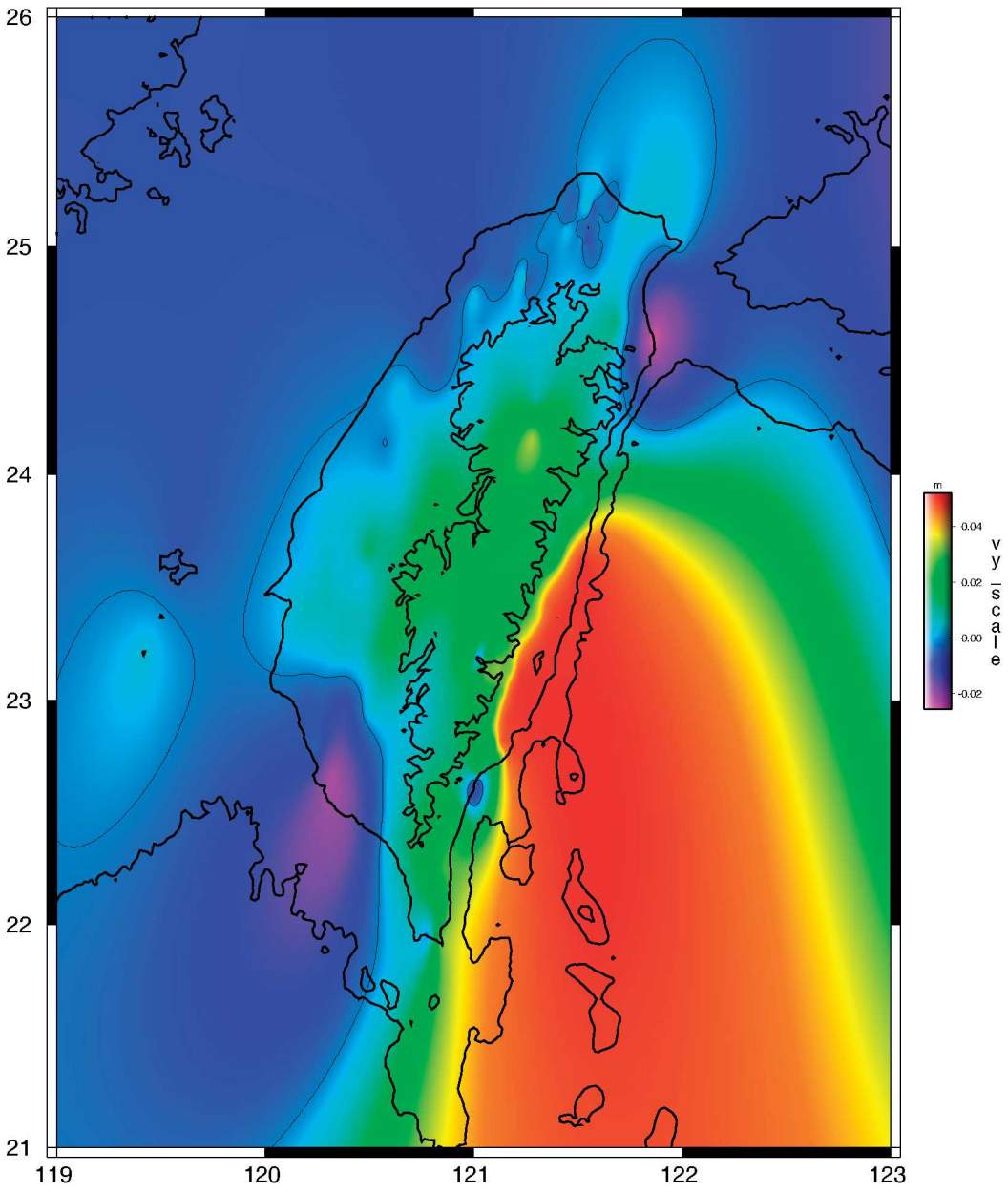

Figure 39. Crustal velocity field in the north-south direction (y component). The velocity field has a positive number for northward motion, negative for southward motion.

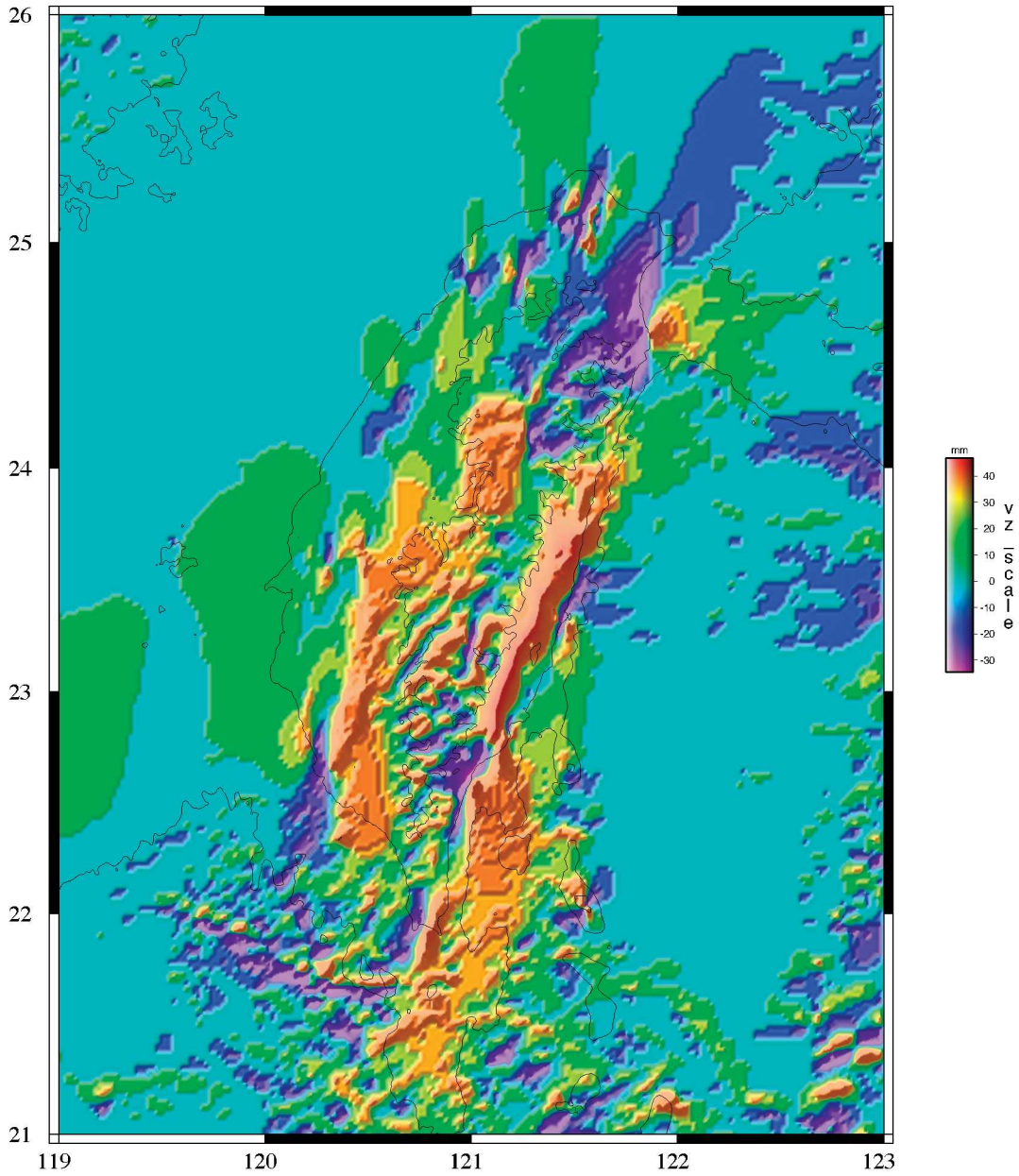

Figure 40. Predicted vertical uplift rate on- and offshore the island of Taiwan.

on marine terraces and reported a Holocene uplift rate of 4.6 mm/yr east of Kenting. The discrepancy between predicted uplift rates, geodedic measured uplift rate, and the Holocene mean uplift rate might be due to the potential of tectonic quiescence within the longer time frame considered.

Figure 41 shows the recent earthquake records of Taiwan. The area in which the predicted uplift rate is high (or slope of uplift rate is high) generally correlates with the areas with seismic activity over the past 100 years, as compiled by Wang and Shin (1998). The localities of the Chi-Chi earthquake in 1999 (2002) coincide with the offset of the high uplift rate zone in central part of Taiwan (Figure 42). In northeastern Taiwan, the predicted uplift rate is negative and the tectonic regime there belongs to the southwest extension of the opening of the Okinawa Trough as a back-arc basin (Teng 1996). The highest uplift rates are associated with the Coastal Range and the central and southern part of the Western Foothills.

With the assumptions mentioned earlier (no rheology, $v_z << v_x$ and v_y), the predicted uplift rate over the island of Taiwan provides interesting information. We can examine the predicted uplift rate in the area around Hengchun Peninsula. The observations are:

1. The neotectonic regime of southern Taiwan is compartmentalized into segments.

2. The eastern part of the Hengchun Peninsula has a much higher predicted uplift rate than the western half of the peninsula.

3. The high uplift rate observed does not continue smoothly north of the Hengchun Peninsula into the southern segment of the Central Range. This boundary coincides with the Fengkang fault. North of the Fengkang fault, the magnitude of predicted uplift is much smaller.

4. To the east of the zone of high uplift rate in the eastern Hengchun Peninsula, there is a region with a more uniform, gentler uplift over a zone about 30 km wide. These gentle uplift zones can be observed as far north as the southern end of the Coastal Range, where the northern end of the Luzon arc massif is actively accreting onto the island and mountain belt of Taiwan.

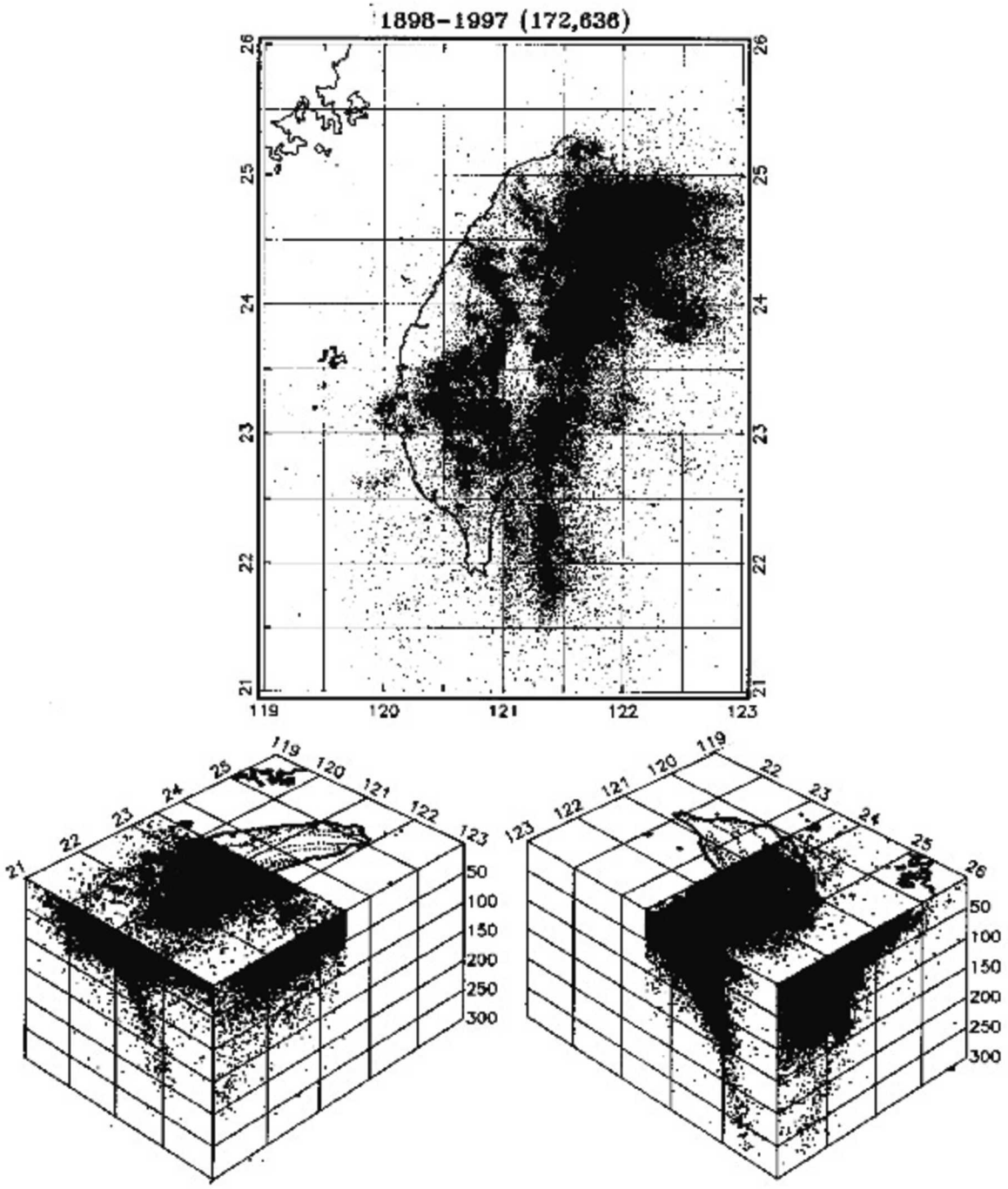

Figure 41. Seismicity near Taiwan over a 100-year period. After Wang and Shin, 1998.

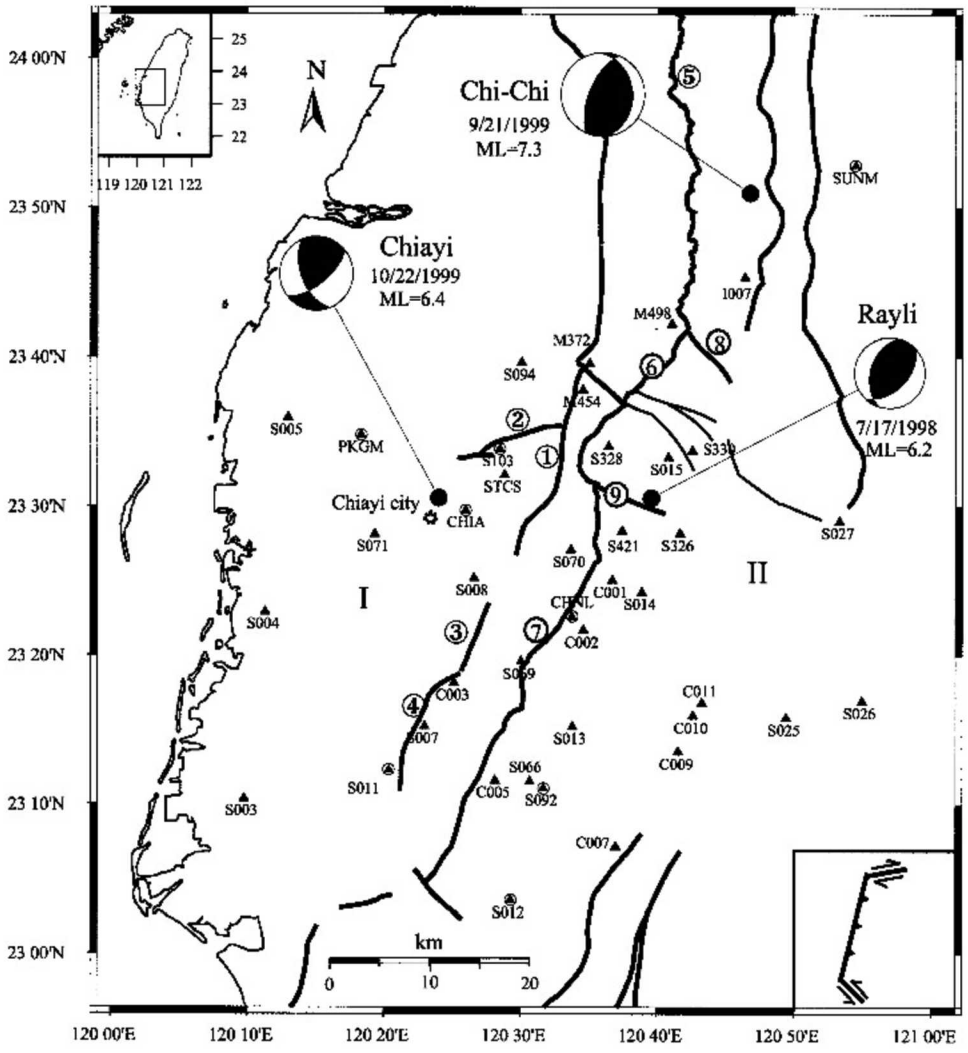

Figure 42. Map showing the location of the Chi-Chi earthquake. (After Hung et al., 2002.)

The observations made from the patterns of predicted uplift rates relate directly with the local structures that appear on and near the Hengchun fault, which separates the peninsula into an eastern and a western part, while the Fengkang fault marks the northern boundary of the peninsula. The high uplift zone in the peninsula seems to be related to the closure of forearc basin to the east, and also seems to be associated to the south with possible buckling of the obducting Philippine Sea Plate.

The implications of these observations are important to the interpretation of the local geology. These observations imply that the high uplift rate in the eastern part of the Hengchun Peninsula extends north only to the vicinity of the Fengkang fault, and not farther. Coupled with the high denudation rate in Taiwan of 2.5-4.6 mm/yr to 5.5 mm/yr (Li 1976; Liu et al., 2000), this model predicts greater cumulative uplift and therefore the exposure of older stratigraphic sequences in the eastern part of the peninsula, provided that there are no complicating structural disturbances. The segmented zones of uplift substantiate the existence of the Fengkang fault, implying the need for offset to take place to allow relatively independent uplift. This is possibly due to the previous structure underlying the island of Taiwan (Ma et al., 2002), the coincidence of the continent-ocean boundary of Eurasia plate along the southern tip of Taiwan (Lallemand et al., 2001), and/or to accommodate the difference in horizontal compression caused by the collision of the relatively straight Philippine Sea plate boundary and the convex-eastward Eurasian continental margin. The northern part of the collision has greater horizontal shortening, with the northern extension of Luzon arc closer to the continental margin. The southern section is farther away from the continental-ocean boundary and the horizontal compression ratio is lower.

2D Bathymetric Profiles on and Offshore Taiwan

Eight elevation profiles were extracted from the NGDC 5-Minute Gridded Elevation Data Selection (etopo5) in order to show the gross morphotectonic features on- and offshore the island of Taiwan. Because the Philippine Sea plate is currently moving toward the Eurasian plate along an azimuth of 307° (Yu et al. 1997), all eight profiles are extracted parallel to this direction. The profiles, spanning from longitude of 118°E to 123°E, are shown in figure 43. In figure 44 the profiles are aligned with one another by the location of the Manila trench or deformation front within each individual extracted line.

From the pre-collision state (profile A) to the fully collided state (profile I), some observations can be made from the morphotectonic profiles:

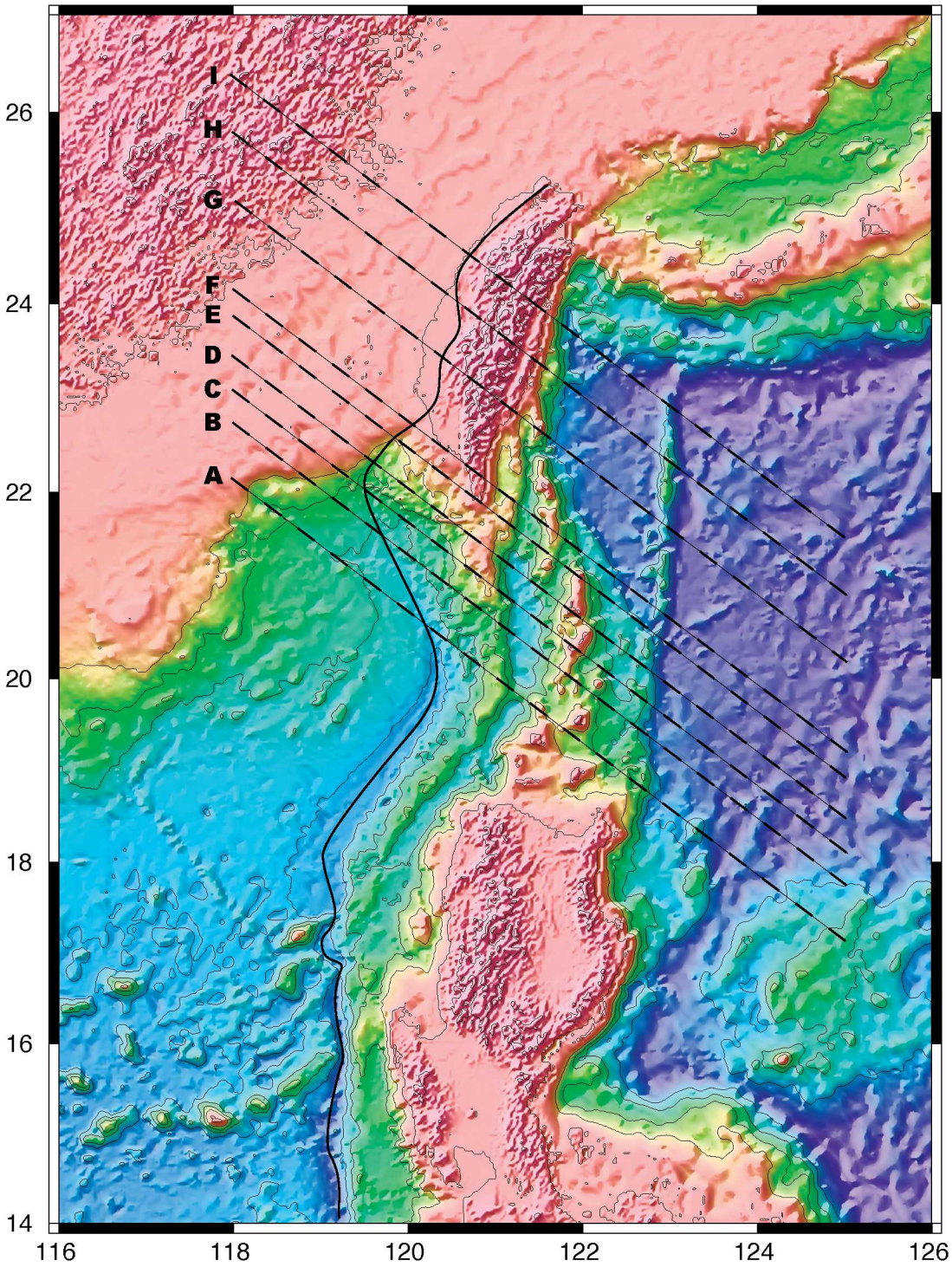

Figure 43. Topographic and bathymetric map of Taiwan and the surrounding area. Morphotectonic profiles are extracted along the eight lines plotted on the map.

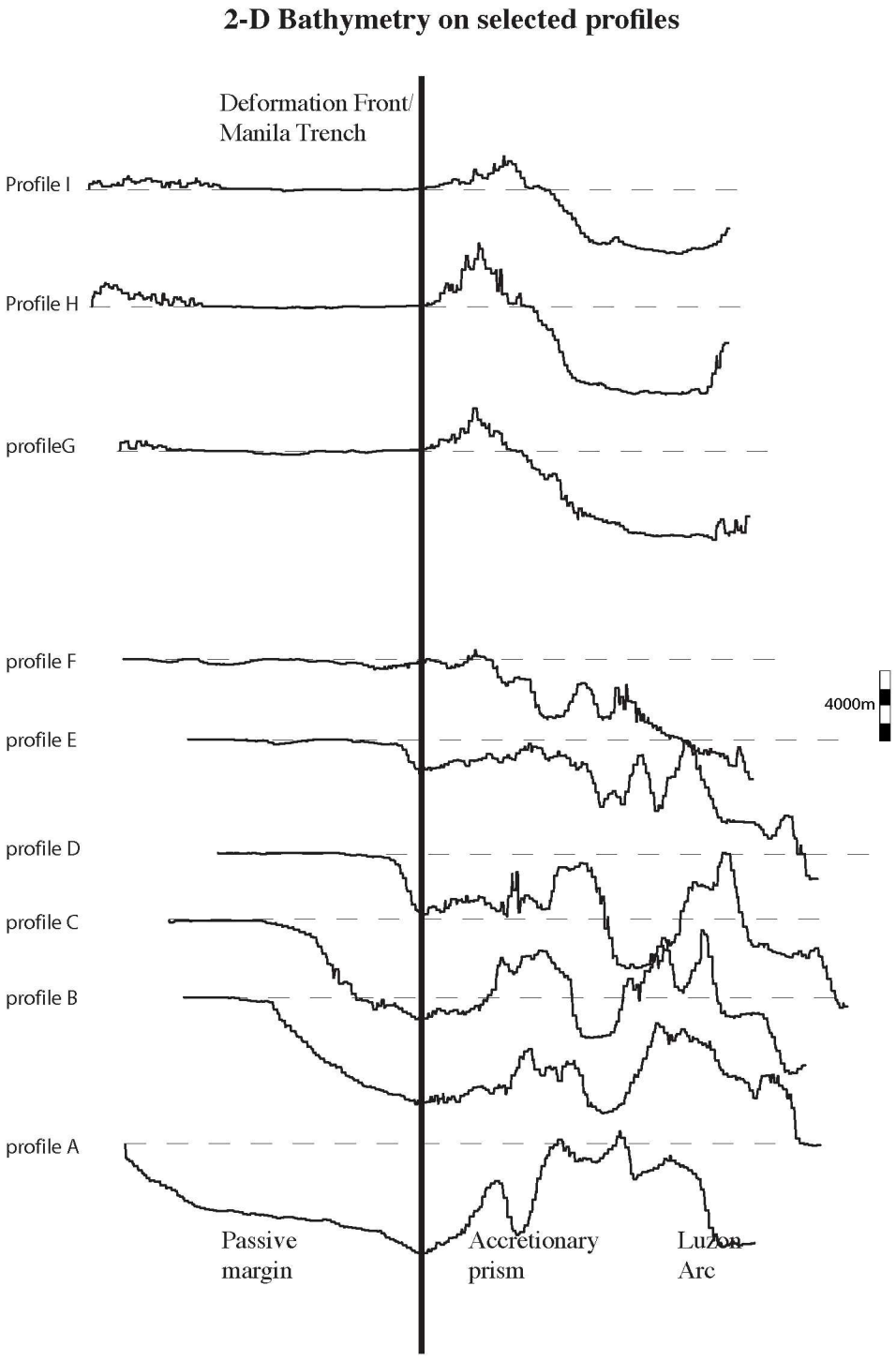

Figure 44. 2-D bathymetric profiles illustrating the transition from subduction-based tectono-morphology (profile 8) to collision-based tectono-morphology (profile 1). The first point on the left hand side of each profile is artificially set to sea-level.

The accretionary prism grows wider toward the north, as it moves toward and closer to the passive margin of the Eurasia continent and this adds to the decrease in width of the South China Sea and passive margin as the collision progresses. The width of the forearc basin, on the other hand, does not change significantly until the basin becomes relatively shallow (<1000m in depth) and its morphologic expression is lost, between profiles D and G.

Accretionary prisms above sea level seem to be self-similar; but the submarine accretionary prism is not self-similar. The crest moves from a more arcward to a more trenchward position.

Implications

If the propagation speed of collision were the same for the past 5 to 10 m.y., the HCP basin would have been at the point of trench closure at about 5 Ma, at which time the main sedimentary sequences of the HCP ceased to further accumulate (i.e. the upper stratigraphic limit of the Mutan Formation). On the continental side of the trench, the broad basin before 5Ma is capable of receiving sediment directly from the continent side. On the other hand, the arc side of the trench, being separated from the continent source by the trench to the west, may not be able to receive coarse sediment directly from the west. However, as indicated by modern day sedimentation, the trench side of the accretionary prism is receiving sediments from the current highest terrane roughly 200 km north of area. The Kaoping Canyon brings sediment from the island of Taiwan and carries it along to the Taiwan Strait and continues southward from there, turning to the east following contours of the accretionary wedge, and depositing sediment along the way. Proto-Taiwan had not emerged above sea level when the HCP basin was receiving sediments. The obvious source at the time was either directly from China or from subaerial rifted terranes offshore of Asia.

The sequences of 2-D bathymetry profiles essentially paint a picture of how the South China Sea is being closed.

1. The filling of the major structural trough of the trench (profile A to profile B).

2. The accretionary wedge extends tectonically to the base of the continental slope (profile B to profile C).

3. The closure and shallowing of the South China Sea continues, bringing the frontal toe of the accretionary prism closer to the continental slope. (profile C to profile D)

4. The South China Sea "shallows up" rather quickly while on the arc side of the accretionary wedge the forearc basin starts to close (profile D to profile E). This profile runs across the southernmost tip of the Hengchun Peninsula.

5. Foreland basin shallows to near sea level (profiles E to profiles F).

6. The accretionary wedge emerges above sea level. The height of the accretionary wedge is now controlled by the uplift and erosion rates (profile E to profile H).

7. The distance between Eurasia and the collided arc stays almost constant among the three profiles of the mature collision (profiles G, H, and I).

The process of accretion at the trench takes in crustal materials from the oceanic plate and passive margin and incorporates them into the accretionary prism. Crustal elements that are separated along the path and direction of the plate convergence can be brought together by this mechanism. The closing of the trench should synchronize with and be sub-parallel to the propagation of the collision of the Luzon arc. Therefore the shallowing of the foreland basin propagates south toward the HCP basin. The HCP basin also becomes shallower as successive material is added to the base of the accretionary wedge.

The transition of subduction-dominant tectonics to collision-dominant tectonics brings the processes of sediment transport/channeling, sediment deposition, possible switch of the sources of sediment, and displacement of sedimentary sequences together in one basin.

CHAPTER SIX
DISCUSSION

Provenance

Petrologic studies of sandstones in each of the upper Miocene sedimentary sequences studied document compositional distinctions between the units in their specific types of lithic fragments. The other major components fail to distinguish between the units, perhaps because the parameters covary, as shown by factor scores produced by principle component analysis.

Four traditional ternary diagrams (QtFL, QmFLt, QpLvmLsm, LsLvLm) of sandstone petrology were contructed by plotting the samples analyzed from the Hengchun Peninsula. The samples from individual stratigraphic units generally cluster together on these plots, although some units overlap. Sandstones from the Shihmen unit consistently differ from samples of other units (Figures 14-17). The mean of the Shihmen sandstones generally falls into the field of "magmatic arc" provenance (QtFL, Figure 14; QmFLt, Figure 15), "mixed magmatic arc and rifted continental margin" provenance and volcaniclastic "type 1" (QpLvmLsm, Figure 16), and "magmatic arc" provenance and volcaniclastic "type 1" (LsLvLm, Figure 17). "Type 1" sandstone is a volcanic-rich sandstone defined by Teng (1979) based on Plio-Pleistoncene sandstones from the Coastal Range of eastern Taiwan. The analysis clearly indicates that the Shihmen sandstones have a high affinity to magmatic arc provenance and suggests a slight influence from rifted continental margin provenance.

In the field, the uppermost Lilongshan unit includes a distinctive layer of conglomerate and very coarse sandstones that contain abundant altered mafic igneous lithic fragments. In this analysis, however, the compositional mean of sandstones from the Lilongshan unit shows more affinity to lithic arenites of "type 3" sandstones (QtFL Figure 14), "recycled orogen" provenance and "magmatic arc" provenance in QmFLt plot (Figure 15), and "mixed magmatic arcs and subduction complexes" provenance (QpLvmLsm Figure 16). "Type 3" sandstones contain large amount of lithic fragments, particularly sedimentary lithic fragments (Teng, 1979). These are more lithic-rich sandstones and do not resemble the very coarse materials that stand out in the field in the uppermost part of the Lilongshan unit.

The mean composition of Shihtzutou sandstones falls into the field of "rifted continental margins" provenance on a QpLvmLsm plot but shows contradictary affinities in other plots

("magmatic arc" provenance in a QmFLt plot, Figure 16; "recycled orogen" provenance in a QtFL plot, Figure 14). None of these ternary plots are capable of compositionally discriminating the sandstones of this unit from those of other units.

The compositions of Loshui and Shihtzutou sandstones are generally very similar. They plot in the field of "recycle orogen" provenance on a QtFL plot and the field of "magmatic arc" provenance on a QmFLt plot. They plot outside of any distinct defined fields in QpLvmLsm and LsLvLm plots.

Mutan sandstones shows affinity to "recycled orogen" provenance on a QtFL plot and to "magmatic arc" provenance in QmFLt plot, and plot near the field of "mixed magmatic arcs and subduction complex" provenance in a QpLvmLsm plot and near the field of "suture belt" provenance in LsLvLm plots.

To summarize the provenance analysis, in chronologic order: the background Mutan of mixed recycled orogen and magmatic arc provenance reflects a consistent sediment source in the region that provides detrital input throughout the duration of the formation of the HCP sequence. In the very early stage of forming the HCP sequence, a source terrane characterized as "magmatic arc with rifted continental margin" provided an abrupt and possibly brief pulse of very coarse mafic detritus into the sequence as the Shihmen unit. Starting at about the same time, the lithic-rich Lilongshan unit began to accumulate in the basin and would continue doing so until the very late stage of HCP deposition when this unit is capped by a very coarse layer of somewhat metamorphosed mafic igneous detritus. The Shihtzutou and Loshui detritus accumulate in a recurring way throughout the course of formation of the HCP sequence, representing deposition of detritus from a rifted continental margin and recycled orogen into the basin at different times and in different specific localities.

The dispersal paths of the Miocene sedimentary units in the HCP are illustrated in the "component-density" plots. From the QpLvmLsm ternary diagram, we know that high Qp value means higher affinity to Loshui and Shihtzutou units, and that the southward decrease in Qp implies a south-propagating sediment dispersal path for the Loshui and Shihtzutou units. This sediment dispersal path conforms with the paleocurrent direction for the Shihtzutou unit but does not agree with the paleocurrents in the Loshui unit. In contrast, Lvm shows the highest concentration on the western flank of the peninsula, and lower values

on the eastern half of the study area. This is indicative of the Shihmen unit and its inferred dispersal path from the west. Lsm shows yet another trend, quite different from the previous two parameters, and is high on both the east and west sides of the peninsula and very low in the central part of the region. This implies that a sedimentary source (or sources) provided detritus for these two areas. This parameter has high affinity to both the Lilongshan and Mutan units.

From the geostatistical representation of petrographic parameters and component loadings, it is clear that volcanic lithic detritus in the Hengchun Peninsula strata came from the west side, and was transported eastward only for a short distance. This trend is clearly indicated in the Lvm plot (Figure 25) and the plot of component 3 (Figure 29). The sandstones of the Shihtzutou and Loshui units are from the north and dispersed southward as imply by Qp plot (Figure 24) and the plot of component 2 (Figure 28). The first component extracted (component 1) is associated with the Mutan and Lilongshan units, as is parameter Lsm. However, the density plot of component 1 and density plot of Lsm show very different patterns. In the Lsm density plot, the high values are located on both sides of the peninsula and slightly higher in the north than the south, and the central longitudinal axis of the peninsula has a relatively low value. This seems to indicate a slight trend of southward transport of this materials. On the other hand, the density plot of component 1 shows no clear trend and no obvious clustering of low values other than on the very southern end of the peninsula. The explanation of this might be that the principle component analysis extracted the common composition in the samples into component 1, and these "common compositions" are particularly high in the Lilongshan and Mutan units. This seems to imply that there are "background" sediments that are pervasive through the whole region and that this component is included in most of the sandstones regardless of which stratigraphic unit it belongs to. Although at times coarse sediments may dilute this "background" influx, this particular composition exists in most of the samples.

Field Relationships

The Loshui unit extends much farther north than indicated on the map published by the Central Geological Survey of Taiwan, although the exposure narrows in its northern extent. The southern part of the Loshui exposure has been mapped as bounded by the Manchou fault, and seems to comprise stratigraphic intercalations of Loshui strata with background strata

of the Mutan Formation. The bedding orientations measured are complex, especially in the northern region that had not previously been mapped as Loshui.

New exposures of Shihtzutou-type lithologies were discovered during the field survey of this study. The discovery of Shihtzutou-type lithologies south of the Fengkang fault and depositionally below the Lilongshan unit paves a way to reconciling the difficulty heretofore in correlating the stratigraphy between the areas north and south of the Fengkang fault.

In the newly discovered exposure, Shihtzutou-type sandstones are clearly depositionally overlain by strata of the Lilongshan unit, while outcrops in several other localities on the Hengchun Peninsula show that the Shihtzutou beds are intercalated in background strata of the Mutan unit. The duration of deposition of the Lilongshan unit spanned almost as long as the whole Mutan Formation (Sung, 1990), and therefore the fact that Shihtzutou-type sandstones underlie the Lilongshan unit suggests that this unit, herein named the Dameitsun member, is the oldest coarse-grained member in the Mutan Formation. On the other hand, other localities with the Shihtzutou beds intercalated in background strata of the Mutan Formation suggest that this detritus is much younger in these localities. The model of Sung and Wang (1986) suggested that the coarse-grained sedimentary units of the Mutan Formation are essentially independent from and unrelated to each other, and are only connected with each other via exposures of the main Mutan unit. The model proposed by Cheng (1984) also suggested that the Shihtzutou unit is independent from the "Shihmen Formation" (equivalent to the Mutan Formation as used in this research). The new discovery indicates that the named stratigraphic members of the Mutan Formation are not all depositionally independent from each other, and it suggests that these units were probably not distant and unrelated, concurrent sedimentary systems that were later brought together by structural means. A more likely scenario is that the named members of the Mutan Formation each represent a specific type of coarse sediment influx into the basin, likely diluting the normal "background" Mutan strata. These members are restricted in time and space, but may recur or alternate temporally rather than simply representing episodes of independent deposition that end up stacking on top of one another depositionally.

There may be recurring changes of the alternate source areas in a rather small sedimentary basin. This suggests the possibility of several small deep-sea fans or fan lobes, co-mingling or in part coalescing to fill a basin. Therefore, the different units may represent deposition at somewhat different times, with different source areas, in slightly different

areas within the basin. Some of the source areas might have experienced recurring tectonic rejuvenation, producing repetitive depositional units of distinctive lithologies.

Loshui Sandstones: Rotation or an Atlantis Problem

The contrasting paleocurrent directions in the Miocene sedimentary sequences in HCP lead to two hypotheses.

First, because it is easier to postulate that there were source terranes along the northwest or west side of the HCP basin, most sediments should have been derived from those directions. Thus a southeast-directed paleoflow should be expected in all the sedimentary units and therefore the Loshui unit, which shows a northwest-directed paleoflow, must have been rotated almost 180° from a larger terrane characterized by southeast flow. This hypothesis requires that the Loshui unit was coherently transferred from an original location to its current location and was rotated 180° during the process.

The second hypothesis is: the paleoflow directions exhibited by the Loshui unit represent a clear indication of an ancient source terrane that lies to the southeast of the HCP. Problematically, there are no known terrane out in the open ocean southeast of the current HCP and, in fact, aside from the Luzon arc, there is no obvious terrane within a couple of hundred kilometers to the southeast of Taiwan.

The first hypothesis seems to require transport of a sedimentary block from somewhere along the continental margin (for it to have a southeast-trending paleoflow direction) to its current location and then rotate 180° to have the paleoflow direction pointing to the northwest. Although the Loshui unit, with along intercalated Mutan strata, is bounded by the Manchou fault, there are no signs of large displacement, and no signs of differential displacement between the northern and the southern exposures of the unit. Furthermore, the Loshui unit extends farther north than is shown on the map published by the Central Geological Survey of Taiwan, based on field observations made during this study, making the shape of the sedimentary unit an elongated strip. Keeping an elongated strip of sedimentary unit coherent while performing a rotation of 180° seems unreasonably difficult.

The second hypothesis is also problematic. Assuming the Loshui unit did not undergo a large rotation, then the paleocurrent information in the Loshui unit clearly suggests a

source terrane to the southeast side of the present-day Hengchun Peninsula, a region mainly occupied by open ocean thousands of meters deep. This creates an "Atlantis problem." This topic will be further discussed later in this chapter.

The Miocene sedimentary rocks exposed and drilled along the western flank of the main island of Taiwan show a dramatic overall southward-fining trend along the main island of Taiwan. In fact seismic reflection data show the basin the Western Foothills deepens southward (Ho, 1982) and most Miocene strata in southern Taiwan is mudstone. In contrast, Miocene sedimentary rocks of the Hengchun Peninsula are quite coarse, especially compared to Miocene strata exposed not far north of the HCP. Many of the HCP sedimentary units contain pebbles 10 cm across or larger, and many of the sandstone units contain coarse sand. This indicates that the source terranes might in fact have been very close to the HCP basin and likely were different from the source terranes of contemporaneous strata of the rest of Taiwan.

Detrital Thermochronometry

Zircons analyzed from the individual stratigraphic units of the Mutan Formation have a common fission-track age component of around 30-40 Ma, while those of the Shihtzutou unit also have a much older age component, around 64 Ma. This is the oldest of three age components extracted from the overall samples. In fact the three older grain ages from the older cluster of the Shihtzutou unit are 62.7, 75, and 90.2 Ma. The southeastern border of China is made up of a series of accreted terranes. The outermost of these (the southeastern coast of China), comprises rocks dated at about 70-140 Ma (Jahn et al., 1990). Therefore, the cluster of samples with older zircon ages may be derived directly from the Chinese continent or a rifted terrane that originated there. The majority of the rest of the samples analyzed cluster around 30 Ma, and the samples from the Shihmen unit seem to be around 40 Ma. According to Liu's hypothesis, these samples may be explained by being partially reset during the modern Penglai orogeny that has generated the island of Taiwan. The age components extracted from sandstones of the Hengchun units are compatible with those of samples from the unmetamorphosed Western Foothills on the main island of Taiwan (Liu et al., 2000; Liu et al., 2001), and structurally the Hengchun Peninsula can be considered the southern extension of the Central Range. However, the sedimentary sequence in the Hengchun Peninsula does not appear to be metamorphosed, and there does not appear to have been a heating event that caused an in-situ partial resetting of ages by the Penglai

orogeny, because many of the samples still retain the "signature" old age similar to that of the southeastern border terrane of the Chinese continent. Although the similarity in ages between samples from the Western Foothills and the Hengchun Peninsula suggests that the sources of these sedimentary rocks may have similar origins, the Hengchun Peninsula is an emerging accretionary prism and the exposed strata in the peninsula are expected to represent a rather shallow part of the accretionary prism. These rocks have apparently undergone very little metamorphism and are very unlikely to have experienced temperatures high enough to reset their zircon fission-track ages. One possible explanation, then, is that the sedimentary rocks of the Hengchun Peninsula were derived from erosion of materials from the northern part of the Taiwan orogen. However, the general consensus on the timing of collision initiation, between 12Ma (Teng, 1990) and 5Ma (Dorsey, 1988), postdates the depositional age of the main sequences of interest in Hengchun Peninsula, and therefore Taiwan had not emerged yet. Also, the eroded material needs to have included an age around 20 M.y. old at the time of deposition, which should not have been available back then, in that the reset age is regarded as a product of the modern Penglai orogeny. This excludes the possibility of self-recycling detritus from the orogeny in this case. Willett (2002) reports an anomalous apatite fission-track date in Hengchun Peninsula with an age of 2Ma, which is younger than its depositional age, and suggested a hot oceanic basin as a possible cause of the post-depositional reset. This does not seem to explain the zircon ages either, because the event is rather young and did not have an universal effect on all the materials on the Peninsula. A partial reset should produce a spectrum of age dates. In contrast, the zircon fission-track dates of Hengchun detritus cluster rather well.

Neotectonics

The process of subduction accretion brings terranes from distinctly different settings together tectonically. Modern horizontal motions predict a greater uplift rate in the east side of the Hengchun Peninsula than in the west, and the tectonic regime on the island is compartmentalized. This situation should tend to expose different crustal levels in different areas.

The observations made from the patterns of predicted uplift rates relate directly to the structures of the Hengchun Peninsula. The Hengchun fault separates the Peninsula into eastern and western parts, while the Fengkang fault marks the northern boundary of the

peninsula. The eastern region of high uplift on the peninsula seems to be related to the closure of the forearc basin to the east.

The implications of these observations are important to the interpretation of the local geology. These observations imply that the high uplift rate in the eastern part of the Hengchun Peninsula extends north only to the vicinity of Fengkang fault. Coupled with the high uplift and denudation rates in Taiwan of 2.5-4.6 mm/yr to 5.5 mm/yr (Li, 1976; Liu et al., 2000), this model predicts greater uplift and the exposure of older stratigraphic sequences in the eastern part of the peninsula, provided that there are no structural disturbances. The segmented zones of uplift substantiate the existence of the Fengkang fault, implying the need for offset to take place to allow relatively independent uplift. This may be due to the older structures underlying southernmost Taiwan, such as the continent-ocean boundary (Lallemand et al., 2001) and the extension of the "Taitung canyon fault zone" proposed by Kao et al. (2000), and/or to the difference in ratio of horizontal compression or the amount of the shortening measured along the convergence direction of the Philippine Sea plate at the island of Taiwan. Northern areas have experienced greater E-W compression, with the northern extension of the Luzon arc now lying quite close to deformed rocks of the continental margin. South of Taiwan, the arc lies farther away from the continental-ocean boundary and the overall compression ratio is lower. The sense of faulting (right lateral) in the "Taitung canyon fault zone" is causing the northern end of the Luzon forearc basin to close, and thus supports the higher uplift rate south of the Fengkang fault in Hengchun Peninsula.

The motion of the Philippine Sea plate is along the azimuth of 307° toward the Eurasia plate, hence the maximum compression and accretion take place along this direction (Crespi et al., 1994; Crespi et al., 1996). The propagation of the arc-continent collision, on the other hand, is nearly perpendicular to this direction as depicted by Suppe (1984) and Byrne (1998). The southward propagation of the collision is 42 km/My (Byrne,1998). The transition from the Manila trench to the deformation front, where the trench starts to lose its physiographic characteristics, is about 200 km south-southwest of the Hengchun Peninsula. Using the time-space equivalence of the oblique collision, the Hengchun Peninsula would be at the stage of this transitional point at around 5 Ma, and north of this point the deformation front should be the more dominant feature of the basin, and to the south the trench can be clearly defined, as depicted in the morphotectonic profiles extracted from the area (Figure 44). As inferred from the calculation earlier, the current HCP at 5 Ma should resemble the morphotectonic features

at the location about 200 km south of the HCP's current location, where the trench starts to lose its identity and became a deformation front (profile A, figure 44).

The sequence of 2-D bathymetry profiles essentially paints a picture of how the South China Sea is being closed. As the crustal materials on the passive margin and the oceanic plate encounter the subduction zone, portions of each may be incorporated into the accretionary prism. The materials that are distributed along the path and direction of the plate convergence can be brought together by this mechanism into the forearc. As the subduction zone encounters the continental margin, it first encounters extended and thinned continental crust with complex rift basins. The closing of the trench should be synchronized with and sub-parallel to the propagation of the collision of the Luzon arc. Therefore, shallowing of the foreland basin should propagate south toward the HCP basin. The HCP basin also shallows through the developing of the deformation front.

The transition of subduction tectonics to collision tectonics brings the processes of sediment transport/channeling, sediment deposition, possible switch of the sources of sediment, and displacement of sedimentary sequences together in one basin.

Palinspastic Setting in Pre-Collisional Stage of HCP Basin

If we reconstruct the tectonic configuration palinspastically using the current convergent rate between the Philippine and Eurasia plates, the sedimentary basin of the modern Hengchun area, if tied to the advancing Philippine Sea plate, will be placed approximately 750km to 820km southeast of its current position circa 10 Ma. The vast area of the South China Sea plate was yet to be consumed by the approaching Manila subduction system, which was located far to the southeast of its current location (Lee and Lawver, 1994). However, several studies (Zhou et al., 1995; Lallemand et al., 1997, 2001; Hall, 2002) have suggested that before 5 Ma, the Philippine Sea plate and the Manila trench – Luzon arc system did not move in the same fashion as they are today relative to Eurasia. Rather, before 10 Ma, the Philippine Sea plate had a more northerly motion relative to Eurasia, and between 10 Ma and 5 Ma, the system transitioned toward the current plate motions slowly. The Manila trench was about 400 km east of its current position, and only slightly farther east at 10 Ma. Sometime around 5 Ma the Philippine Sea plate started to approach Eurasia along a more northwestern course, as it is today. Therefore, before the present day to 5- 10 Ma the

southeastern side of the current Hengchun Peninsula was occupied by the proto South China Sea.

The initial Taiwan collision started in the very northern tip of the early Manila trench when the subduction zone encountered rift basins of continental affinity. This collision is between the northern extension of the present-day Luzon arc and the rifted Chinese continental margin, when the trench first intersected the edge of the rifted continental blocks formed during the second stage of rifting in the South China Sea. This intersection was likely at a relatively high angle, somewhat similar to the Izu-Bonin system in southeast Japan, except here the rift basins substitute for the Mariana arc system in the Izu-Bonin collision. Meanwhile, the rift basins formed during the first rift stage serve to trap sediment coming directly from the Asian continent.

When the rifted basins enter the subduction zone, the buoyancy of their crust is likely to ensure that upper crustal materials will become involved in the collision by accretion, causing the accretionary prism to grow well before the main collision (Boxes 2 and 3 in figure 45). Blocks that enter the forearc at a relatively high position may be elevated high into the forearc, raised above neighboring segment of the accretionary prism to become source terranes. These could include continental blocks from the edge of rift basins (as rifted block, box 1 of figure 45), and could also contain pieces of an oceanic plateau, as often seen in the South China Sea. These blocks were raised to form source terranes for sediment in neighboring depressions.

Sediment eroded from high areas was brought down to form turbidite fans in low areas along and in front of the forearc. Because the point of collision is constantly propagating, the likelihood of sedimentary facies change is high. When there is nothing significant being eroded, then the background sediment, possibly from a more distant collisional point formed from collision of another rifted continental block to the Luzon arc system, rains down into the whole basin, and when there is excess sediment, overbank flow occurs along the submarine channel, spilling across the whole depositional basin. This latter scenario describes the formation of the background Mutan Formation.

There are two scenarios to explain the mafic detritus that is pervasive in Hengchun Peninsula strata in different rock units. The first scenario is, they are derived from mafic volcanism similar to the young Penghu Islands. The second explanation is that these mafic

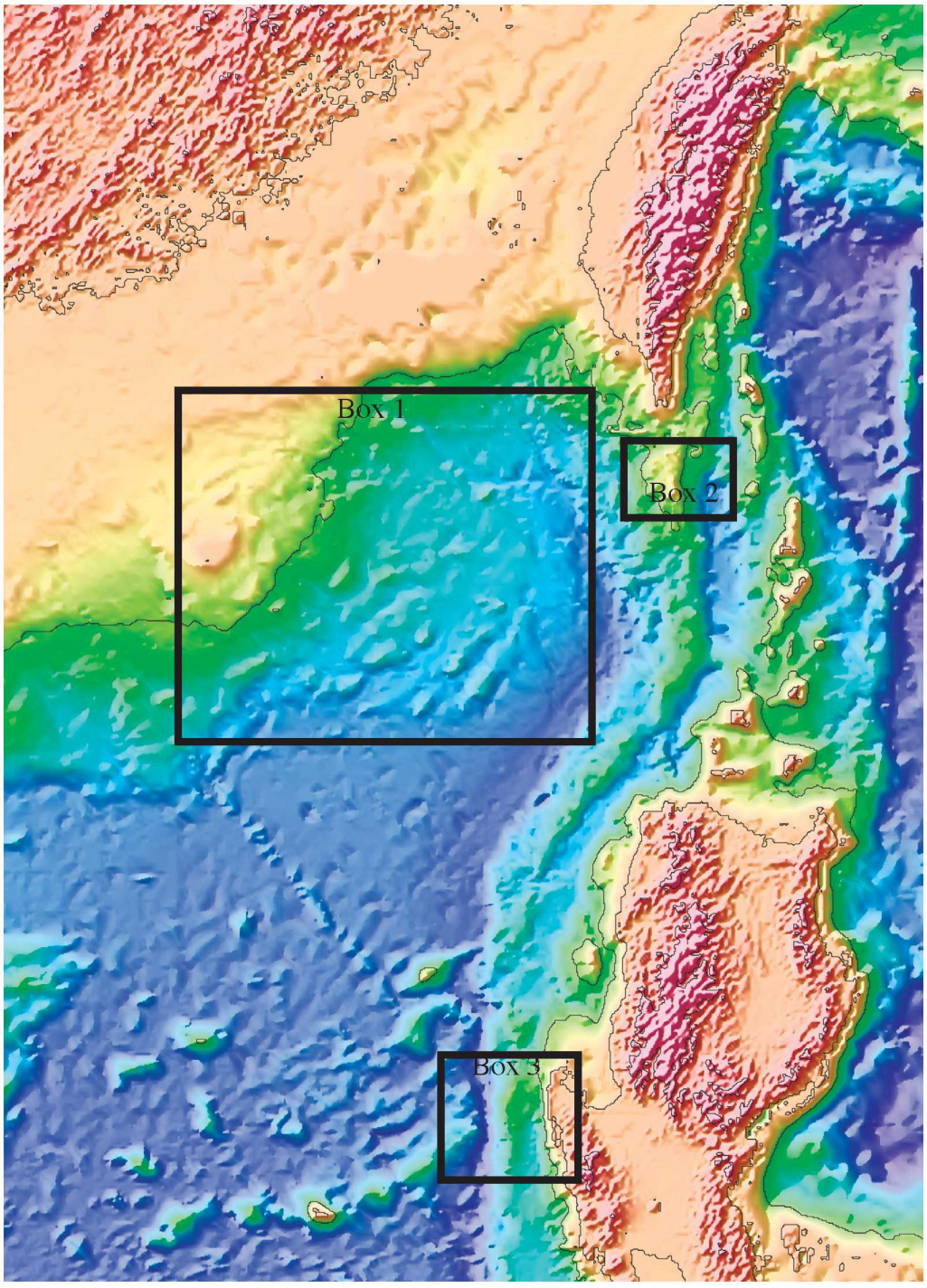

Figure 45. Bathymetric map showing rifted basins in the northern South China Sea. A series of blocks trending NE-SW lie in the northern South China Sea within box 1. Boxes 2 and 3 show the segments of the accretionary prism that are anomoulously high relative to its surroundings.

materials are derived from oceanic crust, possibly a segment of the floor of the South China Sea that has been trapped in the accretionary prism.

In either scenario, the mafic source terrane needs to be in close proximity to the depositional site of the Hengchun Peninsula basin, and provide detritus from the west of the sedimentary system at the time.

Brief History of South China Sea

The South China Sea (SCS) experienced a complex history of rifting with various tectonic elements around it interacting with the SCS. Most researchers agree on the episodic nature of the opening of the South China Sea, but they differ slightly in how to define the stages and the orientation of the spreading (Lee and Lawver, 1994; Pigott and Ru, 1994; Zhou et al., 1995). The two accepted models are summarized in figure 46.

The South China Sea opened in several distinct stages with different orientation of rifting. (Lee and Lawver, 1994; Zhou et al., 1995). Initial NW-SE to WNW-ESE extension in the Late Cretaceous to Eocene produced a series of sedimentary basins along the South China margin, and is inferred to have resulted in a NE-trending "proto" South China Sea. This proto-South China Sea was mostly consumed at the Palawan Trough, a paleo-subduction zone, following southeastward extrusion of Indochina (tectonic escape; Tapponnier et al., 1982). A second stage of opening in the mid or late Eocene to early Miocene involved N-S to NW-SE extension, forming most of the present-day South China Sea plate. In the rift basins off present-day southern China, the upper Eocene-lower Oligocene sequence consists of mainly continental, coarse-grained clastic deposits. A third stage of extension, which Lee and Lawver (1994) suggest trended NW-SE, began and ended in the early Miocene. Opening of the South China Sea stopped by the end of the early Miocene, and spreading moved to the Sulu Sea Basin, apparently due to collision of the North Palawan microcontinental block with the West Philippine block (Lee and Lawver, 1994).

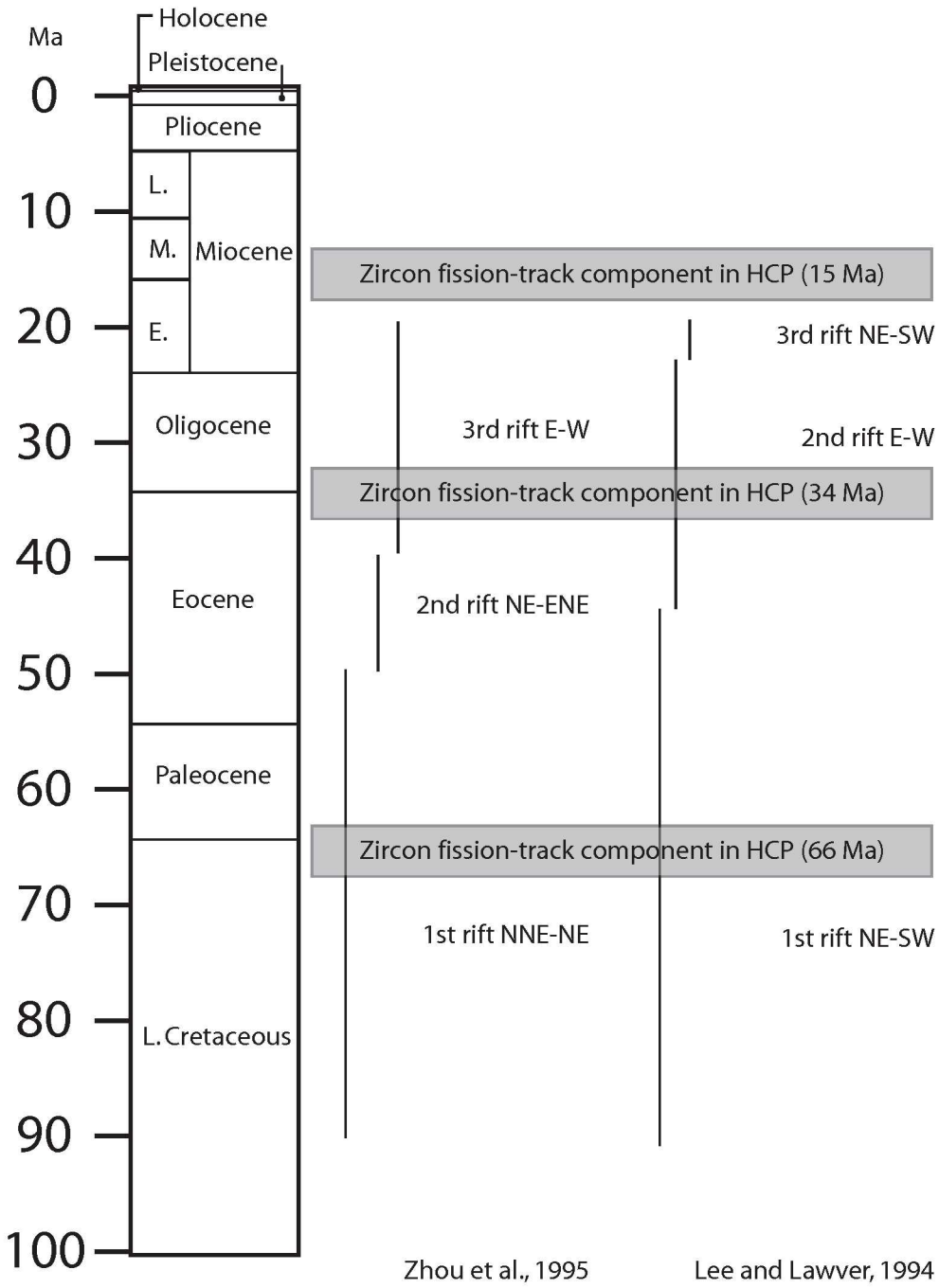

Figure 46. Comparison of models of tectonic history in South China Sea.

Subduction of the South China Sea beneath the Philippine Sea plate along the paleo-Manila trench began by the earliest Miocene, judging by the oldest known arc volcanism in the Luzon arc (26 Ma; Yang et al., 1996). Volcanism has not been continually active throughout the history of this arc, or along its length, which spans at least from the northern part of eastern Taiwan southward to the eastern part of Mindoro.

The complex history of expansion of the South China Sea created a series of rift basins in the region, some of which can be seen in the present-day bathymetric map (Figure 45).

Overall Picture

The above provides a possible scenario for the sediment input from elements of the South China Sea to the HCP basin. The earliest rifting that was related to a ridge trending NNE created rift basins of Late Cretaceous to early Tertiary age, and the thermal event associated with it could have reset ages to Late Cretaceous. The northern end of the NE-SW trending spreading center of the South China Sea extended to about 300 km southeast of the southernmost tip of present-day Taiwan (Figure 47). This mainly Eocene extension generated mid-Tertiary ocean crust, including some that is around 40 Ma as observed in the Shihmen unit. The later Eocene to early Miocene thermal event could lead to the heating of microcontinent blocks created during previous rifting and thus could have reset zircon fission-track ages to around 30 Ma.

A possible scenario is that a microcontinental terrane rifted from the Chinese continental margin during stage one of rifting (Figure 47), and was heated during stage two of rifting of the South China Sea during its expansion (Figure 48). The multiple stages of SCS expansion with different orientations of the spreading centers make it possible to heat a large area of the early SCS basin, and also to form the mafic igneous materials found as detritus in the Shihmen unit in the South China Sea at around 40 Ma. All these elements were later accreted along the approaching Manila trench system during the late Neogene closing of the system.

Source Terrane Created, Expansion of South China Sea

The igneous province of southeasternmost China has an age of around 120 Ma (Jahn et al., 1990). The first episode of South China Sea expansion is in the Late Cretaceous to early Eocene, centering around 60 Ma. This rifting is along an axis trending north-northeast,

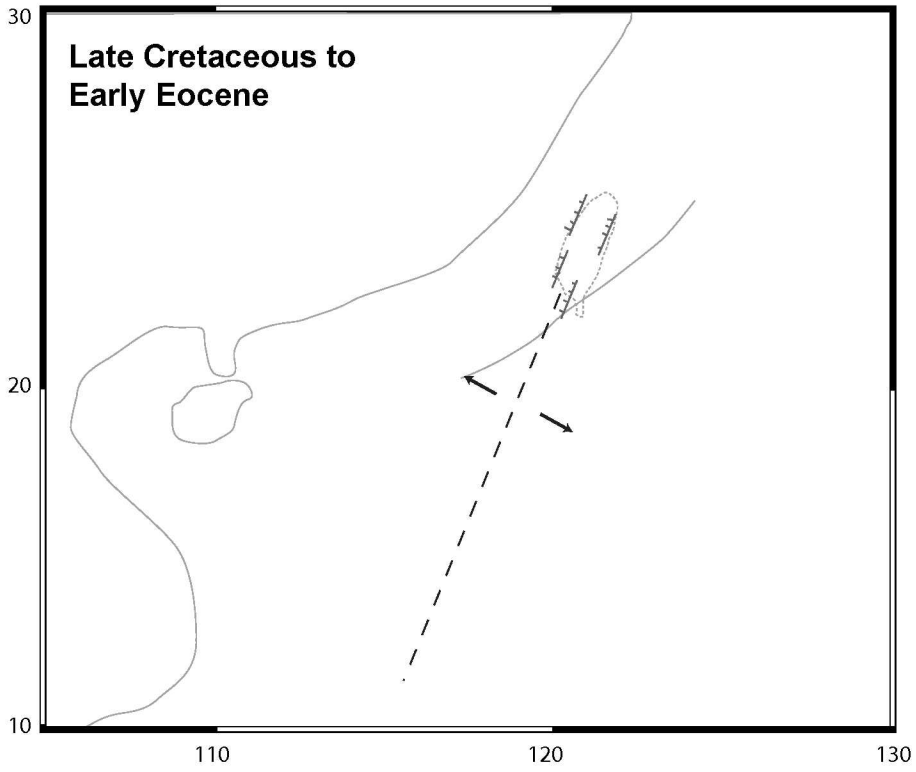

Figure 47. Late Cretaceous to early Eocene rifting of the South China Sea, which created rift basins along southeast China in the East China Sea and South China Sea.

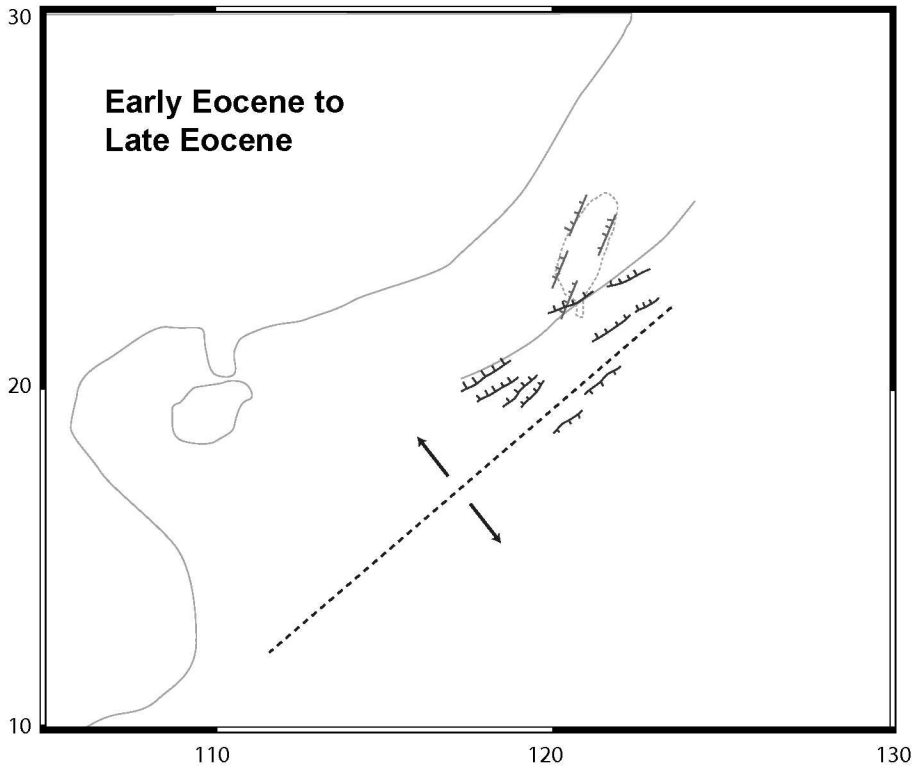

Figure 48. Early Eocene to late Eocene rifting of the South China Sea, which created second series of rift basins and probably dissected some earlier ones. The rift and the South China Sea basin reach as far as 300 km southeast of the current position of Taiwan.

and expands portions of the continental margin toward the east-southeast (Figure 47). This episode of expansion may have generated rifted basins of up to 200 km wide and brought rifted blocks around 200 km off the modern coast of China (Yu and Chow, 1997; Ren et al., 2002). The thermal event associated with this rifting stage may have annealed the zircon fission-tracks recorded in the rifted blocks in addition to generating new sea floor. This expansion of the early South China Sea brought a series of rifted continental-margin terranes out from the Eurasia continent toward the then-opening South China Sea. The second episode of expansion is approximately between early Eocene and late Eocene (Zhou et al., 1995), and centers around 50 to 40 Ma. The expansion axis during this stage trends NE-SW and intersects the previous axis, because they are not sub-parallel and all the axes are centered in the central part of modern SCS. This expansion also likely intersected micro-continental blocks that had rifted from the margin and probably dissected some of them and displaced them farther southeast of China. The possible eastern end of this rift axis is located at around 300 km southeast of the southern tip of Taiwan. The newly generated crust on the far eastern side of the rift may be as old as 40 Ma. The thermal event associated with stage two rifting also reset the fission-tracks accumulated in zircon grains to around 30 Ma; alternatively, the third episode of the rifting, along an E-W axis, may in someway have reset the fission tracks in zircons.

Sedimentation in the HCP basin

The source terranes are in place for erosion by the end of the early Miocene. At this time, subduction of the South China Sea plate beneath the Philippine Sea plate had begun based on the oldest Luzon arc volcanic rocks (26 Ma). The Philippine Sea plate was moving northward toward Eurasia (Hall, 1995; Lee and Lawver, 1995; Zhou et al., 1995; Hall, 2002), and at about 10 Ma, the relative motion of the Philippine Sea plate shifted to its current course to the west-northwest (307° azimuth). The "soft collision" may have begun at the northern part of "proto-Taiwan," i.e. the trench is encroaching on the continental margin and beginning to close in the north as early as 12 Ma (Teng, 1994), first encroaching on the microcontinental blocks rifted off China (figure 49). Some rifted blocks were accreted into the forearc and were raised tectonically to the crest of the accretionary prism (figure 50). These provided a proximal sedimentary source terrane for the HCP basin. The basin-wide "background" Mutan Formation was being deposited in the whole area. The Lilongshan unit is probably a more proximal deep-sea fan that is on the more western side of the HCP basin, while the "background" Mutan Formation might be the more distal part of this fan since they

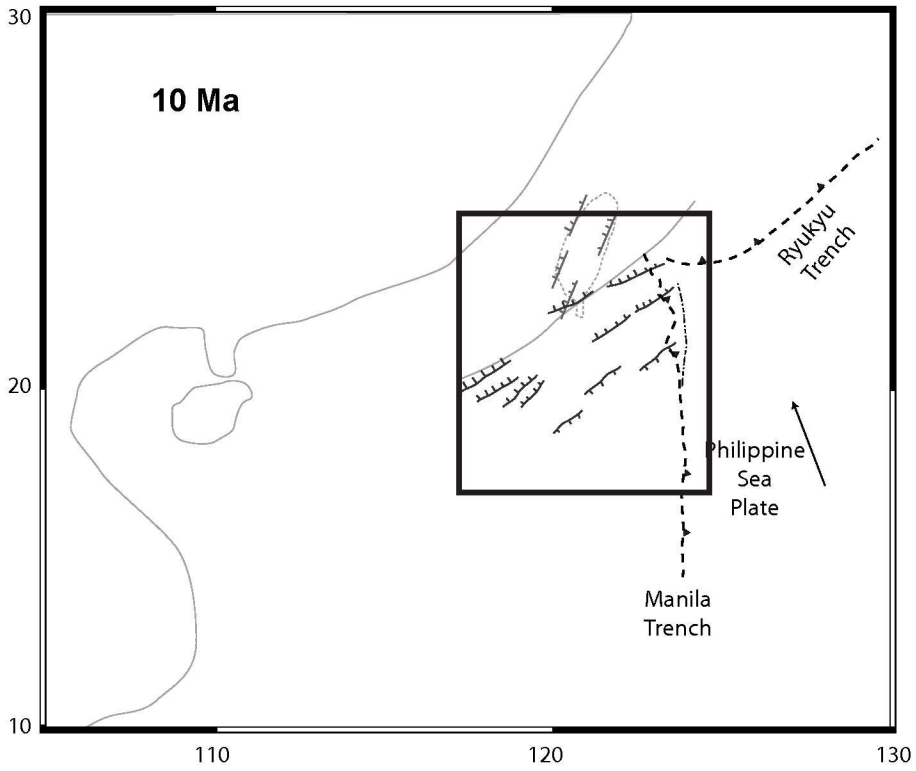

Figure 49. Tectonic configuration circa 10 Ma. The Ryukyu trench is shown located near its present-day location, and the Manila trench is about 400 to 500 km east of its current position. The detail in the area within the black box is shown in next figure.

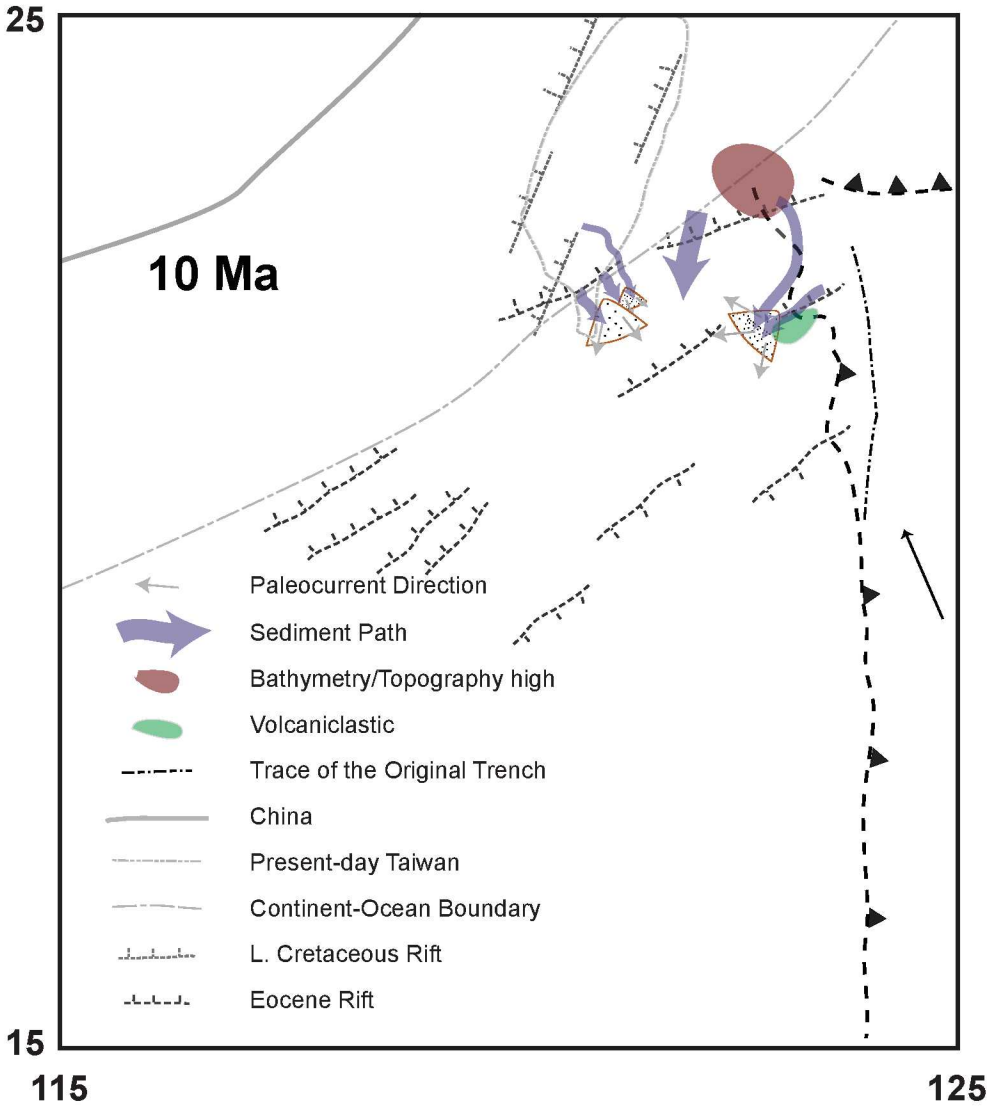

Figure 50. Illustration of sedimentation at about 10 Ma. The forward-migrating deformation front has accreted and uplifted faulted portion of rifted blocks to offer sediments to the HCP basin. Blocks of oceanic crust have been incorporated into the growing accretionary wedge.

share a rather close petrological composition and paleoflow direction. The shallowing of the HCP basin may therefore affect more strongly the proximal part of the fan and less so the distal part of the fan. The Shihtzutou detritus may have a source path that dissects both an older rifted block (block thermally reset by the oldest rifting event, of Late Cretaceous age) and a younger rifted block (block thermally reset by the second expansion event). This could have produced the bi-modal age character of the Shihtzutou unit; whereas the source terrane of the Loshui unit may be derived only from a rifted block that was affected by both thermal events. The source of the Loshui unit can be on the southeast to east side of the HCP basin and could have provided sediments to the west or northwest as turbidites.

Collecting of the sedimentary units by way of accreting (from approaching Manila Trench – Luzon Arc system); this can be depicted by the morphotectonic features offshore southern Taiwan

Most researchers (Hall, 1995; Lee and Lawver, 1995; Zhou et al., 1995; Sibuet et al., 1998; Hall, 2002;) agree that before 10 Ma, the Philippine Sea Plate moved in a more northerly direction compared to its current course relative to Eurasia, and place the Manila trench at about 200 km or less east of the east coast of Taiwan island today. The west-northwest movement of the Philippine Sea plate and the Manila trench would start around 10 Ma and would soon encounter the very northeast end of the spreading center formed in the second episode of expansion of the South China Sea. The approaching Philippine system then encountered remnant rifted continental blocks that have been dissected by the first and second expansions of the South China Sea. This encounter may have actually created the source terrane for the Loshui unit, the detritus of which had to be deposited toward the west side of the intersection of the rift block and the Manila trench (Figure 50), which resulted in paleocurrent directions ranging from trending NW to SW, while the sediment source can be due east or north. Concurrently on the western side of the HCP basin, the Shihtzutou unit is deposited episodically in the HCP basin along with the dominant Lilongshan unit and Mutan unit. These were later swept up by the approaching Manila trench system to form the overgrown accretionary prism.

At 5Ma, the Manila trench and Philippine Sea plate continued to approach Asia (Figures 51, 52). As the two plates converged the vast area of the ancient South China Sea basin was subducted and the HCP basin was accreted, resulting in an overall coarsening-upward

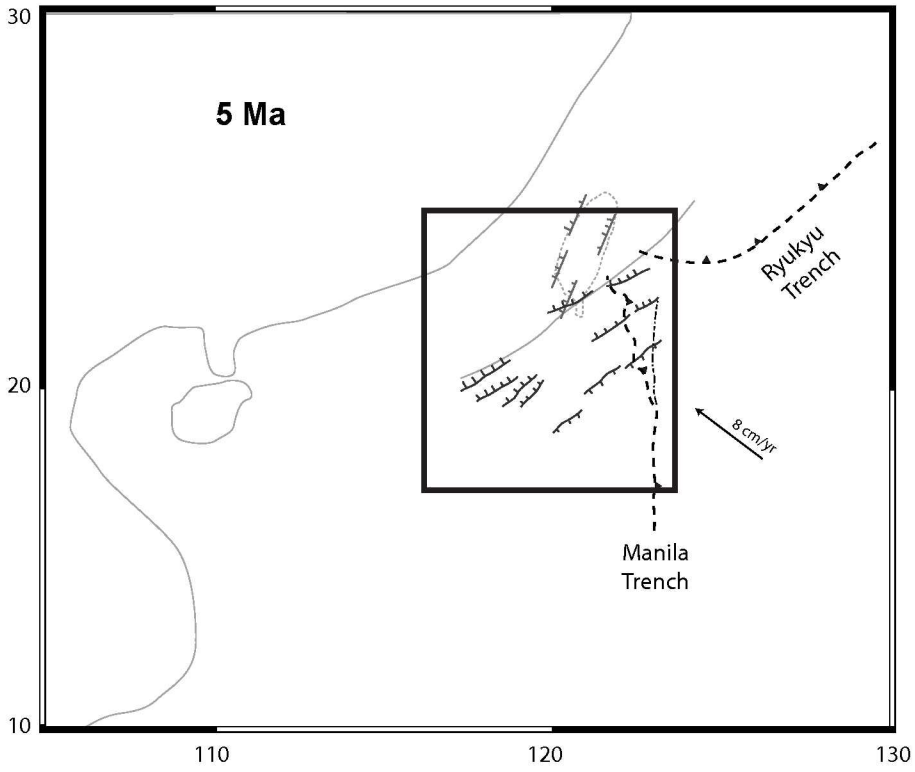

Figure 51. Tectonic configuration circa 5 Ma. The Philippine Sea plate and the Manila trench have begun moving northwest relative to Asia. The collision in the north has just begun. The detail in the area within the black box is shown in the next figure.

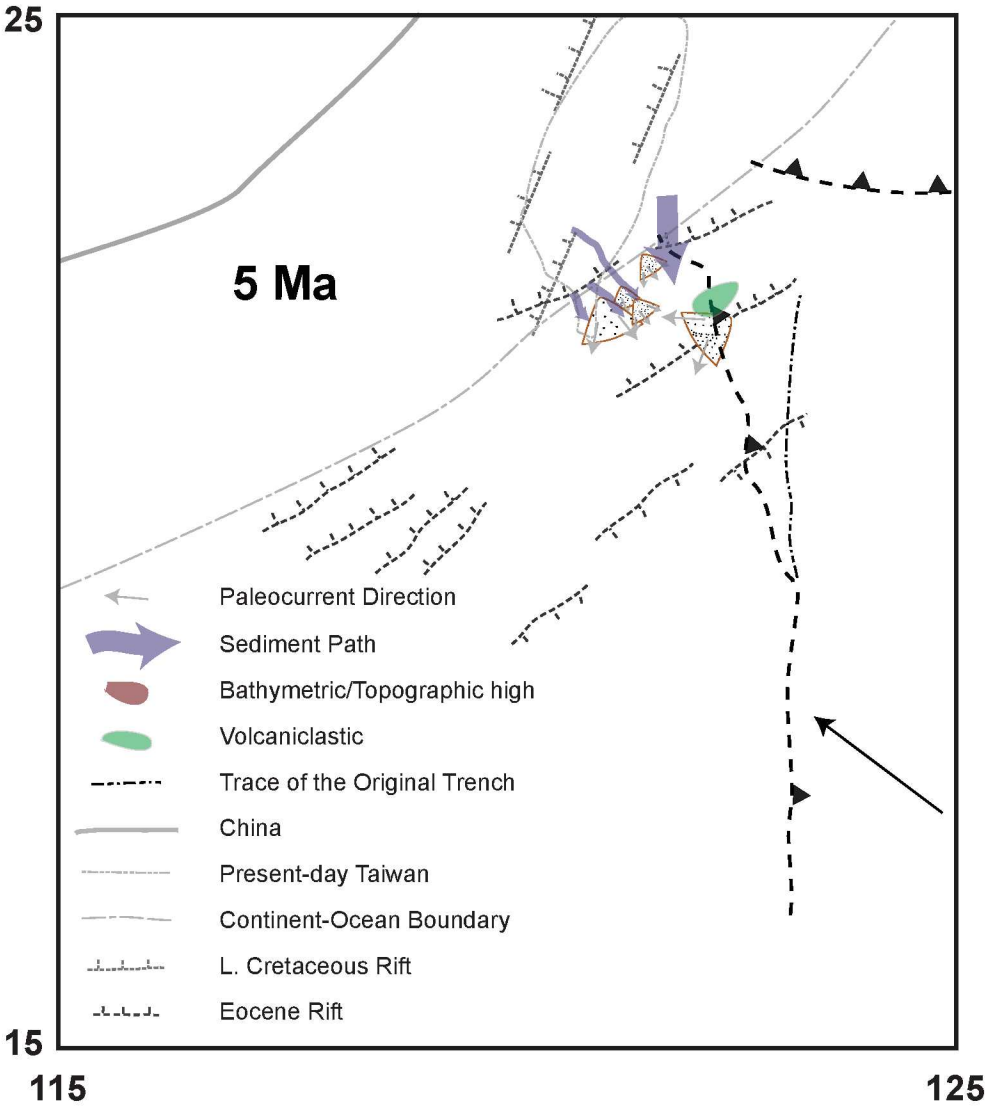

Figure 52. Sediment paths at 5 Ma. The forward-migrating deformation front has carried the deposited fan and mafic materials along the way. The HCP basin has shallowed and input from some sediment sources has recurred multiple times.

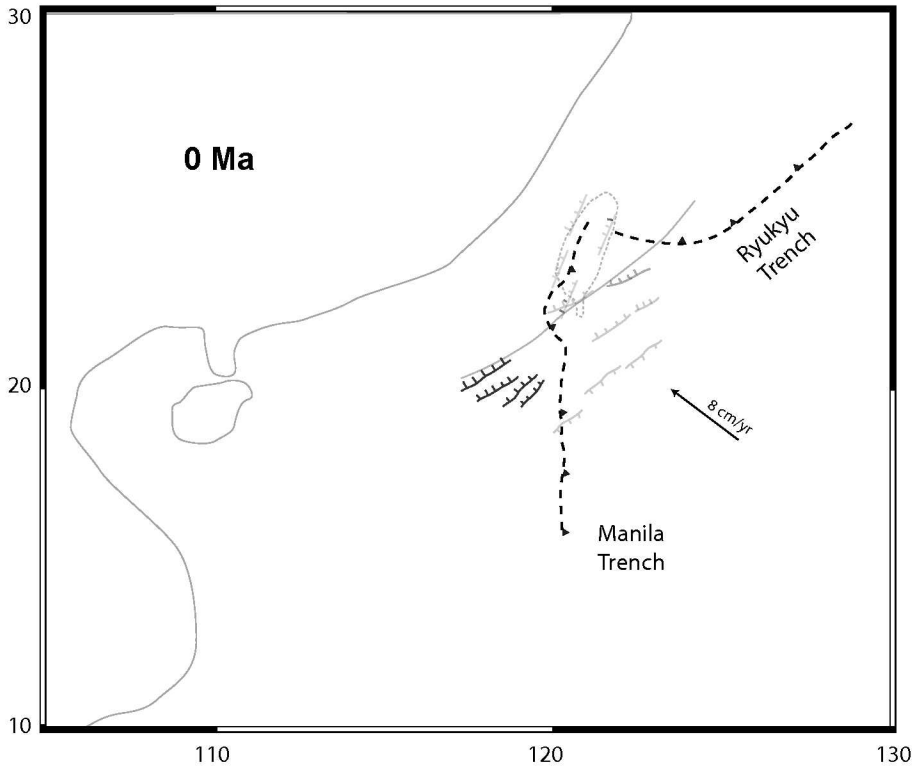

Figure 53. Tectonic configuration at present. The strata derived from mid-Tertiary rift basins have been incorporated into the accretionary prism and are now the newest emerged segment of the Taiwan orogen.

sequence in the Lilongshan unit (with possibly recycled mafic material on the top). The HCP basin was then carried westward by the accretionary prism.

During the latest 5 m.y. the Taiwan collision had begun from the north and propagated southward. Therefore in the southern part of the collision, the Philippine Sea plate is still carrying the accretionary prism and the Luzon arc toward the Eurasia continent. As shown in the east-west component of the interpolated GPS data (figure 38), the northern part of Taiwan is moving slower relative to Eurasia compared to the southeastern and southern parts of Taiwan. The Hengchun Peninsula basin, which had been incorporated into the accretionary prism, rode on the accretionary prism toward the continental margin and has now joined the Taiwan collision as the most recently emerged segment of the accretionary prism (Figure 53). To accommodate the difference in the east-west motion to the north of the Fengkang fault and that south of it, the very southern part of the island has been compartmentalized and is now experiencing different uplift rates.

The Hengchun Peninsula is experiencing different vertical motions than is most of the island north of Fengkang fault. Thus this area, which has a different origin, is being shortened in the E-W direction and has been uplifted to form the southern tip of the island of Taiwan. The differences in GPS motion and thus the predicted uplift rate across the Fengkang fault clearly depict this. The eastern side of the peninsula is experiencing a higher uplift rate, and this might explain why the eastern side exposes older sedimentary units of the Shihmen and Loshui units.

The above model depicts the formation of the Miocene sedimentary sequences in the HCP and explains their existence in the HCP. It incorporates all the known data on Miocene elements into consideration and explains the source terranes of all sedimentary units, in contrast to other models that have been proposed (Chen et al., 1985; Sung and Wang, 1986; Chang et al., 2003). This model also explains the intriguing paleoflow directions in the Miocene sedimentary sequences in the Hengchun Peninsula.

CHAPTER SEVEN
CONCLUSIONS

The sedimentary sequences in the Hengchun Peninsula have, in general, two types of provenance. One is a provenance of "mixed magmatic arc and rifted continental margin," represented by the Shihmen unit; the other is a provenance of "rifted continental margin" and "mixed magmatic arc and subduction complex," represented by all the rest of the Miocene sedimentary sequences in the study area. The composition of sandstones in the Loshui and Shihtzutou units are similar, and those of the Mutan and Lilongshan units are not very different. Shihmen sandstones are quite different from those of all the other units.

Shihtzutou lithologies was deposited during at least two separate times in the Mutan Formation. One was during the very early part of the Mutan Formation, forming the strata that underlie the Lilongshan unit, here named the Dameitsun member of the Mutan Formation; another is much later, during deposition of the younger part of the Mutan Formation. This indicates that not all the coarse sedimentary units are entirely independent of each other, or just pockets of odd sedimentary rocks caught in a larger-scale Mutan Formation. Rather, the short-lived input of Shihtzutou-type detritus apparently recurred, possibly multiple times, by either a swaying fan or episodic supply of detritus.

The elongated shape of the exposure of the Loshui unit and the lack of intense deformation in the field argue against a rotated 180° of the Loshui unit during tectonic transport.

The central age of fission-track analysis of detrital zircon grains taken from Miocene strata of the Hengchun Peninsula is 33.1 Ma. There are three age components in the zircon population, however, of 15, 34, and 66 Ma. There is an age component of around 30 ~ 40 Ma in all the units analyzed. In addition, the Shihtzutou unit has a cluster of grains with dates of 62, 74, and 90 Ma, which are significantly older than other samples analyzed.

The morphotectonic profiles demonstrate major features that change during propagation of the collision, including: loss of identity of the trench; rapid forward (westward) progress of the deformation front; and shallowing of the foreland basin. These changes shed light on how rift basins formed in the ancient South China Sea have likely been disturbed and uplifted.

Uplift rates predicted on the basis of horizontal motions measured by GPS in different parts of the island coincide with major geological features of Taiwan. Differences in predicted uplift rate predict compartmentalization of the island, and substantiate the existence of the Fengkang fault. High uplift rates in the eastern side of the Hengchun Peninsula predict the exposure of older stratigraphic units here.

A tectonic model that incorporates all these data is as follows. Opening of the South China Sea produced rift basins off the southeastern coast of Eurasia during the Late Cretaceous to early Eocene. These rift basins were dissected by the later mid Eocene to late Eocene expansion of the South China Sea and rifted continental blocks were brought farther away from the Asian margin. These rifted continental-margin blocks were incorporated into the accretionary prism of the Manila trench to form source terranes for the Hengchun Peninsula basin in the South China Sea. The Loshui unit is likely to have formed as the southeasternmost fan, whereas the Lilongshan and the Shihtzutou may have been located in the northwest side of the basin. The Shihtzutou unit was deposited episodically as these deposits appear both near the bottom of the Miocene stratigraphic column and in the midle part of the Mutan Formation. The Shihtzutou unit may have a source terrane related to the first episode of rifting in the South China Sea, because it shows a zircon fission-track age component of approximately 60 Ma. The "background" Mutan Formation may have been formed by deposition from the dominant sediment source that provided a constant supply of sediment, which was punctuated at times by coarser sediment provided by local source terranes that emerged sporadically. The basin was then incorporated into the accretionary prism and transported to the current site of the Hengchun Peninsula. It is currently the most recent emerged segment of the mountain belt of the Taiwan collision.

APPENDIX A
FISSION-TRACK DATA FOR LOSHUI UNIT

Datafile: C:\WINNT\Profiles\yen.000\Desktop\loshui\loshui.ftz
Title: Loshui sandstones

NEW PARAMETERS - ZETA METHOD

EFFECTIVE TRACK DENSITY FOR FLUENCE MONITOR (tracks/cm^2): 1.06E+04
RELATIVE ERROR (%): 4.95
EFFECTIVE URANIUM CONTENT OF MONITOR (ppm): 0.82
ZETA FACTOR AND STANDARD ERROR (yr cm^2): 7648.35 2544.06
SIZE OF COUNTER SQUARE (cm^2): 7.13E-08

GRAIN AGES IN ORIGINAL ORDER

Grain no.	RhoS (cm^-2)	(Ns)	Rhol (cm^-2)	(Ni)	Squares	U+/-2s Age	Grain Age (Ma) --95% CI--	
1	1.05E+07	(36)	2.22E+07	(76)	48	1721 429	19.3	12.4 29.3
2	1.10E+07	(63)	2.42E+07	(138)	80	1875 369	18.6	13.3 25.6
3	3.53E+07	(181)	3.82E+07	(196)	72	2960 514	37.4	29.7 47.1
4	4.23E+07	(190)	3.87E+07	(174)	63	3003 543	44.2	35.0 55.8
5	2.65E+07	(51)	3.01E+07	(58)	27	2336 653	35.7	23.7 53.5
6	1.61E+07	(110)	2.43E+07	(166)	96	1880 346	26.9	20.5 35.1
7	1.54E+07	(88)	2.35E+07	(134)	80	1821 362	26.7	19.8 35.7
8	2.92E+07	(100)	4.33E+07	(148)	48	3352 643	27.4	20.7 36.2
POOLED	2.24E+07	(819)	2.97E+07	(1090)	514	2306 268	30.5	26.6 34.8

CHI^2 PROBABILITY (%): 0.0

POOLED AGE W/ 68% CONF. INTERVAL(Ma): 30.5, 28.4 -- 32.6 (-2.1 +2.2)
95% CONF. INTERVAL(Ma): 26.6 -- 34.8 (-3.9 +4.4)

CENTRAL AGE W/ 68% CONF. INTERVAL(Ma): 28.9, 20.3 -- 41.0 (-8.5 +12.1)
95% CONF. INTERVAL(Ma): 14.5 -- 57.3 (-14.3 +28.5)
AGE DISPERSION (%): 24.8

FIT OPTION: Best-fit peaks using the binomial model of Galbraith and Green

INITIAL GUESS FOR MODEL PARAMETERS (number of peaks to fit = 2)

Peak #.	Peak Age	Theta	Fraction(%)	Count
1.	18.70	0.315	35.5	2.84
2.	30.50	0.429	28.3	2.26

Total range for grain ages: 18.6 to 44.2 Ma
Number of active grains (Num. used for fit): 8
Number of removed grains: 0
Degrees of freedom for fit: 5
Average of the SE(Z)'s for the grains: 0.15
Estimated width of peaks in PD plot in Z units: 0.17

PARAMETERS FOR BEST-FIT PEAKS

* *Standard error for peak age includes group error*
* *Peak width is for PD plot assuming a kernel factor = 0.60*

#.	Peak Age(Ma)	68%CI	95%CI	W(Z)	Frac(%)	SE,%	Count
1.	24.5	-7.1 ...+10.0	-12.0 ...+23.4	0.17	65.5	18.0	5.2
2.	40.0	-11.6 ...+16.3	-19.6 ...+38.2	0.13	34.5	18.0	2.8

Log-likelihood for best fit: -32.313
Chi-squared value for best fit: 8.686
Reduced chi-squared value: 1.737
Probability for F test: 1%
Condition number for COVAR matrix: 7.70
Number of iterations: 17

APPENDIX B
FISSION-TRACK DATA FOR MUTAN UNIT

Datafile: C:\WINNT\Profiles\yen.000\Desktop\mutan\mutan.ftz
Title: Mutan sandstones

NEW PARAMETERS - ZETA METHOD

EFFECTIVE TRACK DENSITY FOR FLUENCE MONITOR (tracks/cm^2): 1.06E+04
RELATIVE ERROR (%): 4.95
EFFECTIVE URANIUM CONTENT OF MONITOR (ppm): 0.82
ZETA FACTOR AND STANDARD ERROR (yr cm^2): 7648.35 2544.06
SIZE OF COUNTER SQUARE (cm^2): 7.13E-08

GRAIN AGES IN ORIGINAL ORDER

Grain no.	RhoS (cm^-2)	(Ns)	Rhol (cm^-2)	(Ni)	Squares	U+/-2s Age	Grain Age (Ma) --95% CI--	
1	3.00E+07	(77)	8.88E+07	(228)	36	6886 1138	13.7	10.3 18.2
2	2.81E+07	(36)	3.43E+07	(44)	18	2658 839	33.2	20.5 53.3
3	2.13E+07	(41)	1.66E+07	(32)	27	1289 470	51.8	31.6 85.8
4	7.01E+06	(18)	5.61E+07	(144)	36	4349 842	5.1	2.9 8.4
5	2.81E+07	(96)	5.90E+07	(202)	48	4575 787	19.3	14.7 25.2
6	3.27E+07	(84)	2.03E+07	(52)	36	1570 461	65.2	45.1 95.2
POOLED	2.46E+07	(352)	4.90E+07	(702)	201	3797 473	20.3	17.3 23.9

CHI^2 PROBABILITY (%): 0.0

POOLED AGE W/ 68% CONF. INTERVAL(Ma): 20.3, 18.7 -- 22.1 (-1.7 +1.8)
95% CONF. INTERVAL(Ma): 17.3 -- 23.9 (-3.1 +3.6)

CENTRAL AGE W/ 68% CONF. INTERVAL(Ma): 25.2, 16.0 -- 39.6 (-9.2 +14.4)
95% CONF. INTERVAL(Ma): 10.4 -- 61.0 (-14.8 +35.9)
AGE DISPERSION (%): 72.6

FIT OPTION: Best-fit peaks using the binomial model of Galbraith and Green

INITIAL GUESS FOR MODEL PARAMETERS (number of peaks to fit = 2)

Peak #.	Peak Age	Theta	Fraction(%)	Count
1.	15.00	0.270	17.5	1.05
2.	49.50	0.550	18.0	1.08

Total range for grain ages: 5.2 to 65.0 Ma
Number of active grains (Num. used for fit): 6
Number of removed grains: 0
Degrees of freedom for fit: 3
Average of the SE(Z)'s for the grains: 0.2
Estimated width of peaks in PD plot in Z units: 0.23

PARAMETERS FOR BEST-FIT PEAKS

* *Standard error for peak age includes group error*
* *Peak width is for PD plot assuming a kernel factor = 0.60*

#.	Peak Age(Ma)	68%CI	95%CI	W(Z)	Frac(%)	SE,%	Count
1.	13.5	-4.0 ...+5.6	-6.7 ...+13.1	0.17	50.1	20.4	3.0
2.	50.9	-15.2 ...+21.7	-25.5 ...+51.1	0.24	49.9	20.4	3.0

Log-likelihood for best fit: -35.450
Chi-squared value for best fit: 7.470
Reduced chi-squared value: 2.490
Probability for F test: 1%
Condition number for COVAR matrix: 5.95
Number of iterations: 6

APPENDIX C
FISSION-TRACK DATA FOR SHIHTZUTOU UNIT

Datafile: C:\WINNT\Profiles\yen.000\Desktop\shihtzutou\shihtzutou.ftz
Title: Shihtzutou sandstones

NEW PARAMETERS - ZETA METHOD

EFFECTIVE TRACK DENSITY FOR FLUENCE MONITOR (tracks/cm^2): 1.06E+04
RELATIVE ERROR (%): 4.95
EFFECTIVE URANIUM CONTENT OF MONITOR (ppm): 0.82
ZETA FACTOR AND STANDARD ERROR (yr cm^2): 7648.35 2544.06
SIZE OF COUNTER SQUARE (cm^2): 7.13E-08

GRAIN AGES IN ORIGINAL ORDER

Grain no.	RhoS (cm^-2)	(Ns)	Rhoi (cm^-2)	(Ni)	Squares	U+/-2s	Grain Age (Ma)	--95% CI--	
1	2.10E+07	(27)	3.74E+07	(48)	18	2899 881	22.9	13.6	37.7
2	2.38E+07	(107)	2.05E+07	(92)	63	1588 366	47.1	34.7	63.9
3	4.91E+07	(63)	5.61E+07	(72)	18	4349 1109	35.5	24.5	51.1
4	3.68E+07	(118)	2.37E+07	(76)	45	1836 458	62.7	45.9	86.2
5	2.61E+07	(67)	1.40E+07	(36)	36	1087 376	75.0	48.9	117.1
6	4.01E+07	(103)	1.79E+07	(46)	36	1389 430	90.2	62.4	132.2
POOLED	3.15E+07	(485)	2.40E+07	(370)	216	1862 267	53.0	44.8	62.8

CHI^2 PROBABILITY (%): 0.0

POOLED AGE W/ 68% CONF. INTERVAL(Ma): 53.0, 48.6 -- 57.9 (-4.5 +4.9)
95% CONF. INTERVAL(Ma): 44.8 -- 62.8 (-8.3 +9.8)

CENTRAL AGE W/ 68% CONF. INTERVAL(Ma): 50.6, 34.6 -- 73.9 (-16.0 +23.3)
95% CONF. INTERVAL(Ma): 24.1 -- 106.3 (-26.6 +55.6)
AGE DISPERSION (%): 40.1

FIT OPTION: Best-fit peaks using the binomial model of Galbraith and Green

INITIAL GUESS FOR MODEL PARAMETERS (number of peaks to fit = 2)

Peak #.	Peak Age	Theta	Fraction(%)	Count
1.	22.00	0.352	16.7	1.00
2.	47.00	0.537	30.1	1.81

Total range for grain ages: 23.0 to 89.8 Ma
Number of active grains (Num. used for fit): 6
Number of removed grains: 0
Degrees of freedom for fit: 3
Average of the SE(Z)'s for the grains: 0.18
Estimated width of peaks in PD plot in Z units: 0.21

PARAMETERS FOR BEST-FIT PEAKS

* *Standard error for peak age includes group error*
* *Peak width is for PD plot assuming a kernel factor = 0.60*

#.	Peak Age(Ma)	68%CI	95%CI	W(Z)	Frac(%)	SE,%	Count
1.	31.4	-10.9 ...+16.6	-17.7 ...+40.6	0.23	34.7	22.1	2.1
2.	64.3	-19.0 ...+27.0	-32.0 ...+63.4	0.19	65.3	22.1	3.9

Log-likelihood for best fit: -25.422
Chi-squared value for best fit: 8.017
Reduced chi-squared value: 2.672
Probability for F test: 5%
Condition number for COVAR matrix: 11.61
Number of iterations: 9

REFERENCES

Abbott, L. D., Silver, E. A., Anderson, R. S., Smith, R., Ingle, J. C., Kling, S. A., Haig, D., Small, E., Galewsky, J., and Sliter, W., 1997, Measurement of tectonic surface uplift rate in a young collisional mountain belt: Nature, v. 385, no. 6616, p. 501-507.

Abbott, L. D., Silver, E. A., Thompson, P. R., Filewicz, M. V., Schneider, C., and Abdoerrias, 1994, Stratigraphic constraints on the development and timing of arc-continent collision in Northern Papua-New-Guinea: Journal of Sedimentary Research Section B-Stratigraphy and Global Studies, v. 64, no. 2, p. 169-183.

Alvarez-Marron, J., Brown, D., Perez-Estaun, A., Puchkov, V., and Gorozhanina, Y., 2000, Accretionary complex structure and kinematics during Paleozoic arc-continent collision in the southern Urals: Tectonophysics, v. 325, no. 1-2, p. 175-191.

Andriessen, P. A. M., 1995, Fission-Track Analysis - Principles, methodology and implications for tectonothermal histories of sedimentary basins, orogenic belts, and continental margins: Geologie En Mijnbouw, v. 74, no. 1, p. 1-12.

Barr, T. D., and Dahlen, F. A., 1990, Constraints on friction and stress in the Taiwanfold-and-thrust belt from heat-flow and geochronology: Geology, v. 18, no. 2, p. 111-115.

Barrier, E., and Angelier, J., 1986, Active Collision in Eastern Taiwan: The Coastal Range: Tectonophysics, v. 125, p. 39-72.

Beaumont, C., Fullsack, P., and Hamilton, J., 1992, Erosional control of active compressional orogens, in McClay, K. R., ed., Thrust tectonics, Chapman & Hall, London, United Kingdom, p. 1-18.

Berzin, R., Oncken, O., Knapp, J. H., PerezEstaun, A., Hismatulin, T., Yunusov, N., and Lipilin, A., 1996, Orogenic evolution of the Ural mountains: Results from an integrated seismic experiment: Science, v. 274, no. 5285, p. 220-221.

Biq, C., 1972, Dual-trench structure in the Taiwan-Luzon region: Proceedings of the Geological Society of China, v. 15, p. 65-75.

Brandon, M. T., 1992, Decomposition of fission-track grain-age distributions: American Journal of Science, v. 292, no. 8, p. 535-564.

-, 1996, Probability density plot for fission-track grain-age samples: Radiation Measurements, v. 26, no. 5, p. 663-676.

Brown, D., Alvarez-Marron, J., Perez-Estaun, A., Puchkov, V., Gorozhanina, Y., and Ayarza, P., 2001, Structure and evolution of the Magnitogorsk forearc basin: Identifying upper crustal processes during arc-continent collision in the southern Urals: Tectonics, v. 20, no. 3, p. 364-375.

Byrne, T., 1996, Precollision tectonics and kinematics, and a modern analog for the Lichi and Kenting melanges, Taiwan, International Geological Congress, Abstracts--Congres Geologique Internationale, Resumes: location varies, International Geological Congress, p. 292.

-, 1998, Pre-collision kinematics and a possible modern analog for the Lichi and Kenting melanges, Taiwan: Journal of the Geological Society of China, v. 41, no. 4, p. 535-550.

Cardwell, R. K., and Isacks, B. L., 1978, Geometry of subducted lithosphere beneath Banda Sea in eastern Indonesia from seismicity and fault plane solutions: Journal of Geophysical Research, v. 83, no. NB6, p. 2825-2838.

Carter, A., 1999, Present status and future avenues of source region discrimination and characterization using fission track analysis: Sedimentary Geology, v. 124, no. 1-4, p. 31-45.

Chang, C. P., Angelier, J., and Huang, C. Y., 2000, Origin and evolution of a melange: the active plate boundary and suture zone of the Longitudinal Valley, Taiwan: Tectonophysics, v. 325, no. 1-2, p. 43-62.

Chang, C. P., Angelier, J., Lee, T. Q., and Huang, C. Y., 2003, From continental margin extension to collision orogen: Structural development and tectonic rotation of the Hengchun peninsula, southern Taiwan: Tectonophysics, v. 361, no. 1-2, p. 61-82.

Chen, W.-S., 1992, Consideration on the stratigraphy of the Kenting Formation in the Hengchun Peninsula, Special Publication of the Central Geological Survey, p. 135-142.

Chen, W.-S., and 1991, Origin of the Lichi Melange in the Coastal Range, eastern Taiwan: Special Publication of the Central Geological Survey, v. 5, p. p 257-266.

Chen, W.-S., Cheng, Y.-M., and Huang, C.-Y., 1985, Geology of the Hengchun Peninsula, southern Taiwan: Ti-Chih, v. 6, no. 2, p. 47-74.

Chen, W.-S., Huang, C.-Y., and Chen, Y.-M., 1986, Trace fossils from Miocene Formations in the Hengchun Peninsula, Taiwan: Ti-Chih, v. 7, no. 1, p. 31-48.

Cheng, Y.-M., Huang, C.-Y., Yeh, J.-J., and Chen, W.-S., 1984, The Loshui Formation; deeper-water sandstones on the Hengchun Peninsula, southern Taiwan: Acta Geologica Taiwanica, v. 22, p. 100-117.

Chi, W.-R., 1982, The Calcareous Nannofossils of the Lichi Mélange and the Kenting Mélange and their significance in the interpretation of plate-tectonics of the Taiwan region: Ti-Chih, v. 4, no. 1, p. 99-112.

Chi, W.-r., Namson, J., and Suppe, J., 1981, Stratigraphic record of plate interactions in the Coastal Range of eastern Taiwan, Chung Kuo Ti Ch'ih Hsueh Hui Chuan Kan = Memoir of the Geological Society of China, vol.4, p. 155-194.

Chiu, J. M., Isacks, B. L., and Cardwell, R. K., 1991, 3-D Configuration of Subducted Lithosphere in the Western Pacific: Geophysical Journal International, v. 106, no. 1, p. 99-111.

Chung, S. L., and Sun, S. S., 1992, A new genetic model for the East Taiwan ophiolite and its implications for Dupal domains in the northern-hemisphere: Earth and Planetary Science Letters, v. 109, no. 1-2, p. 133-145.

Crespi, J., Byrne, T., Tillman, K., and Lu, C.-Y., 1994, Deformation partitioning in the active Taiwan arc-continent collision: Abstracts with Programs - Geological Society of America, v. 26, no. 7, p. 109.

Crespi, J. M., Chan, Y.-C., and Swaim, M. S., 1996, Synorogenic extension and exhumation of the Taiwan hinterland: Geology, v. 24, no. 3, p. 247-250.

Crowley, K. D., Naeser, C. W., and Naeser, N. D., 1989, Short Course Manual on Fission-Track Analysis: Theory and Applications: St. Louis, Missouri, Geological Society of America, 297 p.

Dahlen, F. A., and Suppe, J., 1988, Mechanics, growth, and erosion of mountain belts, Geological Society of America, Special Paper, p. 161-178.

Dickinson, W. R., 1970, Interpreting detrital modes of graywacke and arkose: Journal of sedimentary petrology, v. 40, no. 2, p. 695-707.

-, 1985, Interpreting provenance relations from detrital modes of sandstones, in Zuffa, G. G., ed., Provenance of Arenites: Holland, D. Reidel Publishing Company, p. 333-361.

Dorsey, R. J., 1988, Provenance evolution andunroofing history of a modern arc-continent collision - evidence from petrography of Plio-Pleistocene sandstones, eastern Taiwan: Journal of Sedimentary Petrology, v. 58, no. 2, p. 208-218.

Dorsey, R. J., and Lundberg, N., 1988, Lithofacies analysis and basin reconstruction of Plio-Pleistocene collision basin, Coastal Range eastern Taiwan: Acta Geologica Taiwanica, Science reports of the National Taiwan University, v. 26, p. 57-132.

Ernst, W. G., 1983, Mineral paragenesis in metamorphic rocks exposed along Tailuko Gorge, Central Mountain Range, Taiwan: Journal of Metamorphic Geology, v. 1, p. 305-329.

Faure, G., 1986, Principles of Isotope Geology, John Wiley & Sons, 589 p.

Gaedicke, C., Baranov, B., Seliverstov, N., Alexeiev, D., Tsukanov, N., and Freitag, R., 2000, Structure of an active arc-continent collision area: the Aleutian-Kamchatka junction: Tectonophysics, v. 325, no. 1-2, p. 63-85.

Galbraith, R. F., 1981, On statistical-models for fission-track counts: Journal of the International Association for Mathematical Geology, v. 13, no. 6, p. 471-478.

-, 1998, The trouble with "probability density" plots fission track ages: Radiation Measurements, v. 29, no. 2, p. 125-131.

Galbraith, R. F., and Green, P. F., 1990, Estimating the component ages in a finite mixture: Nuclear Tracks and Radiation Measurements, v. 17, no. 3, p. 197-206.

Galbraith, R. F., and Laslett, G. M., 1993, Statistical-models for mixed fission-track ages: Nuclear Tracks and Radiation Measurements, v. 21, no. 4, p. 459-470.

Gallagher, K., Brown, R., and Johnson, C., 1998, Fission track analysis and its applications to geological problems: Annual Review of Earth and Planetary Sciences, v. 26, p. 519-572.

Garver, J. I., 2000, Fission-track Laboratory Procedures at Union College: Union College.

Graham, S. A., Ingersoll, R. V., and Dickinson, W. R., 1976, Common provenance for lithic grains in Carboniferous sandstones from Ouachita Mountains and Black Warrior Basin: Journal of Sedimentary Petrology, v. 46, p. 620-632.

Hall, R., 1995, Cenozoic motion of the Philippine Sea Plate: Paleomagnetic evidence from eastern Indonesia: Tectonics, v. 14, no. 5, p. 1117-1132.

-, 2002, Cenozoic geological and plate tectonic evolution of SE Asia and the SW Pacific: computer-based reconstructions, model and animations: Journal of Asian Earth Sciences, v. 20, no. 4, p. 353-431.

Ho, C. S., 1982, Tectonic evolution of Taiwan: explain text of the tectonic map of Taiwan: Taipei, The ministry of economic affairs, Republic of China, 126 p.

-, 1984, The study of Taiwan melange and its future development: Jingjibu Zhongyang Dizhi Diaochasuo Tekan = Special Publication of the Central Geological Survey, v. 3, p. p 45-60.

Huang, C.-Y., Shyu, C.-T., Lin, S. B., Lee, T.-Q., and Sheu, D. D., 1992a, Marine geology in the arc-continent collision zone off southeastern Taiwan: Implications for Late Neogene evolution of the Coastal Range: Marine Geology, v. 107, p. 183-212.

Huang, C. Y., Shyu, C. T., Lin, S. B., Lee, T. Q., and Sheu, D. D., 1992b, Marine geology in the arc continent collision zone off southeastern Taiwan - implications for Late Neogene evolution of the Coastal Range: Marine Geology, v. 107, no. 3, p. 183-212.

Huang, C. Y., Wu, W. Y., Chang, C. P., Tsao, S., Yuan, P. B., Lin, C. W., and Xia, K. Y., 1997, Tectonic evolution of accretionary prism in the arc-continent collision terrane of Taiwan: Tectonophysics, v. 281, no. 1-2, p. 31-51.

Hung, J. H., Zhan, H. P., Wiltschko, D. V., and Fang, P., 2002, Geodetically observed surface displacements of the 1999 Chi-Chi earthquake near southern termination of the Chelungpu fault: Terrestrial Atmospheric and Oceanic Sciences, v. 13, no. 3, p. 355-366.

Hurford, A. J., and Green, P. F., 1982, A users guide to fission-track dating calibration: Earth and Planetary Science Letters, v. 59, no. 2, p. 343-354.

Hwang, C. W., and Hwang, L. S., 2002, Use of geoid for assessing trigonometric height accuracy and detecting vertical land motion: Journal of Surveying Engineering-Asce, v. 128, no. 1, p. 1-20.

Imbrie, J., and van Andel, T. H., 1964, Vector analysis of heavy mineral data: Geological Society of America Bulletin, v. 75, p. 1131-1156.

Ingersoll, R. V., Bullard, T. F., Ford, R. L., Grimm, J. P., Pickle, J. D., and Sares, S. W., 1984, The effect of grain size on detrital modes: A test of the Gazzi-Dickinson point-counting method: Journal of sedimentary Petrology, v. 54, no. 1, p. 0103-0116.

Ingersoll, R. V., and Suczek, C. A., 1979, Petrology and provenance of Neogene sand from Nicobar and Bengal Fans, DSDP sites 211 and 218: Journal of Sedimentary Petrology, v. 49, p. 1271-1228.

Jahn, B. M., Zhou, X. H., and Li, J. L., 1990, Formation and tectonic evolution of southeastern China and Taiwan - isotopic and geochemical constraints: Tectonophysics, v. 183, no. Iss 1-4, p. p 145-160.

Kao, H., Huang, G. C., and Liu, C. S., 2000, Transition from oblique subduction to collision in the northern Luzon arc - Taiwan region: Constraints from bathymetry and seismic observations: Journal of Geophysical Research-Solid Earth, v. 105, no. IB2, p. 3059-3079.

Kearey, P., and Vine, F. J., 1996, Global tectonics: Boston, Blackwell Science, x, 333 p.

Konstantinovskaia, E. A., 2001, Arc-continent collision and subduction reversal in the Cenozoic evolution of the Northwest Pacific: an example from Kamchatka (NE Russia): Tectonophysics, v. 333, no. 1-2, p. 75-94.

Lacombe, O., Mouthereau, F., Angelier, J., and Deffontaines, B., 2001, Structural, geodetic and seismological evidence for tectonic escape in SW Taiwan: Tectonophysics, v. 333, no. 1-2, p. 323-345.

Lallemand, S., Font, Y., Bijwaard, H., and Kao, H., 2001, New insights on 3-D plates interaction near Taiwan from tomography and tectonic implications: Tectonophysics, v. 335, no. 3-4, p. 229-253.

Lallemand, S. E., Liu, C. S., and Font, Y., 1997, A tear fault boundary between the Taiwan orogen and the Ryukyu subduction zone: Tectonophysics, v. 274, no. 1-3, p. 171-190.

Lee, T. Y., and Lawver, L. A., 1994, Cenozoic plate reconstruction of the South China Sea region: Tectonophysics, v. 235, no. 1-2, p. 149-180.

-, 1995, Cenozoic plate reconstruction of southeast Asia: Tectonophysics, v. 251, no. 1-4, p. 85-138.

Levin, V., Shapiro, N., Park, J., and Ritzwoller, M., 2002, Seismic evidence for catastrophic slab loss beneath Kamchatka: Nature, v. 418, no. 6899, p. 763-767.

Li, Y.-H., 1976, Denudation of Taiwan island since the Pliocene Epoch: Geology, no. FEB., p. 105-107.

Lieske, J., Lundberg, N., and Reed, D. L., 1992, Backthrusting and accretion in the submarine Taiwan orogen: SeaMarc II and seismic reflection data: Acta Geologica Taiwanica, v. 30, p. 131-144.

Liew, P.-M., and Lin, C.-F., 1987, Holocene tectonic activity of the Hengchun Peninsula as evidenced by the deformation of marine terraces: Memoir of the Geological Society of China, v. 9, p. 241-259.

Lin, W.-S., 2003, Debate on the existence of Fengkang Fault, and the stratigraphic system in Hengchun Peninsula; personal communication.

Liu, C.-C., and Yu, S.-B., 1990, Vertical crustal movements in eastern Taiwan and their tectonic implication: Tectonophysics, v. 183, p. 111-119.

Liu, C. S., Liu, S. Y., Lallemand, S. E., Lundberg, N., and Reed, D. L., 1998, Digital elevation model offshore Taiwan and its tectonic implications: Terrestrial Atmospheric and Oceanic Sciences, v. 9, no. 4, p. 705-738.

Liu, T. K., 1982, Tectonic implications of fission track ages from the Central Range, Taiwan: Geological Society of China Proceedings, v. 25, p. 22-37.

Liu, T. K., Chen, Y. G., Chen, W. S., and Jiang, S. H., 2000, Rates of cooling and denudation of the Early Penglai Orogeny, Taiwan, as assessed by fission-track constraints: Tectonophysics, v. 320, no. 1, p. 69-82.

Liu, T. K., Hsieh, S., Chen, Y. G., and Chen, W. S., 2001, Thermo-kinematic evolution of the Taiwan oblique-collision mountain belt as revealed by zircon fission track dating: Earth and Planetary Science Letters, v. 186, no. 1, p. 45-56.

Lundberg, N., and Dorsey, R. J., 1988, Synorogenic sedimentation and subsidence in a Plio-Pleistocene collisional basin, Eastern Taiwan, in Kleinspehn, K. L., and Paola, C., eds., New Perspectives in Basin Analysis: New York, Springer-Verlag, p. 265-280.

-, 1990, Rapid Quaternary emergence, uplift, and denudation of the Coastal Range, eastern Taiwan: Geology, v. 18, p. 638-641.

Lundberg, N., Reed, D. L., Liu, C.-S., and Lieske, J., 1992, Structural controls on orogenic sedimentation, submarine Taiwan collision: Acta Geologica Taiwanica, v. 30, p. 130-141.

Lundberg, N., Reed, D. L., Liu, C. S., and Lieske, J., Jr., 1997, Forearc-basin closure and arc accretion in the submarine suture zone south of Taiwan: Tectonophysics, v. 274, no. 1-3, p. 5-23.

Ma, Z. J., Wang, C. Y., Xu, J., Nie, F. J., and Zhang, J., 2002, Study on the transverse structures across Taiwan Strait: Science in China Series D-Earth Sciences, v. 45, no. 12, p. 1114-1126.

Mueller, C., Pelletier, B., Schaaf, A., Glacon, G., and Huang, T. C., 1986, Age determination of the ophiolitic materials from the Hengchun Peninsula (South Taiwan) and their tectonic implication, Memoir of the Geological Society of China, p. 422.

Page, B. M., and Lan, C. y., 1983, The Kenting melange and its record of tectonic events: Chung Kuo Ti Ch'ih Hsueh Hui Chuan Kan = Memoir of the Geological Society of China, , n, v. 5, p. 227-248.

Page, B. M., and Suppe, J., 1981, The Pliocene Lichi melange of Taiwan; its plate-tectonic and olistostromal origin: American Journal of Science, v. 281, no. 3, p. 193-227.

Pelletier, B., Cotten, J., Beilon, H., Bassoulet, C., and Stephan, J. F., 1986, Field setting, petrography, chemistry, K-Ar ages and origin of the magmatic and sedimentary associated rocks of the Hengchun Peninsula, southern Taiwan: Bulletin of the Central Geological Survey, v. 4, p. 27-54.

Pelletier, B., and Stephan, J. F., 1986, Middle Miocene obduction and late Miocene beginning of collision registered in the Hengchun Peninsula; geodynamic implications for the evolution of Taiwan: Tectonophysics, v. 125, no. 1-3, p. 133-160.

Peng, T. H., Li, Y. H., and Wu, F. T., 1977, Tectonic uplift of the Taiwan island since the early Holocene, in Ho, C. S., ed., Biq Chingchang dedicational volume, Geological Society of China Memoir, p. 57-69.

Pigott, J. d., and Ru, K., 1994, basin superposition on the northern margin of the South China Sea: Tectonophysics, v. 235, p. 27-50.

Price, P. B., and Walker, R. M., 1962, Observation of fossil particle tracks in natural micas: Nature (London), v. 196, no. 4856, p. 732-734.

Reed, D. L., Lundberg, N., Liu, C. S., and Kuo, B. Y., 1992, Structural relations along the margins of the offshore Taiwan accretionary wedge: Implications for accretion and crustal kinematics: Acta Geologica Taiwanica, v. 30, p. 105-122.

Ren, J. Y., Tamaki, K., Li, S. T., and Junxia, Z., 2002, Late Mesozoic and Cenozoic rifting and its dynamic setting in Eastern China and adjacent areas: Tectonophysics, v. 344, no. 3-4, p. 175-205.

Seno, T., Stein, S., and Gripp, A. E., 1993, A model for the motion of the Philippine Sea Plate consistent with NUVEL-1 and geological data: Journal of Geophysical Research, B, Solid Earth and Planets, v. 98, no. 10, p. 17,941-17,948.

Sibuet, J. C., Deffontaines, B., Hsu, S. K., Thareau, N., Le Formal, J. P., and Liu, C. S., 1998, Okinawa trough backarc basin: Early tectonic and magmatic evolution: Journal of Geophysical Research-Solid Earth, v. 103, no. B12, p. 30245-30267.

Stephan, J. F., Blanchet, R., Rangin, C., Pelletier, B., Letouzey, J., and Muller, C., 1986, Geodynamic evolution of the Taiwan-Luzon-Mindoro belt since the late Eocene: Tectonophysics, v. 125, p. no.1-3.

Sung, Q., 1990, Stratigraphy of the Hengchun Peninsula, Special Publication of the Central Geological Survey, p. p 225-237.

-, 1991, Some characteristics of sedimentary blocks in the Lichi Melange, Coastal Range, Taiwan, Special Publication of the Central Geological Survey, p. 231-256.

Sung, Q., and Wang, Y., 1986, Sedimentary environments of the Miocene sediments in the Hengchun Peninsula and their tectonic implication: Memoir of the Geological Society of China, v. 7, p. p 325-340.

Sung, Q.-C., and Wang, Y., 1985, Petrofacies of Miocene sediments in the Hengchun Peninsula and its tectonic implication: Proceedings of the Geological Society of China, no. 28, p. 23-44.

Suppe, J., 1981, Mechanics of mountain building and metamorphism in Taiwan: Memoir of the Geological Society of China, no. 4, p. 67-89.

-, 1984, Kinematics of arc-continent collision, flipping of subduction, and back-arc spreading near Taiwan: Memoir of the Geological Society of China, no. 6, p. 21-33.

-, 1988, Tectonics of arc-continent collision on both sides of the South China Sea: Taiwan and Mindoro: Acta Geologica Taiwanica, Science reports of the National Taiwan University, v. 26, p. 1-18.

Tapponnier, P., Peltzer, G., Ledain, A. Y., Armijo, R., and Cobbold, P., 1982, Propagating extrusion tectonics in Asia - new insights from simple experiments with plasticine: Geology, v. 10, no. 12, p. 611-616.

Teng, L. S., 1979, Petrographical study of Neogene sandstones of the Coastal Range, eastern Taiwan (1. Northern Part): ACTA geologica Taiwanica, v. 20, p. 129-155.

-, 1990, Geotectonic Evolution of late Cenozoic arc-continent collision in Taiwan: Tectonophysics, v. 183, p. 57-76.

-, 1994, Tectonic evolution and depositional history of Southeast China continental margin basins: International Sedimentological Congress, v. 14, p. 82.

-, 1996, Extensional collapse of the northern Taiwan mountain belt: Geology, v. 24, no. 10, p. 949-952.

Tsan, S. F., 1974, The Kenting Formation: a note on Hengchun Peninsula stratigraphy: Proceedings of the Geological Society of China, v. 17, p. 131-133.

Vita-Finzi, C., and Lin, J. C., 1998, Serial reverse and strike slip on imbricate faults; the Coastal Range of East Taiwan: Geology, v. 26, no. 3, p. 279-281.

Wang, C. H., Liew, P. M., Liu, T. K., and Burnett, W. C., 1989, The Holocene uplift rates on both sides of the active plate-collision boundary in Taiwan: Eos (Transactions, American Geophysical Union), v. 70, p. 403.

Wang, C. Y., and Shin, T. C., 1998, Illustrating 100 years of Taiwan seismicity: Terrestrial Atmospheric and Oceanic Sciences, v. 9, no. 4, p. 589-614.

Willett, S., Fisher, D., and Anonymous, 1995, Plate boundaries, relative motion and thin-skinned deformation in Taiwan, Eos, Transactions, American Geophysical Union, p. 603-604.

Willett, S. D., 1999, Steady-state mountain belts; definitions and models, Abstracts with Programs - Geological Society of America, p. 296.

Willett, S. D., Fisher, D., Yeh, E.-C., and Anonymous, 2001, High erosion rates in Taiwan from apatite and zircon fission track ages.

Yang, M., Tseng, C. L., and Yu, J. Y., 2001, Establishment and maintenance of Taiwan geodetic datum 1997: Journal of Surveying Engineering-Asce, v. 127, no. 4, p. 119-132.

Yang, T. F., Tien, J. L., Chen, C. H., Lee, T., and Punongbayan, R. S., 1995, Fission-track dating of volcanics in the northern part of the Taiwan-Luzon arc - eruption ages and evidence for crustal contamination: Journal of Southeast Asian Earth Sciences, v. 11, no. 2, p. 81-93.

Yen, J.-Y., 1998, Sediment compositions and their relations to the source rocks in modern arc-continent collision zone : examples from offshore southern Taiwan, x, 127 leaves p.

Yu, H. S., and Chow, J., 1997, Cenozoic basins in northern Taiwan and tectonic implications for the development of the eastern Asian continental margin: Palaeogeography Palaeoclimatology Palaeoecology, v. 131, no. 1-2, p. 133-144.

Yu, S.-B., and Chen, H.-Y., 1994, Global positioning system measurements of crustal deformation in the Taiwan arc-continent collision zone: Terrestrial Atmospheric and Oceanic Sciences, v. 5, no. 4, p. 477-498.

Yu, S. B., Chen, H. Y., and Kuo, L. C., 1997, Velocity field of GPS stations in the Taiwan area: Tectonophysics, v. 274, no. 1-3, p. 41-59.

Yu, S. B., and Kuo, L. C., 2001, Present-day crustal motion along the Longitudinal Valley Fault, eastern Taiwan: Tectonophysics, v. 333, no. 1-2, p. 199-217.

Zhou, D., Ru, K., and Chen, H. Z., 1995, Kinematics of Cenozoic extension on the South China Sea continental margin and its implications for the tectonic evolution of the region: Tectonophysics, v. 251, no. 1-4, p. 161-177.

BIOGRAPHICAL SKETCH

Jiun-Yee Yen, born in Taipei, Taiwan in 1969, spent much of his youth messing around with gears and engines to figure out how they work. In high school he became fascinated with folklore but still dreamt about becoming a mechanic.

After high school graduation he took a university entrance exam, and the score determined which school and department he might go to. Largely by accident he was admitted to Earth Science, and he accepted, knowing that he could later transfer out from that into either Chemistry or Mechanical Engineering.

But that idea soon vanished after he found out that, for geological field work, he could get to go to exotic places that he had never dreamt or heard of. His early fascination with folklore became transformed into a love of history, and his dream of getting his hands dirty fixing engines in a garage was fulfilled by getting hands-on experience in the field with a hammer, hand lens, and compass.

He graduated from the Earth Science Department, National Cheng-Kung University, in Tainan and received his B.S. degree in 1992 with an honors thesis titled "*The Effect Of Oxidation On The Microtexture Of Titano–Magnetite In Basaltic Rock Using Scanning Electron Microscopy*."

After serving in the army as a Second Lieutenant in Quemoy from July 1992 to May 1994, he held a Research Assistantship at National Sun Yat-Sen University, working on the sedimentary aspects of a national groundwater project.

In Fall 1995 he started graduate study at Florida State University in the Department of Geology and received the M.S. degree in Summer 1998. Thereafter he entered the doctoral program and chose to investigate problems of mysterious sediment sources and the evolutionary history of southern Taiwan.

His current research utilizes the two fields he especially liked when growing up, a love of history and getting his hands dirty by practical work in the field.

Jiun-Yee Yen is a member of the Geological Society of America, Society for Sedimentary Geology, American Geophysical Union, and American Association of Petroleum Geologists.